



Microcavity Supported Lipid Bilayers; biomimetic models of the cell membrane

By

Nicola McConnell, B.Sc. (Hons)

A thesis submitted to Dublin City University for the award of MSc.

Supervisor:

Prof Tia Keyes

Declaration

I hereby certify that this material, which I now submit for assessment on the programme of study leading to the award of MSc. is entirely my own work, that I have exercised reasonable care to ensure that the work is original, and does not to the best of my knowledge breach any law of copyright, and has not been taken from the work of others save and to the extent that such work has been cited and acknowledged within the text of my work.

Signed: _____

ID No.: _____

Date: _____

Acknowledgments

First and foremost I would like to sincerely thank my primary supervisor Prof. Tia Keyes for all of her guidance, time and encouragement with me during the past two years. Without her support and encouragement throughout the course of this work, I wouldn't be here. A huge thank you to Sean Maher, who kindly and patiently taught me all he could this past year and for always being available to answer my many questions and to Dr Sivaramakrishnan Ramadurai, for his never ending words of encouragement and generous contribution to the FCLS data. I learned a lot from both of you and I really appreciated all of your help and support. A special thank you to my project student, Amanda Kunaka, for her contribution to the characterisation of the MSLB, using CV. My gratitude extends to SFI and the Daniel O' Hare Research Scholarship scheme for providing much needed financial assistance throughout the year and additionally to Prof. Gabius for generously providing the galectins.

A massive thank you to all the technical staff: Ambrose, Nicola, Aisling, Veronica, Damien, John, the two Marys, Catherine and Vinny and all other staff in DCU. I really appreciate all your hard work.

I am so grateful to all those who made the research experience enjoyable; Sean, Mohammad, Siva, Kerrie, Leanne, Laura, Ruth, Léa, Brian, Nicky, Kae, Andrew, Natasha, Kellie, Elaine, Hazel, Hannah, Andy, Saorla, Sarah and Orla. Thank you for all the great memories, the laughter and for lending your ears to me when things weren't going great. Thanks also to Aisling, Chris, Aurélien, Samantha, Vinnie, Kerileng and Ciarán and all of those who supported me in any respect during the course.

Finally, a huge thank you goes to my family: Mam, Dad, Peter, Eileen, John and Brendan, for their unconditional love and understanding. I would not be here today if it wasn't for your never-ending support, belief and encouragement. Throughout my years in education, you have advised and guided me to the best of your ability, and always listened when I needed you. I will be forever grateful. Thank you.

This thesis is dedicated to my family.

|

Table of Contents

Acknowledgments.....	iii
Table of Contents.....	v
Abstract.....	viii
List of Acronyms/Symbols.....	ix
Chapter 1: Introduction.....	1
1.0 Introduction to Biological Membranes.....	2
1.0.1 Membrane Lipids.....	3
1.1 Introduction to Model Cell Membranes.....	8
1.1.1 Monolayers.....	8
1.1.2 Supported Lipid Bilayers.....	9
1.1.3 Black Lipid Membrane.....	11
1.1.4 Liposomes.....	12
1.1.5 Giant unilamellar vesicles.....	13
1.3 Introduction of Microcavity arrays.....	18
1.3.1 Fabrication of cavity arrays.....	18
1.3.2 Interfacial Self-Assembly.....	20
1.3.3 Formation of Self-Assembled Monolayers.....	22
1.3.4 Electrochemical Characterisation of Monolayers.....	25
1.4 Conclusions.....	28
1.5 References.....	29
Chapter 2: Experimental Methods and Instrumentation.....	34
2.0 Instrumentation.....	35
2.0.1 Scanning Electron Microscope (SEM).....	35
2.0.2 Cyclic Voltammetry.....	36
2.0.3 Water Contact Angle.....	36
2.0.4 Langmuir-Blodgett.....	38
2.1 Materials and Methods.....	41
2.1.1 Materials.....	41
2.1.2 Methods.....	41
2.1.2.1 Fabrication of Gold Cavity Arrays.....	41
2.1.2.2 Surface Modification of the Gold Cavity Arrays.....	43
2.1.2.3 Preparation of Lipid Bilayer.....	44

2.2 Results and Discussion	46
2.2.1 Optimisation of Microcavity Array Gold Deposition Protocol.....	46
2.2.2 Characterisation of Gold Cavity Arrays.....	48
2.2.3 Characterisation of Lipid Bilayer	56
2.3 Conclusions.....	60
2.4 References.....	61
Chapter 3: EIS Study of Drug Interactions with Lipid Membrane	62
3.0 Introduction.....	63
3.0.1 Log P and Log D Values	64
3.0.2 Cell-based Methods.....	66
3.0.3 PAMPA	67
3.1 Effect of Drug Binding	68
3.1.1 Ibuprofen and Diclofenac.....	69
3.2 Materials and Methods.....	73
3.2.1 Materials.....	73
3.2.2 Experimental Equipment.....	73
3.2.3 Methods.....	73
3.2.3.1 Preparation of Ibuprofen and Diclofenac Stock Solutions	73
3.2.3.2 EIS	74
3.3 Results and Discussions.....	75
3.3.1 EIS Analysis of Drug Interaction	75
3.3.1.1 Ibuprofen	75
3.3.1.2 Diclofenac.....	84
3.3.2 Enhancing the Ibuprofen EIS response	91
3.3.3 Improving the stability of the EIS response	95
3.4 Conclusions.....	99
3.5 References.....	100
4.0 Introduction.....	104
4.1 Glycobiology.....	105
4.2 GM1 and Galectins 1 and 3	111
4.3 Materials and Methods.....	116
4.3.1 Materials.....	116
4.3.2 Experimental Equipment.....	116

4.3.3 Methods.....	116
4.3.3.1 Preparation of Lipid Bilayer	117
4.3.3.2 Preparation of Human Galectins.....	118
4.4 Results and Discussions.....	119
4.4.1 EIS Analysis of Galectin – GM1 Interaction.....	119
4.4.2 EIS Analysis of Galactose Inhibition	132
4.4.3 GM1 Bilayers incorporating Cholesterol	140
4.5 Conclusions.....	142
4.6 References.....	144
Chapter 5: Conclusions and Future Work.....	148
5.0 Conclusions and Future Work	149
Appendix 1: FLCS Results	I

Abstract

Biomimetic models of the cell membrane are sought after as they have the potential to provide a realistic representation of an organism's lipid bilayer. They can be used to understand lipid dynamics, signalling, drug permeability and membrane protein diffusion in an environment that is away from the complexity of the real living cell. This thesis examines the application of a new type of lipid membrane model, the micro-cavity supported lipid bilayer (MSLB), to study drug-membrane interactions and glycolipid containing bilayers using electrochemical impedance spectroscopy (EIS). Chapter 1 outlines the structure and function of the cell membrane and describes current models used to replicate the functions of the cellular bilayer. The limits of these models are also discussed particularly in the context of stability, lipid fluidity and addressability of both sides of the bilayer. The biomimetic MSLB system is then explored as a viable alternative in this thesis and is described in Chapter 2. $2.80 \pm 0.04 \mu\text{m}$ diameter gold arrays were used and their surfaces were chemically modified to render them hydrophilic which aided the assembly of lipid bilayers using Langmuir Blodgett to form the initial monolayer and vesicle disruption to create the final bilayer structure.

This model is applied in Chapter 3 as a means of assessing drug plasma membrane interactions of two representative non-steroidal anti-inflammatory drugs; ibuprofen and diclofenac. These drugs were chosen as their log P values are well established and their interactions with membranes have been characterised by other methods. Their impact on the cavity array supported lipid membrane was investigated using EIS. Chapter 4 uses the MSLB model to study the interactions between the ganglioside, GM1, and disease relevant lectins by fabricating asymmetric GM1 containing lipid bilayer membranes. The influence of lipid/sterol composition on GM1-lectin recognition and aggregation was also considered.

Overall, this work demonstrates that, using EIS as the interrogation method, it is possible to sensitively explore interactions between external molecules and the lipid bilayer using these MSLBs. The MSLBs are a significant advance on current lipid membrane models as they permit accurate representations of cell membrane in elements of composition, fluidity, asymmetry and deep aqueous well on either side of the membrane.

List of Acronyms/Symbols

BLMs - Black Lipid Membranes

CV - Cyclic Voltammetry

DAG - Diacylglycerol

DOPE - 2-dioleoyl-sn-glycero-3-phosphoethanolamine

ECM - Extracellular Matrix

EIS - Electrochemical Impedance Spectroscopy

FLCS – Fluorescence Lifetime Correlation Spectroscopy

GSLs - Glycosphingolipids

GUVs - Giant Unilamellar Vesicles

IIRAS - Infrared Reflection-Absorbance Spectroscopy

ITO - indium tin oxide

LB - Langmuir Blodgett

LC/MS - Liquid Chromatography Mass Spectrometry

LC/UV - Liquid Chromatography Ultraviolet

LUVs - Large Unilamellar Vesicles

MDCK - Madin Darby Canine Kidney

MLVs - Multilamellar Vesicles

MSLB – Microcavity Supported Lipid Bilayer

NSAID - Nonsteroidal Anti-Inflammatory Drug

PA - Phosphatidic acid

PAMPA - Parallel Artificial Membrane Permeability Assay

PBS - Phosphate Buffer Saline

PEG - Polyethyleneglycol

PtdCho - Phosphatidylcholine

PtdEtn - Phosphatidylethanolamine

PtdIns - Phosphatidylinositol

PtdSer - Phosphatidylserine (PtdSer)

SA – Surface Area

SAM - Self-Assembled Monolayer

SEM - Scanning Electron Microscopy

SLBs - Supported Lipid Bilayers

SM - Sphingomyelin

SUVs - Small Unilamellar Vesicles

THF - Tetrahydrofuran

A - Electroactive Surface Area

C = Concentration

D = Diffusion Coefficient, cm^2/s

F - Faradays Constant

i_p = Peak Current

n = Electron Stoichiometry

Q – Charge

r – Radius

v = Scan Rate

π - Pi

Γ - Monolayer Surface Coverage

Chapter 1: Introduction

1.0 Introduction to Biological Membranes

The plasma membrane, illustrated in Figure 1.1, functions in compartmentalisation, acts as a scaffold for biochemical activities, provides a selective permeable barrier, transports solutes, responds to external signals and plays a significant role in intercellular signalling and energy transduction. The lipid bilayer is a selectively permeable barrier or interface that also regulates the exchange between the outer and inner cellular environments and is the “solvent” for supporting fragile membrane proteins important in signalling. Therefore the plasma membrane is a vital component of all organisms as it encloses every cell and regulates molecular transfer between the cell and the extracellular environment and marks the cell as being unique to the particular organism i.e. specialised features of the plasma membrane that allow communication between neighbouring cells to aid in the coordination of the activities of tissues and organs (Mader 2001).

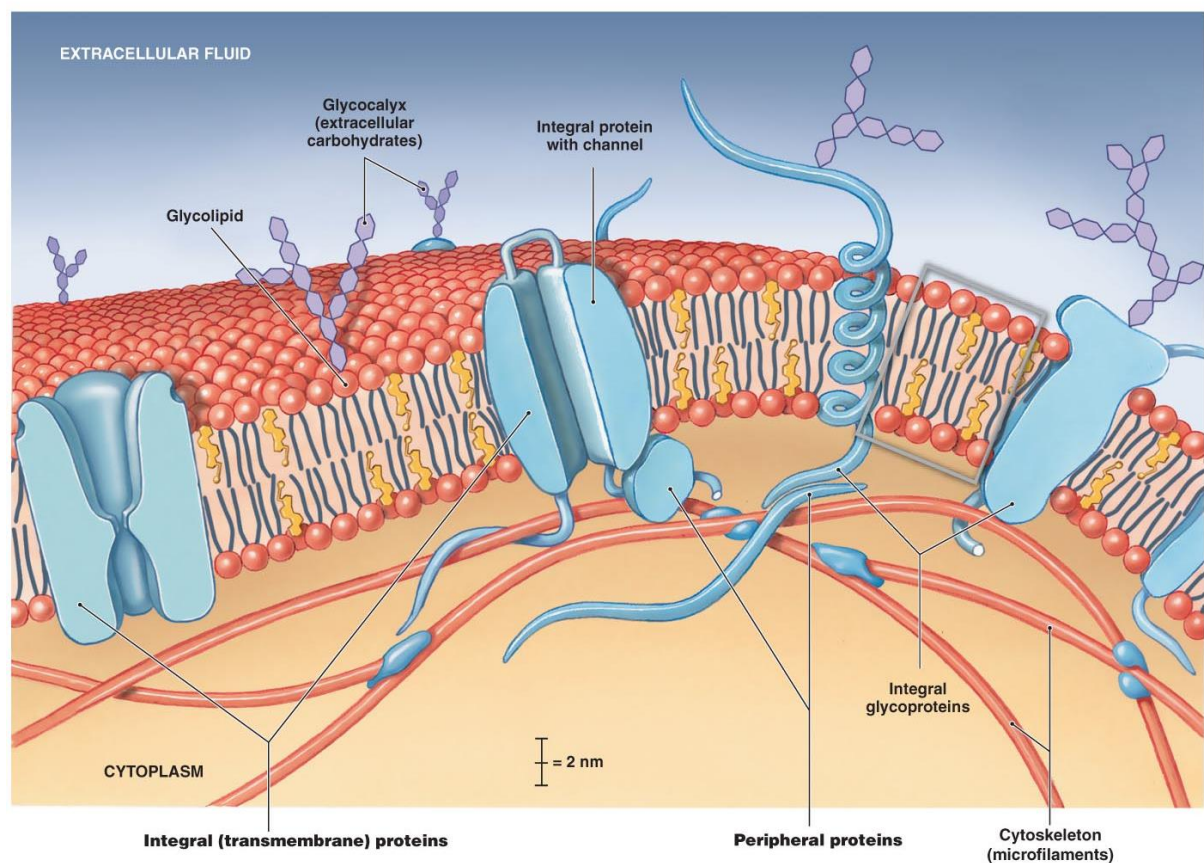


Figure 1.1: Structure of the plasma membrane (Reece, 2011).

The study of the lipid bilayer membrane and its physical properties is recognised as having a beginning in the 20th century but surprisingly many insights originated in

observations from the prehistoric era (Stillwell, 2013). The understanding of interfaces began in 55 A.D. whereby cooking oils were employed to still water surfaces, which was again observed by Benjamin Franklin in 1775, when a teaspoon of oil was dropped in the Derwent Water lake, wherein the oil spread covering half an acre in a thin film (Tanford 1989, Franklin, Brownrigg and Farish 1774, Wang et al. 2013). Again this experiment was repeated by Lord Rayleigh in 1889, with the exception that the molecular size of triolein, the major component of olive oil, was calculated to be 16 Å (Rayleigh 1889). Additional oil on water experiments conducted by Agnes Pockles and Irwing Langmuir, led to the development of the Langmuir-Blodgett trough (Pockles 1891, Langmuir 1917). Osmotic studies were conducted by William Hewson in 1773 in which he concluded the presence of a cell (plasma) membrane (Kleinzeller 1996), which was then visualised by C.H. Schultz in 1836 by staining the outer membrane surface with iodine and estimating the membrane thickness to be approximately 220 Å, just above today's recognised value of 50 – 100 Å. Wilhelm Pfeffer concluded that the cell barrier must be a thin and semi-permeable structure in 1877 which led to Overton in 1899 concluding that membranes must include a lipid-like barrier and hypothesised the presence of cholesterol and phosphatidylcholine (Kleinzeller 1997, Kleinzeller 1999, Stillwell 2013). Evert Gorter in 1925 provided experimental proof that membranes were in fact lipid bilayers (Gorter and Grendel 1925, Zwaal et al. 1976). These discoveries, pioneered over 250 years ago, were the foundations of our current understanding of the biological membrane structure and function; knowledge has advanced rapidly since. However, there are still many aspects of the biological membrane and its components that we have yet to fully comprehend.

The biological membrane functions in compartmentalization; separating the interior of the cell from its external environment, and is so called the 'thread of life', however, the many aspects of complex membrane structure and function remain unresolved (Stillwell 2013). These dynamic membranes consist of two major components, lipids and proteins which form a barrier only a few nanometres thick.

1.0.1 Membrane Lipids

Lipids fulfil three functions in the cell, membrane formation, intracellular signalling and primarily energy storage, mainly as triacylglycerol and steryl esters. The lipids involved in the structural formation of the cell membrane are polar lipids, encompassing a hydrophobic and a hydrophilic portion. These polar lipids self-assemble into a stable

structure, the bilayer, due to the hydrophobic interactions of the lipids. The physical basis of this spontaneous membrane formation is due to the tendency of the hydrophobic moieties to self-associate, driven by water entropically, and the propensity of the hydrophilic moieties to interact with aqueous environments and with each other (Van Meer, Voelker and Feigenson 2008). Aside from the barrier function of the lipids, they additionally allow certain proteins within the membrane to aggregate and others to disperse; finally, they play a role in signal transduction and molecular recognition processes by acting as first and second messengers (Van Meer, Voelker and Feigenson 2008).

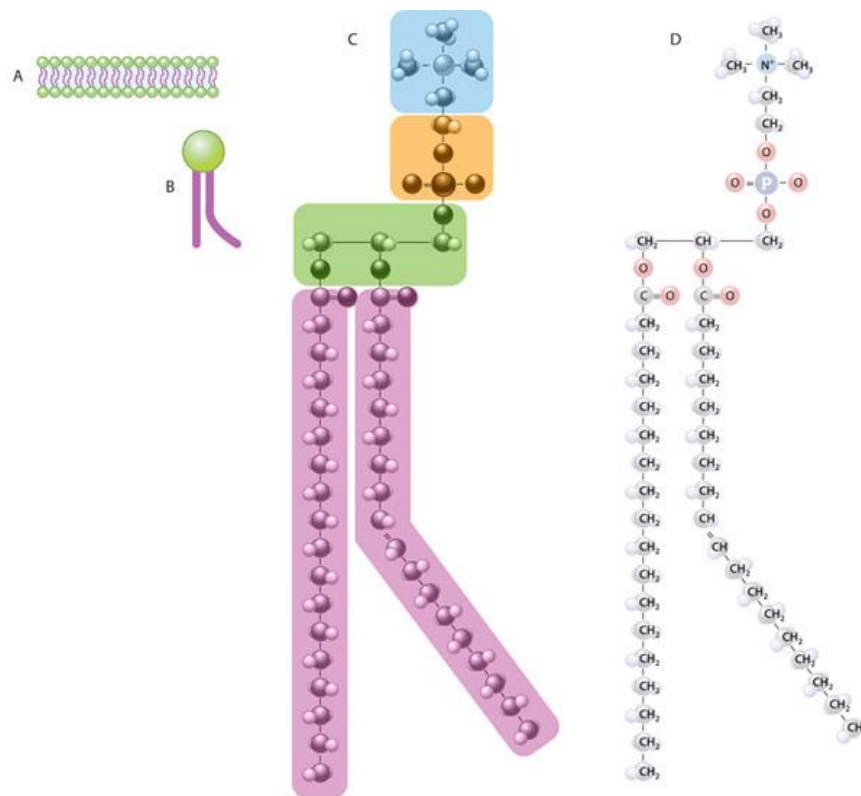


Figure 1.2: Structure and composition of the major structural lipid, glycerophospholipids. (A) The cell is enclosed by a plasma membrane, a bilayer of lipids, primarily glycerophospholipids. (B) There are two major regions of a single glycerophospholipid molecule: a hydrophilic head (green) and hydrocarbon tails (purple). (C) As an example of the subregions of a single glycerophospholipid, phosphatidylcholine is employed. The composition of the hydrophilic head is a choline

structure (blue) and a phosphate (orange). This head is bonded to a glycerol (green) with two hydrophobic tails (purple) called fatty acids. (D) This illustration shows the specific atoms within the various subregions of the phosphatidylcholine molecule where the kink can be identified as been related to a double bond between two carbon atoms (O'Connor, Adams and Fairman 2014).

Glycerophospholipids are the major structural lipids of the cell membrane whose structure is illustrated in Figure 1.2. Glycerophospholipids are molecules composed of a glycerol, a phosphate group and two fatty carbon chains (O'Connor, Adams and Fairman 2014). Various groups are attached to the phosphate group and this allows for lipid variation in the glycerophospholipid family, including phosphatidylcholine (PtdCho), phosphatidylethanolamine (PtdEtn), phosphatidylserine (PtdSer), phosphatidylinositol (PtdIns) and phosphatidic acid (PA). The primary component of glycerophospholipids is a diacylglycerol (DAG), containing various lengths of saturated or cis-unsaturated fatty acyl chains which makes up the hydrophobic portion. The DAG chain in this family of lipids carries a phosphatidic acid which is then esterified to a choline, ethanolamine, serine or inositol forming the various members of this family, with phosphatidylcholine accounting for > 50% of the phospholipids in most cell membranes, specifically eukaryotes (Van Meer, Voelker and Feigenson 2008). Another class of structural lipids found within the biological membrane are sphingolipids, which differ from phospholipids as the hydrophobic backbone constitutes of ceramide in place of phosphate. Sphingomyelin (SM) and the glycosphingolipids (GSLs) are the major sphingolipids of mammalian cells, with gangliosides falling under the umbrella of GSLs. Glycolipids have a similar structure to phospholipids with the exception that in glycolipids, the head group is a variety of sugars joined to form a carbohydrate chain either straight or branching, which function in protection and other various roles that will be discussed later (Mader 2001, Schnaar, Suzuki and Stanley 2009). Sphingolipids differ from phospholipids structurally as their tails are saturated allowing for cylinders that are taller and narrower than PtdCho lipids of identical length and thus they pack more tightly. Sphingolipids are also fluidized by sterols, which are the major non-polar lipids of biological membranes with cholesterol predominating in mammalian cell membranes and ergosterol as the most prevalent in yeast cell membranes. The chemical structures of membrane lipids are shown in Figure 1.3.

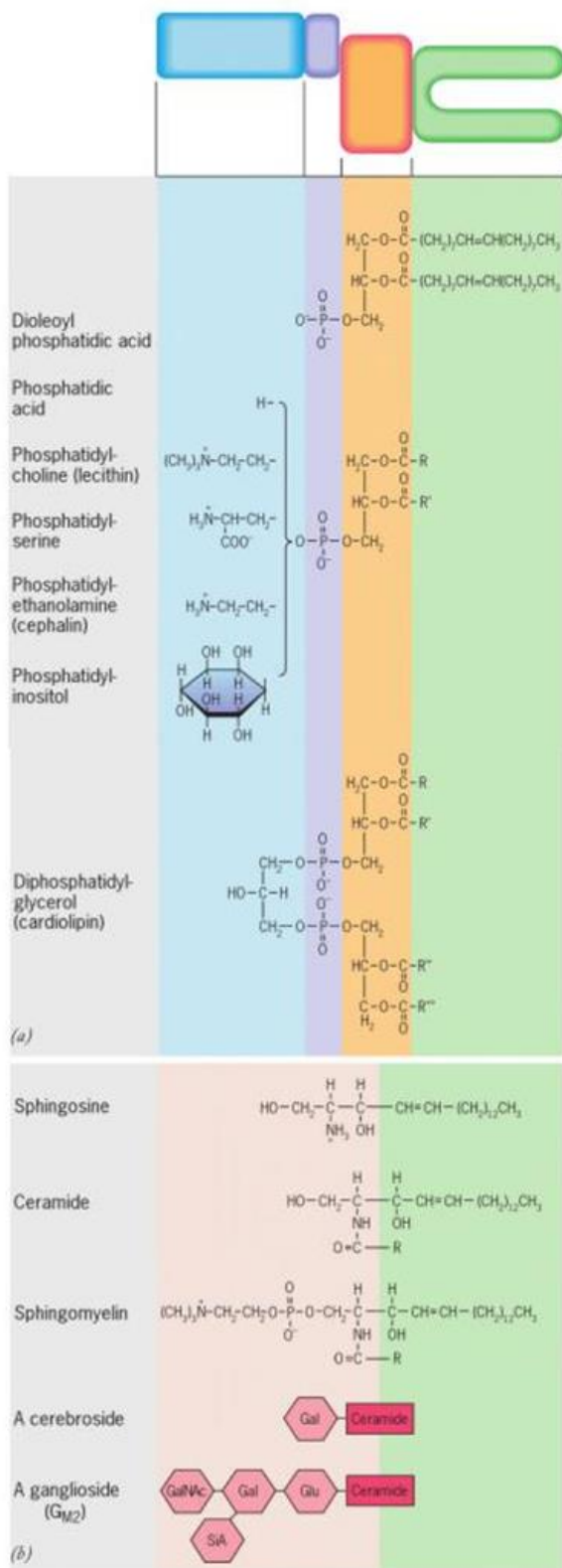


Figure 1.3: Membrane lipids and their chemical structure. (a) Phosphoglycerides are illustrated here where the hydrophobic region is in the green portion. (b) The structures of sphingolipids, the phospholipid sphingomyelin and the glycolipids cerebroside and gangliosides (Karp 2009).

Huang and Feigenson (1999) conducted numerous experiments into the presence of cholesterol in cell membranes and concluded their experiments with an umbrella model, stating that the preferential mixing of sterols with sphingolipids arises due to the shielding of the nonpolar component of cholesterol from water exposure, attributable to the phospholipid headgroups providing 'cover'. Therefore phospholipid headgroups act like umbrellas and the space under the polar headgroups is shared by acyl chains of the phospholipid and cholesterol. These polar phospholipid headgroups then undergo a reorientation as the concentration of cholesterol increases, in order to provide more coverage per headgroup for the increasing cholesterol elements (Huang and Feigenson 1999). Cholesterol presence in the bilayer increases thickness and compressibility of the membrane and also causes the acyl chains to pack together more tightly whilst decreasing the polar lipids rates of translational diffusion (Luckey, 2014).

The amphiphilic nature of lipids enables them to spontaneously assemble to form a fluid bilayer at an aqueous interface additionally, the variation in types of lipid leads to diversity in lipid structures; both factors which define and characterise the biomembrane structure in all organisms. Aside from structure, membrane lipids have many more biological functions in controlling membrane elasticity, governed by non-lamellar lipids, and in cellular communication and intra-cellular trafficking which involves the specialised functions of lipid rafts (Luckey, 2014). Of course, proteins are key contributors to the properties of cell membrane they are beyond the scope of this review.

1.1 Introduction to Model Cell Membranes

Progress in biochemistry, biophysics and structural biology tends to rely on the isolation of purified biological components of interest. However, the purification of membrane components is complex due to the amphiphilic nature of the lipids and their consequent low solubility in water, since they aggregate in aqueous buffer once they are removed from the membrane (Luckey, 2014). An alternative approach is to build model membranes of defined lipid constitution; this allows study of the unit function of lipid or inserted protein in a controlled but biomimetic environment. This section reviews the various approaches applied to modelling lipid bilayers that have been most widely reported in the literature.

1.1.1 Monolayers

Monolayers are films that have a thickness of a single molecule. Although structurally, these films are only representative of a single-leaflet of the lipid bilayer of natural membranes, they have been widely used as model membranes (Czogalla et al., 2014). Lipid monolayers are formed when amphipathic lipid molecules reorganise on an air-water interface with their hydrophobic tails in the air. A Langmuir trough, is usually used to prepare a lipid monolayer, it comprises a container with a moveable barrier which allows control over the monolayer's surface area and pressure. This method is discussed in more detail in Chapter 2. Model monolayer membranes allow lipid composition to be controlled and they have the advantages of homogeneity, stability, planar geometry and controllable lateral packing density of lipids (Czogalla et al., 2014). Monolayers have been used to appraise how lateral pressure, pH, ionic strength and addition of multivalent versus monovalent ions affect the lipids (Luckey, 2014). However, the model is not ideal as leaflet-coupling interactions are not considered and, as it is planar in structure, it does not account for any effects relating to curvature.

Blume and Kerth (2013) used lipid monolayers to assess how peripheral proteins, polypeptides and proteins containing hydrophobic membrane anchors bound to membrane interfaces using infrared reflection-absorbance spectroscopy (IRRAS) and concluded that this approach provides an insight into the conformational properties and orientation of proteins within a lipid environment. They argue that using a monolayer model advances a bilayer model as the structure can be more easily controlled, however

the model presented is not truly biomimetic as it is only presenting proteins interaction with half of an organism's membrane.

1.1.2 Supported Lipid Bilayers

Supported lipid bilayers (SLBs) are a commonly used model of the cell membrane. They comprise two leaflets of lipids forming a bilayer on a hydrophilic planar solid substrate such as fused silica, borosilicate glass, mica or oxidised silicon. The phospholipid SLB is constructed using the absorption and fusion of small or large unilamellar vesicles (SUVs or LUVs respectively) is one of the simplest approaches implemented (Czogalla et al., 2014). However, a major flaw of this model is the necessary rinsing off of excessive vesicles this process can lead to defects in the membrane. Additionally the ionic interactions between the lipid and the support affect the process of membrane deposition and the membrane's physical properties. An alternative approach is to deposit the first monolayer using the Langmuir-Blodgett (LB) technique and transfer the second by dipping the substrate into a Langmuir trough horizontally (Czogalla et al., 2014). Combining both methods is the gentlest approach to constructing a bilayer where the initial leaflet is deposited using the LB and the upper leaflet is formed from liposome fusion. This approach is also superior in that an asymmetric bilayer can be formed.

SLBs have a water phase between the lower leaflet and the substrate which promotes membrane fluidity; this aqueous interface is typically 1 - 2 nm (Czogalla et al., 2014). In spite of this gap there are still frictional interactions of lipids within the bilayer and the underlying substrate in SLBs leading to slower lipid diffusion than at true aqueous interfaces. Additionally large extra-membrous portions of integral proteins that are reconstituted into the SLB are not accommodated for, leading to protein immobilization or denaturation. This can be overcome somewhat by use of a chemical support to which the SLB lipids are tethered or by depositing a spacer such as a polymeric cushion onto the support which decouples lipid or protein from the underlying substrate promoting fluidity. In the former approach ligand-receptor pairs can be used to form a tethered SLB where the membranes composing of biotinylated lipids are tethered to a low-density streptavidin sublayer (Czogalla et al., 2014). The polymer-supported approach usually involves one of two major classes: lipopolymers and polyelectrolytes, such as polyethylenimine. Wagner and Tamm (2000) combined these approaches by developing a tethered polymer SLB on

a cushion of polyethyleneglycol (PEG) on quartz and glass substrates to try and combat the nonphysiological interactions of integral membrane proteins with the solid support. They observed an increase in stability as the membrane which was now covalently linked to the substrate. Protein diffusion increased also when diffusion values of cytochrome b_5 and annexin V were compared when the bilayer was supported on quartz directly and on the polymer-SLBs. However, Wagner and Tamm (2000) did report that 'a significant fraction of these membrane proteins exhibit restricted lateral diffusion' which was concluded to be due to viscous coupling of the polymer support to the proteins.

Czogalla et al. (2014) discussed the value of SLBs in studying a broad range of biophysical phenomena: protein-lipid interactions, lipid-order changes, structural transitions of proteins that are lipid-driven, lateral diffusion of lipids and proteins and also self-assembly of proteins on and within membrane surfaces. Their review discusses the advantages of using SLBs to study these phenomena as a broad variety of biophysical methods can be applied. Vallejo and Gervasi (2002) used electrochemical impedance spectroscopy (EIS) to analyse ion transport through gramicidin channels on an SLB supported on mercapto-carboxylic acid modified gold, with the aim of developing an electrochemical circuit which could represent their data. In their work, they acknowledged the presence of defects within the bilayer using the SLB model and accounted for it in their circuit with an additional resistor, R_{defect} . Their work also had a second limitation in that they are analysing gramicidin on a supported platform which is not allowing the ions to physically pass through the channels, instead they adsorb at the surface and in the channel, a process which is not biologically reflective of an ion channel.

Nascimento et al. (2012) developed an SLB on a gold support modified with mercaptopropyltrimethoxysilane to evaluate the effect of the antimicrobial peptide Magainin I on the lipid membrane using EIS and fitted their data to the Randles equivalent circuit. They showed that the phospholipid-magainin I complex caused a disruption of the bilayer at the electrode surface, but as their bilayer is supported on a mercaptopropyltrimethoxysilane modified planar gold substrate, it is possible that the disruption is due to the magainin I interacting with the model components. This example highlights one of the limits of SLBs as model of the cell membrane.

1.1.3 Black Lipid Membrane

Planar bilayers were historically termed black lipid membranes (BLMs) as when they were fabricated on a Teflon sheet, they appeared black (Luckey, 2014). BLMs are free-standing planar bilayers and pore-suspended membranes that separate two aqueous compartments. They attempt to maintain the stability of SLBs but eliminate the effects caused by the support. BLMs are often used to study electrical properties of membranes as electrodes can be placed at either side of the membrane to investigate ion-channel activity as pure lipid bilayers are not permeable to ions. BLMs are fabricated when lipids are dissolved in an organic solvent and then painted onto an orifice. The final result is a lipid layer stretching across an aperture that is formed when the solvent dissipates and the lipid thins. The painting method is not well controlled and frequently lipid multilayers result. Various membrane components such as peptides, small proteins and other lipids can be added to one of the aqueous compartments and to diffuse into the bilayer (Luckey, 2014). Issues arise when trying to incorporate larger proteins as BLMs have poor stability and often contain residual organic solvents resulting in artefacts that interfere with lipid diffusion and affect protein reconstitution (Czogalla et al., 2014). Winterhalter (2000) discussed a solvent free membrane approach to preparing BLMs where the lipids are spread on top of an aqueous buffer using an organic solvent which was developed by Montal and Mueller. Subsequently the buffer level is lowered below the aperture in the substrate, creating the primary monolayer. The second leaflet is then obtained by raising the buffer level. Advantages in this technique is that asymmetric membranes can be formed, however similar issues arise as previously mentioned, whereby solvent residues can still be present. Incorporation of proteins has also been advanced in BLMs as Schindler designed a further modification by spreading monolayers from lipid vesicles, where proteins can be introduced and are specific to one leaflet (Czogalla et al., 2014).

Zhu et al. (2012) investigated the mechanical properties of solvent-containing BLMs in relation to size dependence of the nanopores using EIS. Their work focused on BLMs fabricated on 200, 400, and 700 nm silicon nitride chip-based nanopores and they concluded that there was increased lifetime and stability on 200 nm diameter nanopores. The impedance data was fitted to an equivalent circuit involving a double layer resistor and capacitor and showed the BLMs lifetime on a 200 nm pore to be at least 144 hours, however, when gramicidin was embedded within the bilayer, the lifetime was decreased

to a single day, thus indicating that increasing the complexity of BLM model reduce their already limited stability.

1.1.4 Liposomes

Liposomes are closed bilayer vesicles that form spontaneously in water during dispersion of phospholipids and prevent any access to the inner aqueous compartment. Liposomes can be a single bilayer, unilamellar or encompass multiple bilayers within each other, multilamellar. Liposomes are characterised by size and lamellarity (number of bilayers that constitute a single vesicle) and are used to study effects of various lipid compositions and membrane protein function, folding and assembly (Luckey, 2014). However, not all lipid compositions spontaneously form vesicles, including those that have a high percentage of cholesterol (> 50%) or charged lipids (Czogalla et al., 2014).

Multilamellar vesicles (MLVs) are not ideal cell membrane models as they can range from diameters of 0.2 – 50 μm incorporating anything up to 20 concentric bilayers, resulting in a structure that prevents molecular binding and surface interaction of the inner bilayers. MLVs can be extensively sonicated or extruded through defined pore size polycarbonate filters to yield 20 – 50 nm SUVs; alternatively SUVs can be formed when the lipids are dissolved in organic solvents and are injected into aqueous media where the organic solution is subsequently removed. Asymmetry is present in SUVs due to the nature of the curvature in their structure as the inner leaflet will always contain less lipid molecules. One issue with SUVs is that polydiverse populations can arise as stable small vesicles will not be affected by the extrusion approach which can potentially impact experimental results. LUVs encompass diameters ranging from 100 nm – 5 μm and can be yielded from freeze-thawing SUVs or forcing them through specific pore sized polycarbonate filters under nitrogen pressure and extruding this repeatedly. However, similar to SUVs there is a disadvantage in heterogeneous size distributions and they are fragile due to their large structure (Luckey, 2014).

Integrity of liposomes can be preserved when they are immobilised, for instance by using oligonucleotides covalently coupled to cholesterol on solid supports of microcavities or sensors (Czogalla et al., 2014). Bhuvana et al. (2013) immobilised 2-dioleoyl-sn-glycero-3-phosphoethanolamine (DOPE) liposome-gold nanoparticles onto a gold surface using

3-mercaptopropionic acid and assessed using EIS for DNA sensing. DNA sensing using this liposome-gold nanoparticle composite tethered to a gold electrode showed a low detection of 0.1 fM, however the impedance data was conducted in PBS buffer (pH 7.4) in the presence of 1 mM $[\text{Fe}(\text{CN})_6]^{3-/4-}$ and not fitted to a circuit. Additionally the layer on the electrode was only stable for four repeated measurements which prevented EIS analysis over long periods.

1.1.5 Giant unilamellar vesicles

The primary advantage of giant unilamellar vesicles (GUVs) as membrane models is their geometry, as they encompass diameters ranging from 5 – 300 μm , which are equivalent to the size of cells (Luckey, 2014). Their large size allows microelectrode insertion and surface section visualisation using optical microscopy. Their elastic compressibility can be investigated by micropipette manipulation (Czogalla et al., 2014). GUVs allow for unconstrained diffusion within the bilayer as there is no supporting surface which can hinder fluidity and movement, however their size can also be their disadvantage due to the large internal volume which leads to fragility when proteins are introduced. One method of GUV formation is by slowly hydrating a dry lipid film. Sufficient yield and quality of vesicles is achieved by the addition of charged/ionic phospholipids as these are necessary in providing electrostatic repulsion between bilayers (Czogalla et al., 2014).

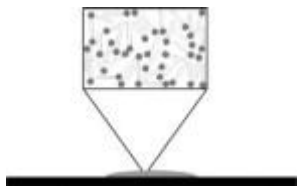
Currently, a more widely adopted approach is GUV formation by vesicle electroformation which is a faster, more reproducible and higher yielding method than the aforementioned methods. Lipid molecules in an ionic strength solution are deposited on electrodes, for example indium tin oxide (ITO)-covered microscopic slides or platinum wires, where an AC current is applied. This current exerts an ordering effect on the lipids, aiding their bilayer-packing and arrangement into unilamellar structures (Czogalla et al., 2014). GUV preparation at high ionic strengths, comparable to physiological salt concentrations, requires a low content (10 – 20 %) of charged phospholipids and millimolar concentrations of Mg^{2+} or Ca^{2+} . Temperature and electrode-catalysed oxidation and decomposition of lipids need to be considered as factors that affect vesicle quality.

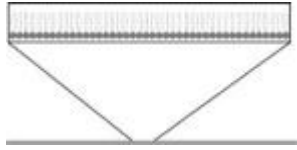
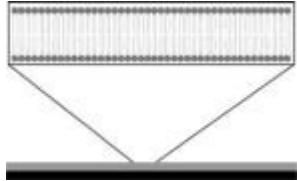
Czogalla et al. (2014) discussed issues concerning GUVs and highlighted the limited control of membrane lipid composition of individual vesicles, for instance selective binding of proteins to vesicles in one population may lead to phenomena that is observed

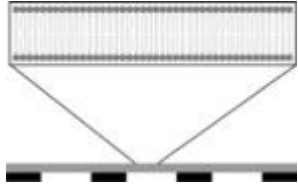
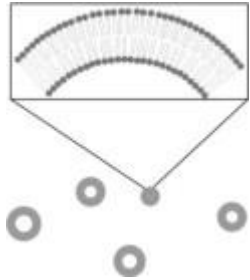
but only in a fraction of the total vesicle population, which on average may not exhibit these distinctive effects. EIS analysis is also a technique that is not applied to assess GUVs, implied by the lack of literature in this area. This gap is probably due to the instability of the large vesicles which makes it difficult to tether it to an electrode.

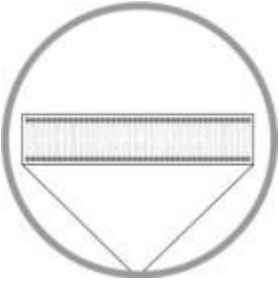
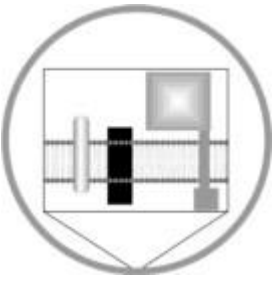
Table 1.1 presents many of the approaches that have been used to act as models of the cell membrane and the major advantages and disadvantages they involve. Most of these models do not represent the lipid bilayer as a barrier between two solutions, which is its function in biological organisms. Those that do successfully mimic the bilayer between two aqueous environments usually involve a system where both aqueous solutions cannot be differentiated and characterised (liposomes) or the bilayer is unstable and fragile (BLMs). This review will discuss the development and fabrication approaches of gold substrates incorporating cavities and their potential application as models of the cell membrane.

Table: 1.1 Overview of the most commonly used membrane model systems (Adapted from Czogalla et al., 2014)

Experimental approach	Controllable parameters	Major advantages	Major disadvantages
Protein–lipid overlay 	lipid composition	fast and easy to perform relative high throughput	lipid presentation in non-physiological context difficult to quantitate variable deposition efficiency susceptibility to removal during the incubation and wash cycles

<p>Monolayers</p> 	<p>lipid composition</p> <p>tunable lateral pressure</p>	<p>defined geometry of lipid assembly (flat membrane)</p> <p>homogeneity of the system</p> <p>accessibility to fluorescence (confocal) microscopy, FCS, Brewster angle microscopy, AFM (after transfer to support)</p>	<p>single leaflet presentation</p> <p>requirement for relatively large amount of protein.</p> <p>restricted to planar lipid monolayers</p>
<p>Supported lipid bilayers</p> 	<p>lipid composition</p> <p>incorporation of integral proteins/compounds</p> <p>membrane curvature/patterning</p>	<p>flat geometry</p> <p>asymmetric lipid distribution is amenable</p> <p>accessibility to broad range of biophysical methods (e.g. AFM, TIRF, SPR)</p> <p>accessibility of both leaflets (polymer-cushioned systems)</p>	<p>interactions with support may result in restricted fluidity of lipids and segregation between the leaflets (partially overcome in polymer-cushioned systems)</p> <p>possible defects within a bilayer</p>

<p>Pore-suspending membranes</p> 	<p>lipid composition</p> <p>incorporation of integral proteins/compounds</p>	<p>flat geometry</p> <p>asymmetric lipid distribution is amenable</p> <p>suitable for broad range of biophysical methods (particularly for conductance measurements, fluorescence microscopy)</p> <p>accessibility of both leaflets</p>	<p>reduced stability comparing to SLB</p> <p>presence of residual organic solvents (primarily in BLMs)</p>
<p>Liposomes</p> 	<p>lipid composition</p> <p>membrane curvature/lipid packing (vesicle size-dependent)</p> <p>incorporation of integral proteins/compounds</p>	<p>simple preparation procedure</p> <p>free-standing membrane</p> <p>compatibility with multiple methodical approaches</p>	<p>possible polydispersity in terms of size and multilamellarity</p> <p>symmetric lipid distribution</p> <p>size below optical resolution</p> <p>only one leaflet accessible</p>

<p>GUVs</p> 	<p>lipid composition</p> <p>membrane tension</p> <p>membrane deformation can be induced (deflation, tubulation)</p> <p>incorporation of integral proteins/compounds</p>	<p>micrometer-scale structure</p> <p>free-standing membranes</p> <p>microscopically accessible</p> <p>compatibility with multiple methodical approaches</p>	<p>heterogeneity in lipid composition at the individual specimen level</p> <p>increased fragility compared to SUVs and LUV</p>
<p>GPMVs</p> 	<p>protein content by overexpression</p>	<p>relatively high population homogeneity</p> <p>micrometer-scale structure</p> <p>free-standing membranes</p> <p>complex lipid and protein composition</p> <p>microscopically accessible</p>	<p>undefined lipid and protein composition</p> <p>chemically induced crosslinking of lipids and proteins</p> <p>possible depletion of specific lipid classes</p>

1.3 Introduction of Microcavity arrays

Microcavity arrays are cavities or hollows on a self-assembled monolayer substrate that can be used as an alternative support for lipid membrane. The size and density of the microcavities can be controlled on the surface. The surface chemistry or materials of these microcavities can be altered to optimise the stability of the lipid bilayer.

1.3.1 Fabrication of cavity arrays

Cavities at the micro and nano scale have been developed for sensing applications, photonics and surface-enhanced spectroscopy by a number of approaches. This research aims instead to utilise microcavity arrays to build lipid bilayers that span across the cavity, providing a deep aqueous interface on both sides of the bilayer. Porous alumina templates, electron beam lithography, nanosphere lithography and nanoimprint lithography are several methods used to build nanostructured arrays (Murphy *et al.*, 2013). Murphy *et al.*, (2013) produced gold coaxial rod-tube nanocavities using porous alumina oxide fixed to a glass substrate as a template with gold nanorods being electrodeposited into the pores. Following this, a shell was etched around these rods of gold using NaOH where deposition of the polymer could take place, before further pore widening using NaOH again with a second deposition of gold (Figure 1.4). The diameter and height of the rods can be controlled by etching and electrodepositing time where rod diameters of 20 nm, 25 nm and 50 nm were fabricated.

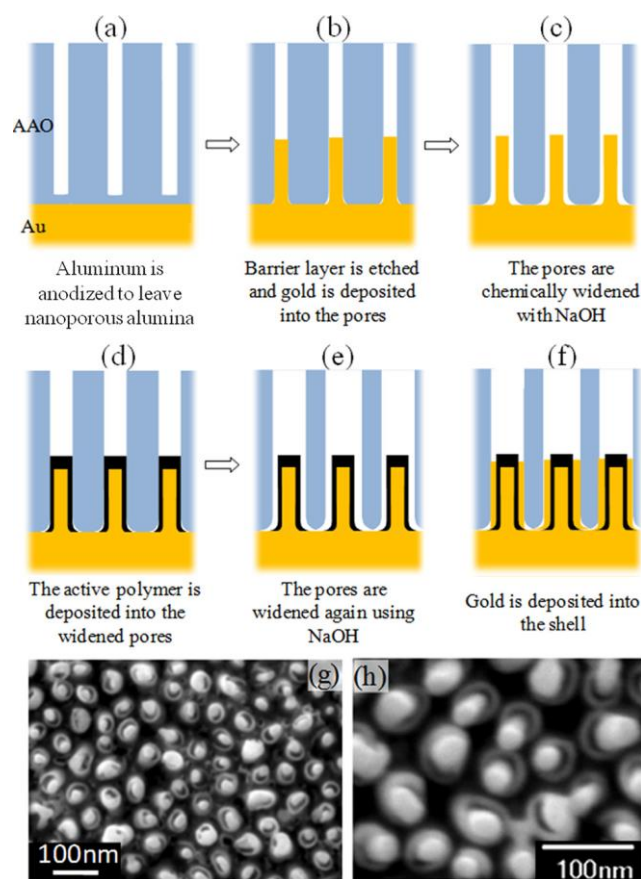


Figure 1.4: Fabrication of gold nanocavities using porous alumina (Adapted from Murphy *et al.*, 2013).

Bartlett *et al* (2004) also employed the electrodeposition of gold approach to fabricate cavities on templates of lyotropic liquid crystalline phases with diameters of 2 – 10 nm and colloidal crystalline templates (20 – 1000 nm) and illustrated how these arrays of nanoscale pores altered the material’s physical properties in optics, magnetism and conductance, providing applications in sensors alongside storage and conversion of energy, electroanalysis and catalysis.

Gold substrates are preferred for cavity arrays because of its value as an electrode material, ideal to study electrical properties of various compositions of bilayers and the effect of interacting molecules, and also enhances plasmonic spectroscopic signals, if such studies are required (Jose *et al.*, 2011). These can be used as sensors, for instance Jose *et al.* (2011) developed lipid bilayers where gold nanocavities were prefilled with buffer causing a lipid membrane to form on the top of the array allowing aqueous environments on both sides of a suspended membrane, instead of in a dry cavity where the membrane is localized within it. This research can lead to the production of uniform

lipid bilayers where drug-cell and protein incorporation interactions can be studied by naturally mimicking these molecular interactions. The advantage of the plasmonic behaviour of nanocavity arrays is the control over the nanoscale features such as size, aperture and thickness and the possibility of solution filling aiding sensor development (Jose *et al.*, 2009). Nanocavity arrays can use this phenomenon of plasmonic behaviour to detect the luminescence of weakly emitting species particularly as the pores can be filled with analyte whose luminescence can be enhanced. This was demonstrated by Jose *et al.* (2009) where the emission intensity of $[\text{Ru}(2,2'\text{-bipyridyl})_2(2,2':4,4'':4,4''\text{-quarterpyridyl})]^{2+}$ and fullerene (C_{60}) increased by an order of magnitude in nanocavities (820 nm in diameter) compared with the emission intensity of the bulk solution using conventional confocal fluorescence microscopy; when SAMs of this molecule formed on the array the Raman signal was enhanced by seven orders of magnitude. The advantages of this enhanced signal intensity are increased sensitivity in analytical applications particularly using gold as it is chemically and structurally stable and high quality arrays are produced (Lordan *et al.*, 2012).

Liu *et al.*, (2004) developed a biosensing technique using nanocavities with a diameter of 200 nm and average spacings of 1 μm where the fluorescence signal, produced due to binding of immobilized oligonucleotides in the nanocavity with complementary target oligonucleotides in solution, was monitored. Target molecules that have bound within the cavity will produce enhanced fluorescence while target molecules that are unbound and lie outside the nanocavity will not efficiently transmit their fluorescent emission through the structure, demonstrating real-time affinity biosensing.

1.3.2 Interfacial Self-Assembly

The chemical composition and physical structure of a solid surface is difficult to control and reproduce, and bilayer instability is an issue in many cell membrane models, however this can be overcome by the use of self-adsorbing monolayers that spontaneously organise themselves on a surface. A self-assembled monolayer (SAM) first appeared in publication in 1946, when Zisman published the fabrication of a surfactant onto a clean metal surface by self-assembled adsorption, igniting the work then carried out by Nuzzo and Allara, who demonstrated SAMs of alkanethiolates onto a gold surface (Ulman, 1996). This self-assembly system of gold and alkanethiolates has undergone the most research, however

aside from this system, silanes on hydroxylated surfaces and fatty acid derivatives have been developed. Supramolecular structures can also be produced using SAMs, particularly using long chain hydrocarbons as building blocks. Gold metal surfaces strongly adsorb disulphides (R-S-S-R), sulphides (R-S-R) and thiols (R-SH) due to the sulphur donor atoms, the monolayer is further stabilised and orientated by Van der Waals forces between the methylene groups (Wink *et al.*, 1997). Hydroxylated surfaces are required for alkylchlorosilanes, alkylalkoxysilanes, and alkylaminosilanes where there is a formation of polysiloxane that is linked to surface silanol groups (-SiOH) through Si-O-Si bonds on substrates such as silicon oxide, aluminium oxide, quartz, mica, zinc selenide, germanium oxide and gold (Ulman, 1996). The structure and defect density of the monolayer is affected by the chosen surface.

Gold is the metal/surface used in this study as it is reasonably inert (Wink *et al.*, 1997). Gold is not oxidised in air, can withstand treatment with harsh chemicals and can be deposited in thin films onto surfaces from ceramics to quartz by a series of methods, such as physical vapour deposition, electrodeposition or sputtering, and are patterned using an amalgamation of lithographic tools. (Forster *et al.*, 2003). After gold, silver is the most studied substrate for alkanethiols however in air it oxidises and is toxic to cells (Love *et al.*, 2005).

Sulphur atoms covalently bind through the sulfhydryl (R-SH) functional group to gold, leading to stabilised nanostructures and simultaneously allowing transmissions of electrons between molecules containing gold and sulphur (Häkkinen, 2012). This RS-Au bond strength is close to that of an Au-Au bond requires deprotonation of the sulfhydryl functional group, thus forming a radical that binds to the gold atoms at the top of the crystal lattice. R-SH can also bind by weaker interactions via the lone pair of electrons on the sulphur atom (Häkkinen, 2012). This gold-sulphur bond has a strength in the area of 100 kJ/mol.

Thiol bound self-assembled monolayers have numerous applications including modelling electron transfer reactions, biomimetic membranes, nanoscale photonic devices, solar energy conversion, catalysis, chemical sensing and nano-scale lithography (Forster *et al.*, 2003). Self-assembly, as shown in Figure 1.5, has become a popular area of research for

those mentioned applications due to its ease of use, variety of shapes and forms, flexibility and low-cost.

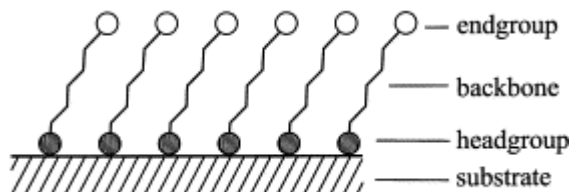


Figure 1.5: Schematic illustration of self-assembled monolayer which can vary in the substrate, headgroup and endgroup (adapted from Schreiber, 2000).

1.3.3 Formation of Self-Assembled Monolayers

The self-assembly of alkanethiols on a gold substrate is a kinetically straight forward and stable process. Conditions such as anaerobic, anhydrous or vacuum are not required contributing to the ease of formation particularly significant for industrial and manufactural processes. Subsequently, a wide range of chemical reactivities and hydrophobicities can be prepared due to the range of functional groups that can be terminated on the thiol (as listed in Figure 1.6), for instance halide, ether, alcohol, aldehyde, carboxylic acid, amide, ester, amine and nitrile and also the specificity of the monolayer can also be altered by addition of heteroatoms, aromatics, conjugated unsaturated links and sulfones and amides that are rigid-rod structures (Forster *et al.*, 2003). In this project, an alcohol functional group on alkanethiols is used to improve hydrophilicity of the gold substrate to aid stability and orientation of the lipid molecules during bilayer formation. Thermodynamic stability also increases with longer chain lengths.

Ulman (1996), discussed the kinetics of the adsorption of the thiol to the gold substrate, observing two distinct steps, initially fast (taking minutes) where the contact angles are close to their limiting values and a final slow step (hours) where final values of contact angles and thickness are achieved. This is noted at relatively dilute solutions (10^{-3} M) where the initial fast step is in relation to the surface-head group reaction i.e. thiol to the gold substrate, and the slower final step is associated with the components and mobility of the chains and how they interact with each other via Van der Waals forces etc. The

surfaces can be analysed for spectroscopic and physical characterisation by numerous techniques such as reflectance absorption infrared spectroscopy (RAIRS), Raman spectroscopy, X-ray photoelectron spectroscopy (XPS), high-resolution electron energy loss spectroscopy (HREELS), near-edge X-ray absorption fine structure spectroscopy (NEXAFS), helium atom scattering, x-ray diffraction, contact angle goniometry, optical ellipsometry, surface plasmon resonance (SPR) spectroscopy, mass spectrometry and scanning probe microscopy (SPM) (Love *et al.*, 2005).

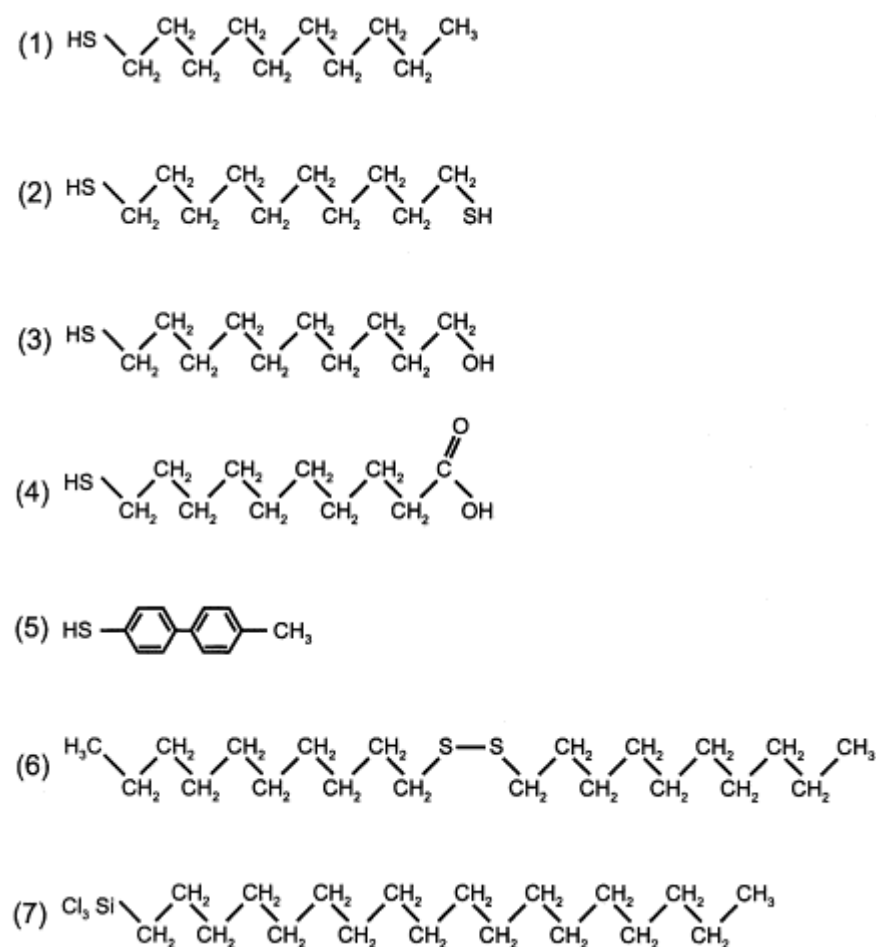


Figure 1.6: Compounds that are commonly used in SAMs with variations in headgroup, chain length, chain structure and end group (adapted from Schreiber, 2000).

Numerous factors aside from solvent, temperature and potentials affect the rate of formation and the structure of SAMs. These include concentration and structure of the adsorbant (which affects surface coverage), oxygen concentration (which can oxidise the adsorbant thiols to sulfonates) and substrate cleanliness (affects kinetics of formation).

These factors can also cause defects. At maximum coverage, the typical surface density is $\approx 4.5 \times 10^{14}$ molecules cm^{-2} due to longer immersion times resulting in greater coverage.

After the bond between the gold substrate and the sulphur from the alkane thiol, the alkyl chain tilts at an angle from the headgroup relative to the surface normal. This angle is determined by the headgroups and their packing density on the substrate and the optimization of the interactions between chains, i.e. Van der Waal forces and is shown in Figure 1.7(a). Aside from these intermolecular forces, the degrees of freedom of the molecular backbone alter their conformational shape (Schreiber, 2000). The orientation of the molecules is governed by the tilt angle, α , of the linear backbone relative to the surface normal which can be a positive or negative value and the angle of rotation, β , about the long axis of the molecule which can range from $0^\circ - 90^\circ$ (Love *et al.*, 2005). The terminal group's alignment is an odd or even effect which can depend on the number of methylenes in the chain that separate it from the headgroup, as shown in Figure 1.7(b). Alkanethiols on gold have the tilt angle, α , at an absolute value close to 30° and an average angle of rotation, β , at approximately 50° . These values vary depending on the surface used and the packing density of the headgroups of the alkyl chains, Figure 1.7(c). The average spacing between alkane thiols in the transformation on the hexagonal gold lattice surface is 5.0 \AA .

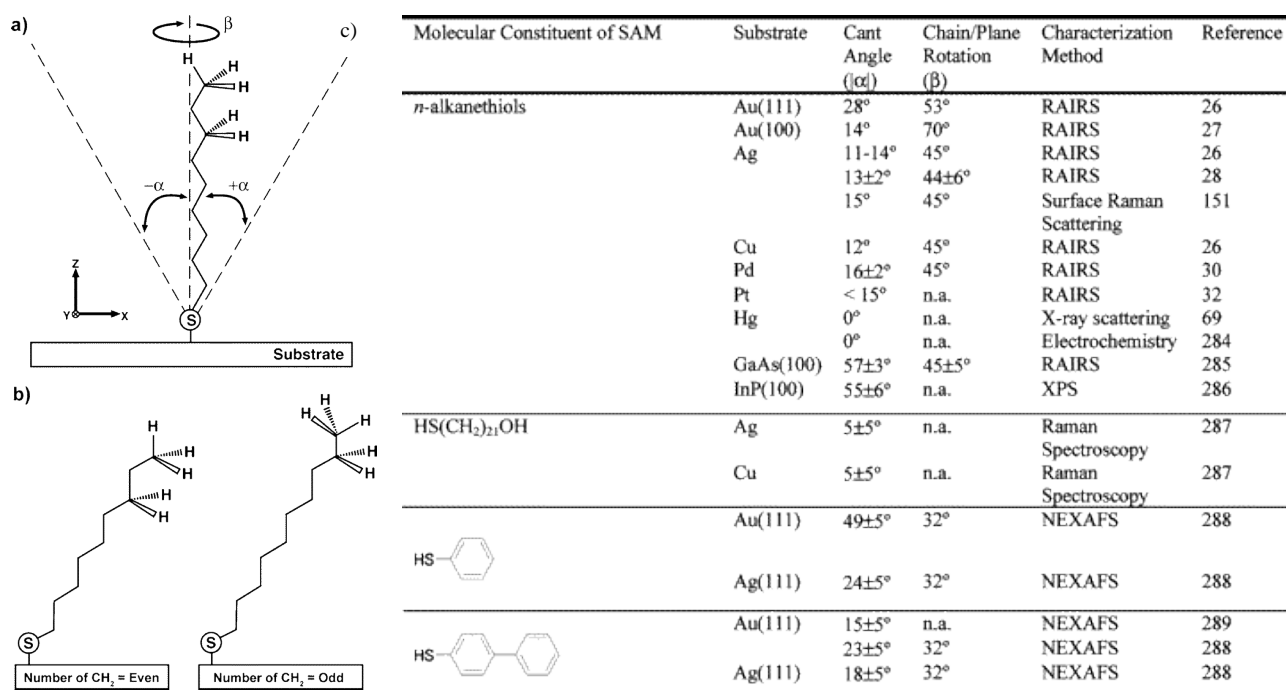


Figure 1.7: a) This schematic illustrates the tilt angle, α , relative to the surface normal and the angle of rotation, β , or twist angle of the molecule relative to α and the surface normal. b) This illustrates how the backbone alters the conformational shape of the molecule and α and β . c) This table contains information on how α and β for alkanethiols can change depending on the substrate used. This variation on angles is due to the packing densities of these surfaces. (Adapted from Love *et al.*, 2005)

1.3.4 Electrochemical Characterisation of Monolayers

As mentioned previously, defects can occur in the monolayer due to external and intrinsic factors such as substrate cleanliness, substrate preparation, solution purity and adsorbate purity. These pinhole defects (molecular vacancies) in the monolayers can be analysed by spectroscopic and microscopic methods such as scanning tunnelling microscopy (STM) which provides topographic information and the non-invasive optical technique, ellipsometry, which determines numerous features of the surface such as refraction index, extinction coefficient, thickness of the film, roughness of the interface and multilayer and thin surface layer composition (Forster *et al.*, 2003). Numerous defects can present themselves on the monolayer that can affect the reactivity of the electrode surface. In the

case of alkanethiols on an Au (111) surface, these include missing rows (specifically evident in short alkanethiols), vacant Au islands, absence or disorder of the adsorbing molecules and domains or boundaries where there is enhanced disorder (Vericat *et al.*, 2005). Vericat *et al.* (2005) discussed how these defects can result from inadequate annealing procedures, partial extension of hydrocarbon chains leading to a change in the tilt angle or possible desorption of Au resulting in pit formation. These defects expose the substrate as the imperfect structure leads to direct access of electrons to the electrode surface instead of electron tunnelling across the monolayer, therefore efficient electron transfer occurs as mass transport of the electrons to the electrode is facilitated.

Subsequently, voltammetry can be used to detect these defects as it is sensitive enough to detect nanoamp and picoamp current levels that correspond to redox reactions (Forster *et al.*, 2003). Cyclic voltammograms can indicate the defect density of a SAM due to the current ratio of bare and modified electrodes, as large currents correspond to surfaces that are not coated with a monolayer due to a strong electron transfer rate to the electrode from the electrolyte probe and a decreased current is indicative to a SAM presence on the surface as it blocks redox reactions. Cyclic voltammograms characteristic for pinholes illustrate a sharp rise in the Faradaic current (Forster *et al.*, 2003).

Porter *et al.* (1987) used electrochemical measurements of heterogeneous electron transfer to examine the nature and extent of structural defects using a $\text{Fe}(\text{CN})_6^{3-}$ probe as it is an electrochemically reversible, one-electron redox couple. Their work also investigated differential capacitance which indicates the ion permeability between the electrode and the monolayer and provides an additional measurement of film thickness. Capacitance increases when the distance or separation between the electrode surface and ionic species decreases and subsequently decreases when there is a film blocking the electrode from the ions, therefore determining the pinhole defects on the surface.

Another characteristic of SAMs that can be determined by electrochemistry is surface coverage of the electrode. Stability of the monolayer varies at different potentials resulting in reductive or oxidative desorption if the potential is too negative or too positive (Sun *et al.*, 2011). Walczak *et al.* (1991) used voltammetric measurements to determine the surface coverage of three different monolayers film by reductive desorption where the charge for the one-electron reductive desorption of the Au-S bond was

measured voltammetrically in an alkaline solution: $\text{Au-SR} + \text{e}^- \rightarrow \text{Au}^{(0)} + \text{SR}^-$. The monolayers experimented were dodecanethiol and two ferrocene-terminated thiols that varied in chain length where the thiol was displaced by applying a potential. This charge, Q (measured in coulombs, C), was recorded which is proportional to the surface coverage and subsequently determined using the following equation, $\Gamma = Q/nFA$, where Γ is the monolayer surface coverage (mol cm^{-1}), n is the number of electrons involved in the transfer, F is Faradays constant (C mol^{-1}) and A is the electroactive surface area (cm^2) (Ding *et al.*, 2005).

1.4 Conclusions

Models of the cell membrane have been researched and developed for many years; however each approach has several key drawbacks. This review discussed the composition of cell membranes in relation to their phospholipids, as well as various developments that are present in the literature as models of the cell membrane. Current approaches to date have been conducted using monolayers, SLBs, BLMs, liposomes and GUVs. However, the use of gold microcavities, particularly surfaces modified with SAMs, is an enticing area of research as such substrates allow bilayers to span and be assessed for their electrical properties, enabling understanding of how various classes of molecules interact with the cell membrane. The potential of these models is based on the ability to suspend a lipid bilayer across buffer filled cavities to selectively study electrical properties of the membrane. This chemically constructed platform can aid research into the areas of drug permeability in the cell membrane and also provides a unique insight into glycobiology, both of which will be discussed in Chapter 3 and 4 respectively.

1.5 References

- Bartlett, P.N., 2004. Electrodeposition of Nanostructured Films Using Self-Organizing Templates. *Interface-Electrochemical Society*, 13, pp.28-33
- Bhuvana, M. Narayanan, J.S., Dharuman, V., Teng, W., Hahn, J.H. and Jayakumar, K. 2013. Gold surface supported spherical liposome – gold nano-particle nano-composite for label free DNA sensing. *Biosensors and Bioelectronics*, 41, pp.802-808.
- Blume, A. and Kerth, A. 2013. Peptide and protein binding to lipid monolayers studies by FT-IRRA spectroscopy. *Biochimica et Biophysica Acta (BBA) – Biomembranes*, 1828(10) pp.2294-2305.
- Czogalla, A., Grzybek, M., Jones, W. and Coskan, U. 2014. Validity and applicability of membrane model systems for studying interactions of peripheral membrane proteins with lipids. *Biochimica et Biophysica Acta (BBA) – Molecular and Cell Biology of Lipids*, 1841(8), pp.1049-1059.
- Ding, S.J., Chang, B.W., Wu, C.C., Lai, M.F. and Chang, H.C. 2005. Impedance spectral studies of self-assembly of alkanethiols with different chain lengths using different immobilization strategies on Au electrodes. *Analytica Chimica Acta*, 554, pp. 43–51.
- Forster R.J., Keyes T.E. and Vos J.G. 2003. *Interfacial supramolecular assemblies*, England: John Wiley & Sons, Ltd.
- Franklin, B., Brownrigg, W. and Farish, M. 1774. Of the stilling of waves by means of oil. Extracted from Sundry Letters between Benjamin Franklin, LL. D.F.R.S. William Brownrigg, M.D.F.R.S. and the Reverend Mr. Farish. *Philosophical Transactions*, 64, pp.445-460.
- Gorter, E. and Grendel, F. 1925. On bimolecular layers of lipoids on the chromocytes of the blood. *The Journal of Experimental Medicine*, 41(4), pp.439-443.
- Häkkinen, H. (2012). The gold-sulfur interface at the nanoscale. *Nature Chemistry*, 4, pp. 443–455.

Huang, J. and Feigenson, G.W. 1999. A microscopic interaction model of maximum solubility of cholesterol in lipid bilayers. *Biophysical Journal*, 76(4), pp.2142-2157.

Jose, B., Mallon, C., Forster, R.J. and Keyes, T.E. 2011. Lipid bilayer assembly at a gold nanocavity arrays. *Chemical Communications*, 47, 12530-12532.

Karp, G. 2009. *Cell and Molecular Biology: Concepts and Experiments*. 6th Ed ed. John Wiley & Sons.

Kleinzeller, A. 1999. Charles ernest overton's concept of a cell membrane. *Current Topics in Membranes*, 48pp.1-22.

Kleinzeller, A. 1997. Ernest overton's contribution to the cell membrane concept: A centennial appreciation. *Physiology*, 12(1), pp.49-53.

Kleinzeller, A. 1996. William hewson's studies of red blood corpuscles and the evolving concept of a cell membrane. *The American Journal of Physiology*, 271(1 Pt 1), pp.C1-8.

Langmuir, I. 1917. The constitution and fundamental properties of solids and liquids. II. liquids. 1. *Journal of the American Chemical Society*, 39(9), pp.1848-1906.

Liu, Y., Bishop, J., Williams, L., Blair, S., and Herron, J. 2004. Biosensing based upon molecular confinement in metallic nanocavity arrays. *Nanotechnology*, 15, pp. 1368–1374.

Lordan, F., Rice, J.H., Jose, B., Forster, R.J. and Keyes, T.E. 2012. Effect of Cavity Architecture on the Surface-Enhanced Emission from Site-Selective Nanostructured Cavity Arrays. *Journal of Physical Chemistry C*, 16, pp. 1784-1788.

Love J. C., Estroff L.A., Kriebel J.K., Nuzzo R.G. and Whitesides G.M. 2005. Self-assembled monolayers of thiolates on metals as a form of nanotechnology. *Chemical Reviews*, 105, pp. 1103-1169.

Luckey, M. (2014). *Membrane Structural Biology: With Biochemical and Biophysical Foundations*. Cambridge University Press.

Mader, S.S. 2001. *Biology*. 7th ed. New York: McGraw-Hill.

Murphy, A., Sonnefraud, Y., Krasavin, A.V., Ginzburg, P., Morgan, F., McPhillips, J., Wurtz, G., Maier, S.A., Zayats, A.V. and Pollard, R., 2013. Fabrication and optical properties of large-scale arrays of gold nanocavities based on rod-in-a-tube coaxials. *Applied Physics Letters*, 102, pp. 103103.

Nascimento, J. Franco, O.L., Oliveira, M.D.L. and Andrade, A.S. 2012. Evaluation of Magainin I interactions with lipid membranes: An optical and electrochemical study. *Chemistry and Physics of Lipids*, 165, pp.537-544.

O'Connor, C., Adams, J.U. and Fairman, J.E. 2014. *Essentials of Cell Biology*. Nature Education.

Pockles, A. 1891. Surface tension. *Nature*, 43pp.437-439.

Porter, M.D., Bright, T.B., Allara, D.L. and Chidsey, C.E.D. 1987. Spontaneously Organized molecular assemblies 4. Structural Characterization of n-alkyl thiol monolayers on gold by optical ellipsometry, infrared spectroscopy and electrochemistry. *Journal of the American Chemical Society*, 109, pp. 3559-3568.

Rayleigh, L. 1889. Measurements of the amount of oil necessary in order to check the motions of camphor upon water. *Proceedings of the Royal Society of London*, 47(286-291), pp.364-367.

Reece, J.B. 2011. *Campbell Biology*. Benjamin Cummings/Pearson

Schnaar, R.L., Suzuki, A. and Stanley, P. 2009. Chapter 10 Glycosphingolipids *IN: Varki, A., Cummings, R.D., Esko, J. and et al. (eds.) Essentials of Glycobiology. 2nd edition.*

Schreiber, F. 2000 Structure and growth of self-assembling monolayers. *Progress in Surface Science*, 65, pp. 151–257.

Stillwell, W. 2013. *An Introduction to Biological Membranes: From Bilayers to Rafts*. Newnes.

Sun, K., Jiang, B. and Jiang, X. 2011. Electrochemical desorption of self-assembled monolayers and its applications in surface chemistry and cell biology. *Journal of Electroanalytical Chemistry*, 656, pp. 223–230.

Tanford, C. 1989. *Ben Franklin Stilled the Waves*. Durham and London: Duke University Press.

Ulman A. (1996). Formation and structure of self-assembled monolayers. *Chem Rev*, 96, pp. 1533-1554.

Vallejo, A.E. and Gervasi, C.A 2002. Impedance analysis of ion transport through gramicidin channels in supported lipid bilayers. *Bioelectrochemistry*, 57, pp.1-7.

Van Meer, G., Voelker, D.R. and Feigenson, G.W. 2008. Membrane lipids: Where they are and how they behave. *Nature Reviews Molecular Cell Biology*, 9(2), pp.112-124.

Vericat, C., Vela, M.E., and Salvarezza, R.C. 2005. Self-assembled monolayers of alkanethiols on Au(111): surface structures, defects and dynamics. *Physical Chemistry Chemical Physics*, 7, pp. 3258 – 3268

Wagner, M.L. and Tamm, L.K. 2000. Tethered Polymer-Supported Planar Lipid Bilayers for Reconstitution of Integral Membrane Proteins: Silane-Polyethyleneglycol-Lipid as a Cushion and Covalent Linker. *Biophysical Journal*, 79, pp.1400–1414.

Wang, D., Stieglitz, H., Marden, J. and Tamm, L.K. 2013. Benjamin franklin, philadelphia's favorite son, was a membrane biophysicist. *Biophysical Journal*, 104(2), pp.287-291.

Walczak, M.M., Popenoe, D.D., Deinhammer, R.S., Lamp, B.D., Chung, C., and Porter, M.D. 1991. Reductive Desorption of Alkanethiolate Monolayers at Gold: A Measure of Surface Coverage. *Langmuir*, 7, pp. 2687-2693.

Wink T., Van Zuilen S.J., Bult A. and van Bennekom W.P. 1997. Self-assembled monolayers for biosensors. *Analyst*, 122, pp. 43-50.

Winterhalter, M. 2000. Current Opinion in Colloid & Interface Science. *Black Lipid Membranes*, 5, pp.250-255.

Zhu, Z.W.Z., Wang, Y., Zhang, X., Sun, C.F., Li, M.G., Yan, J.W. and Mao, B.W. 2012. Electrochemical Impedance Spectroscopy and Atomic Force Microscopic Studies of

Electrical and Mechanical Properties of Nano-Black Lipid Membranes and Size Dependence. *Langmuir*, 28, pp.14739-14746.

Zwaal, R., Demel, R., Roelofsen, B. and Van Deenen, L. 1976. The lipid bilayer concept of cell membranes. *Trends in Biochemical Sciences*, 1(2), pp.112-114.

Chapter 2: Experimental Methods and Instrumentation

2.0 Instrumentation

2.0.1 Scanning Electron Microscope (SEM)

Scanning electron microscopy (SEM) is a technique that images and analyses specimens using a focussed beam of high-energy electrons, Figure 2.1, illustrates the operation of an SEM microscope. The beam of electrons is generated by thermionic emission from an electron gun (cathode) and is accelerated by a voltage difference between the cathode and the anode that can be set between low and high values; 0.1 keV and 50 keV. This beam follows a vertical straight path through the instrument within a vacuum environment. It traverses through lenses which are subsequently focused coarsely and finely onto the sample area to obtain a well-defined image. This image is formed from the secondary electrons and backscattered electrons which relay information relating to the surface topography, morphology and composition in high resolution images. The SEM has numerous advantages as a characterisation technique as it is easy to operate, requires minimal sample preparation, acquires data rapidly and can image samples in the nanometre size range. However If the sample is electrically insulating, a sputter coater is used to coat the sample in a conducting metal. Another key limitation is that ‘wet’ samples cannot be analysed as they are likely to outgas at low pressures, which is an issue for biological and organic samples. There are a number of ways this can be addressed.

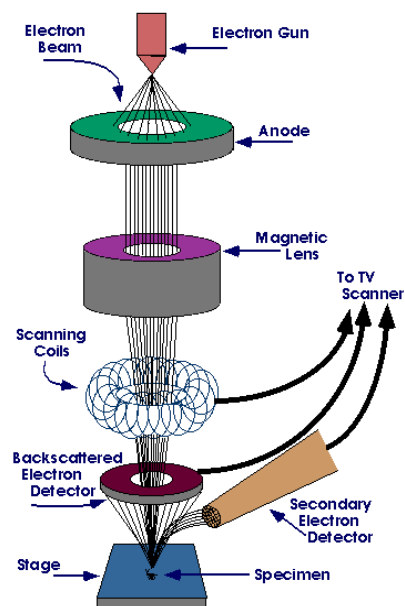


Figure 2.1: Schematic representation of a scanning electron microscope (Obtained from Purdue University, 2014).

2.0.2 Cyclic Voltammetry

Cyclic Voltammetry (CV) is an electrochemical technique that is used for elucidating electrode mechanisms by measuring the current that develops in an electrochemical cell. It operates by scanning the potential linearly of a working electrode where the resulting peaks are a result of the diffusion at the electrode-electrolyte interface from an electrochemical reaction, therefore it provides thermodynamic information of redox properties, kinetics of electron transfer and adsorption processes. In terms of the theoretical voltammetric response, diffusion and adsorption can be predicted as a function of scan rate. In a reversible scan cycle, a difference between the two peak potentials mainly results from the effects of analyte diffusion rates whereas adsorption processes can result in a symmetrical voltammogram which can be further investigated by exploring the effect of scan rate. The potentiostat can similarly be used for electrochemical deposition, which is achieved by placing a negative charge on the object to be coated and immersing it in a solution containing the metallic ions (positively charged). Gold electrodeposition and CVs were measured on a CH instrument model 660 electrochemical workstation potentiostat.

2.0.3 Water Contact Angle

The water contact angle measurement is a technique employed in materials science to measure the hydrophilicity of an interface. When a drop of liquid is placed on a solid surface the triple interface formed between the solid (substrate), liquid (water) and gas (air) will move until an equilibrium is established, which is a response to the forces arising from the three interfacial tensions (Gentle and Barnes 2005). This scenario is illustrated below in Figure 2.2 which demonstrates the change in shape of a single drop of liquid on a planar, solid surface with the third gaseous interface constituting of air.

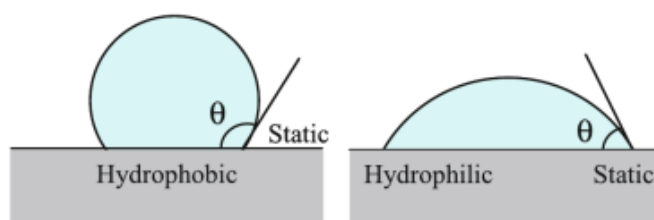


Figure 2.2: Illustration of a liquid drop placed on a solid substrate and its response at equilibrium due to the interface tensions arising from the solid, liquid and gas (Dongqing 2008).

The contact angle refers to the angle, θ , which is located at the interface between the solid surface and the tangent to the liquid surface at the exact point of contact (Gentle and Barnes 2005). The magnitude of the water contact angle is controlled by cohesive and adhesive forces. Cohesive forces describe the balance of forces within the liquid droplet that arise between the molecules whereas adhesive forces are those between the surface and liquid molecules. For instance, a surface that comprises of primarily polar groups, such as hydroxyl groups (-OH), is hydrophilic and will have strong adhesive forces with the liquid water molecule, leading to a low contact angle typically of between 10 - 80°. Conversely, if the primary interface is hydrophobic, there is a low affinity for water, resulting in a large contact angle, typically in the range of 80 – 120°. Water contact angle measurement is an insightful technique which gives rapid and quantitative insight into a surface's chemical nature as shown in Figure 2.3, where three substrates of varying contact angles are presented.

Instruments which provide this measurement operate by depositing a single drop of liquid on a surface which is then viewed by a magnifying lens. A digital image is subsequently taken, where the drop can be measured optically and the contact angle can be determined using software (Gentle and Barnes 2005).

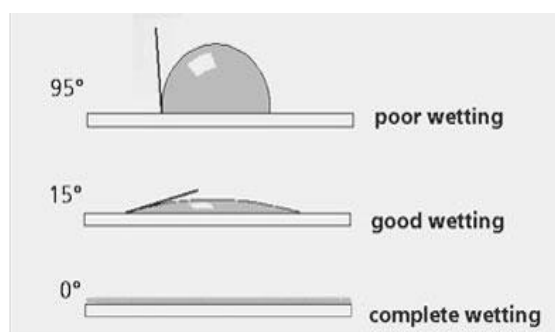


Figure 2.3: Three different water contact angles are illustrated showing the shape variation of the water droplet on three different surfaces.

The water contact measurements were conducted throughout this thesis using a contact angle analyser FTA 200.

2.0.4 Langmuir-Blodgett

The Langmuir-Blodgett (LB) technique is used for the fabrication of molecular monolayer films. Amphiphilic molecules are used to create these films as they assemble at the interfaces between a gas and a liquid or a liquid and a liquid when deposited on an aqueous sub-phase in a trough, by spreading rapidly to cover the area. As the solvent with which the amphiphile molecule was dissolved in evaporates, a monolayer forms at the interface between the air and water, creating a Langmuir film, which can be further compressed by the software-controlled barriers in the trough top, which is a hydrophobic material that improves containment of the sub-phase i.e. the water (Biolin Scientific, 2014). A film is organised under compression in a typical surface pressure-area isotherm measurement starting from a two dimensional gas phase moving through a liquid phase to a fully organised solid phase as shown in Figure 2.4 (Biolin Scientific, 2014). Information regarding the packing density of the monolayer is provided by the surface pressure sensor, which is usually a Wil-helmy plate. In the first phase, the gaseous phase, the molecules are not strongly interacting with each other as they are spaced apart. As the barriers close, the surface area decreases, causing the molecules to interact more as they become more packed (the liquid phase). As the surface area continues to decrease, the molecules enter the solid phase where they are organised completely and the surface pressure increases.

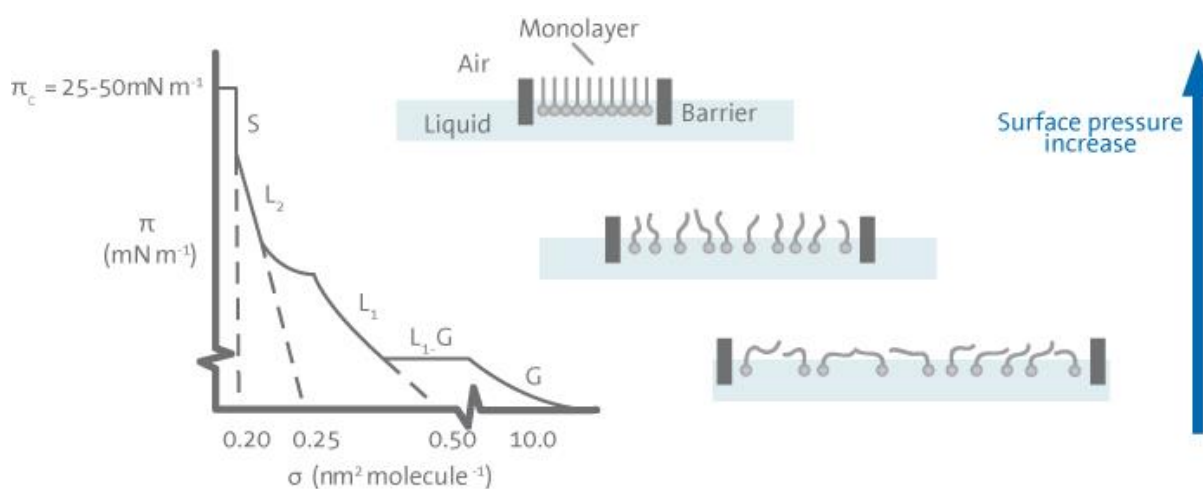


Figure 2.4: This diagram illustrates the three phases of the monolayer: gas (G); liquid (L); and solid (S). The three phases are depicted in a surface area-pressure isotherm demonstrating the formation of the film, i.e. as surface area decreases, pressure increases, resulting in an organised, stable arrangement of the molecules (Biolin Scientific, 2014).

The transfer of the monolayer to a solid substrate is carried out when the surface pressure is at a certain point, usually greater than 10 mN/m and less than 40 mN/m, that ensures sufficient cohesion in the monolayer i.e. that the forces of attraction between the molecules within the monolayer is sufficient enough that the monolayer is prevented from falling apart during transfer (Biolin Scientific, 2014). Figure 2.5 illustrates the two approaches of monolayer transfer to a solid substrate, which is catered for by the well in the centre of the trough which provides space for the dipping mechanism to place the solid substrate through the monolayer and into the liquid phase in a controlled fashion. A Langmuir-Blodgett film is the term applied when this Langmuir film is transferred vertically onto a solid surface. Langmuir-Schaefer films are those that are transferred horizontally. LB deposition troughs can be utilised to transfer this monolayer thick film onto various substrates to create films of monolayers or multilayers with precise control of film thickness, molecular orientation and packing density.

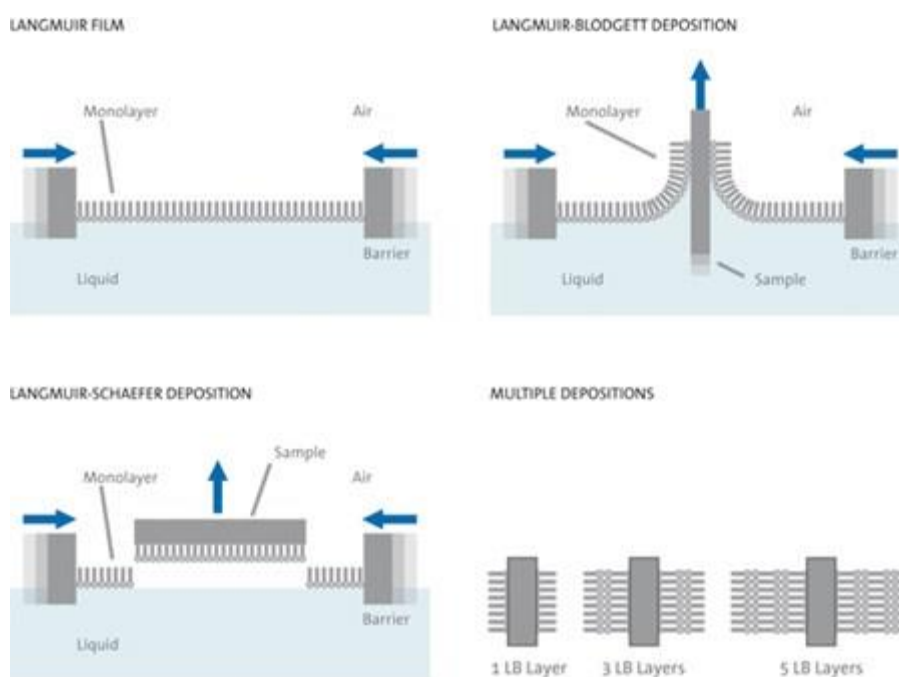


Figure 2.5: Schematic depicting various methodologies to create and transfer Langmuir films onto solid substrates via Langmuir-Blodgett (LB) and Langmuir-Schaefer (Biolin Scientific, 2014).

The solid substrate's affinity for water dictates the method with which to transfer the LB film and also decrees the orientation of the monolayer. When a solid substrate is hydrophilic, as is the case in our model, the first layer is deposited by raising the solid substrate from the sub-phase through the monolayer, resulting in a monolayer with the polar moieties bound to the solid substrate and the non-polar moieties in the gas phase. The type of LB film produced is also varied by several parameters: the nature of the spread of the film; the sub-phase composition and temperature; the surface pressure and the dipper speed during the deposition; the type and nature of the solid substrate; and the time the solid substrate is stored in air or in the sub-phase between the deposition cycles (Biolin Scientific, 2014).

DOPC monolayer was prepared and transferred to the gold cavity array using a NIMA model 102M Langmuir Blodgett trough.

2.1 Materials and Methods

2.1.1 Materials

Silicon wafers coated with 1000 Å gold (Au) 525 µm thickness over a 50 Å titanium adhesion layer were purchased from Amsbio, UK. A polystyrene microsphere solution, containing microspheres of diameter 2.88 ± 0.28 µm at a concentration of 13.8 w/v %, was supplied by Bang Laboratories Inc., USA. The gold salt solution used in the fabrication of the microcavity arrays, is a commercial gold plating solution, purchased from Technic Inc, Sodium Gold Sulfite Solution, Cranston, RI, USA. 1,2-Dioleoyl-sn-glycero-3-phosphocholine (DOPC, > 99%) was supplied by Avanti Polar Lipids, Alabaster, USA. Tetrahydrofuran (THF, 99%.), 2-merceptoethanol ($\geq 99\%$), chloroform ($\geq 99.5\%$), ethanol ($\geq 99.5\%$), phosphate buffer saline (PBS, pH 7.4) were all purchased from Sigma Aldrich, Ireland.

2.1.2 Methods

Figure 2.6 illustrates the steps required to build the MSLBs, from deposition of gold around the templating spheres through the deposition of the bilayer.

2.1.2.1 Fabrication of Gold Cavity Arrays

Gold cavity arrays are the substrates with which the lipid bilayers were suspended across. All methods involved in the fabrication of the arrays were conducted at room temperature, 20 °C. In the following EIS measurements, it was this substrate that acted as the working electrode. Silicon wafers, were purchased from Amsbio, UK, that were coated with a 525 µm thickness with 1000 Å gold (Au) over a titanium adhesion layer, were cut to create a 1 cm² final working electrode surface area, using a diamond pen..

The electrodes were washed thoroughly with deionised water and acetone. Polystyrene (PS) latex spheres with an average diameter of 2.88 ± 0.28 µm in 13.8 wt % stock

solutions, obtained from Bangs Laboratories, USA, were diluted to approximately 1 % solution in deionised water. 150 μL of the 1 % sphere solution was deposited on the gold plated silicon wafers and evaporated over night at room temperature, to form a monolayer of spheres of uniform coverage.

Gold electrodeposition and EIS were measured on a CH instrument model 660 electrochemical workstation potentiostat at 20 $^{\circ}\text{C}$. The gold electrochemical deposition process was carried out in a standard electrochemical cell containing three electrodes: the Ag/AgCl (sat. KCl) was the reference electrode; the gold wafer with PS spheres was the working electrode; and a platinum mesh was the counter electrode.

Prior to gold deposition, the gold salt solution (Technic Inc. USA) was covered with parafilm and degassed with nitrogen for 30 mins. A potential of -0.95 V versus an Ag/AgCl (sat. KCl) electrode was then applied. The Ag/AgCl (Sat KCl) reference electrode was placed in a salt bridge to prevent chloride ion contamination. A series of trial and error experiments were carried out to identify the best conditions for deposition of the gold to achieve a smooth substrate.

It has been found that the conditions required to produce the desired deposition depth (i.e. to 70% above equator of the spheres) had to be re-established for each new batch, but can then be reliably applied across all experiments using that single batch of deposition solution. For all of the arrays produced for this thesis, all employed the same batch of deposition solution and a potential of -0.95 V was found to produce optimal deposition of a smooth layer of gold onto the wafer. The amount of charge (C) passed in the electrochemical deposition step was used to control the thickness of the cavities, in this case gold was deposited electrically up to 0.7 C to form cavities that are 70 % above the equator of the spheres.

Once deposition has been completed up to the optimised charge value, the gold array was allowed to dry for a few minutes before being washed with deionised water to remove any salts from the surface. $2.88 \pm 0.28 \mu\text{m}$ PS spheres and subsequent gold deposition fabricated cavities of $2.80 \pm 0.04 \mu\text{m}$ gold arrays, characterized by SEM. See Figure 2.6 for schematic.

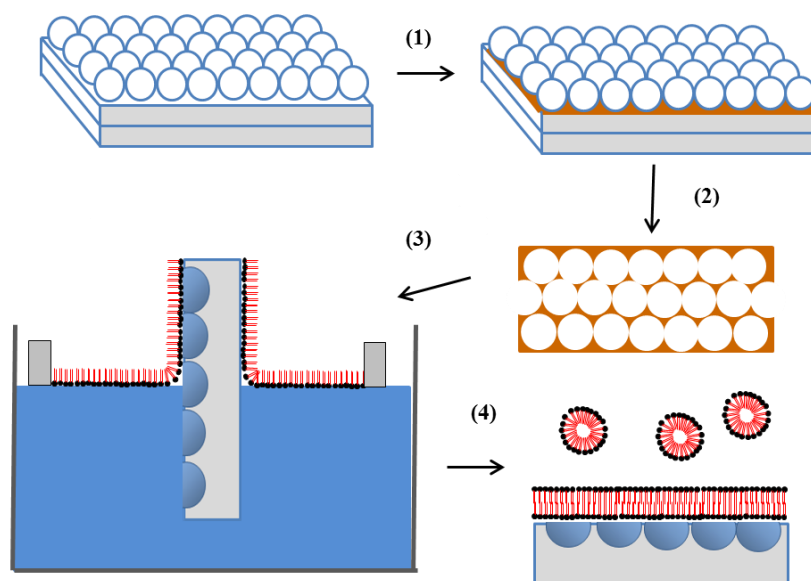


Figure 2.6: Schematic showing steps involved in fabrication of the microcavity array supported lipid bilayers and protein insertion. (1) The arrays are prepared from polystyrene sphere (PS) templating through electrodeposition of gold onto gold coated silicon wafer. (2) A mercapto-ethanol layer is assembled prior to elimination of the PS template, i.e. only the top surface is modified. (3) The cavities are buffer filled and then a phospholipid monolayer is deposited at the cavity surface using Langmuir Blodgett deposition. (4) The second layer, representing the external cytoplasmic layer is deposited by vesicle fusion. Pore diameters of $2.80 \pm 0.04 \mu\text{m}$ have been demonstrated, as these have been shown to be really robust. Once formed the lipid bilayer assembled across such an aqueous filled pore persists with unmodified fluidity for up to a week.

2.2.1.2 Surface Modification of the Gold Cavity Arrays

Selective SAM assembly at the top surface of the cavities was carried out before the templating spheres were removed from the gold array. Leaving the PS spheres in, prevented the modification of the inner cavities, meaning that only the top surface was available for binding. Three different SAMs were employed in this work; 2-mercapto-ethanol, 6-mercapto-1-hexanol and 11-mercapto-1-undecanol. Microcavity substrates were modified with the thiol by immersing the substrate in each case in a $1 \mu\text{M}$ solution of the thiol in ethanol overnight at room temperature. Following this, the substrates were sonicated in THF for 30 mins to remove the polystyrene spheres. Complete removal of

the spheres was confirmed by SEM. It has been previously confirmed that the ethanol deposition solution does not remove the templating spheres (Mallon et al., 2010).

2.2.1.3 Preparation of Lipid Bilayer

DOPC vesicles were prepared by pipetting 20 μL of a 50 mg/mL solution of DOPC in chloroform into a glass vial where the chloroform was evaporated under a stream of nitrogen. This dry lipid film was then placed under vacuum for 30 mins to ensure adequate drying of the DOPC lipids. Following this, the dry lipid film was solvated by addition of 1 mL of 0.01 M phosphate buffer saline (PBS) solution, pH 7.4. To ensure complete detachment of the lipid film from the glass vial, the suspension was vortexed. This solution now containing multilamellar polydisperse vesicles was then extruded repeatedly through a polycarbonate membrane using an extruder from Avanti Polar Lipids, Inc., USA. Unilamellar vesicles of a narrow size distribution were prepared by 11 extrusions of the vesicle solution through a polycarbonate membrane of 0.1 μm in between two filter supports, which improve flow rate and provide extra support to the polycarbonate membrane by eliminating tearing. After extrusion, vesicles were added to 3 mL of 0.01 M PBS buffer, pH 7.4.

Prior to assembly of the first leaflet of the bilayer, the $2.80 \pm 0.04 \mu\text{m}$ gold microcavity arrays, prepared as described above, were sonicated in 0.01 M PBS buffer, pH 7.4 for 30 minutes in order to fill the cavities with solution. In this manner, the bilayer is suspended across aqueous filled pores, providing a biomimetic model of the cell membrane. Langmuir Blodgett (LB) films prepared in chloroform at a concentration of 50 mg/ml were suspended in the LB trough on the water sub-phase. Fifteen minutes were allocated for evaporation of the chloroform, prior to lipid monolayer compression. The rate of compression was $30 \text{ cm}^2/\text{min}$ and a constant surface pressure of 35 mN/m was maintained for the transfer of a DOPC monolayer from the water-air interface to the aqueous filled, gold microcavity arrays. During LB transfer, the rate of the dipper movement was 5 mm min^{-1} to ensure adequate transfer. Following DOPC monolayer deposition, the slides were incubated at room temperature horizontally in a solution of the prepared vesicles to facilitate vesicle disruption at the lipid monolayer and the formation of a DOPC bilayer.

The resulting bilayer modified substrates were then placed in 0.01 M PBS buffer, pH 7.4 until required for analysis.

For electrochemical analysis, a cavity array of dimensions of 1 cm² containing 2.80 ± 0.04 μm diameter spherical pores was used as a working electrode and this was placed in an electrochemical cell containing 20 mL of 0.01 M PBS buffer, pH 7.4

2.2 Results and Discussion

2.2.1 Optimisation of Microcavity Array Gold Deposition Protocol

Careful optimisation of the deposition conditions was carried out to identify the parameters which lead to most the reproducible and defect free $2.80 \pm 0.04 \mu\text{m}$ diameter porous array. This diameter corresponds to a cavity depth of just over the equator of the deposition sphere. This was carried out originally for cavities created using $1.6 \mu\text{m}$ diameter PS spheres and then extended to the $2.88 \mu\text{m}$ PS.

An initial potential of -0.9 V (scan rate 100 mV/s) was used to deposit gold until the following charges were accumulated: 0.2 , 0.4 , 0.6 , 0.8 and 1.0 C respectively. Characterisation of the resulting arrays was then conducted by SEM and the optimum charge was selected using SEM images. Figure 2.7 shows two microcavity arrays, with differing charges of electrodeposition. Figure 2.7 (a) shows cavities where the gold has deposited to the extent that only small apertures are available, resulting in an array that appears to have great separations between each cavity. This was due to over-deposition of the gold. For this sphere size, the optimised charge was 0.2 C . Within this value, further optimisation was conducted; 0.20 , 0.22 , 0.24 , 0.26 , 0.28 and 0.30 C . Figure 2.7 (b) shows the array when a charge of 0.22 C was applied where the resulting arrays have a greater cavity to top surface ratio, the lowest number of defects and are packed. Subsequently the optimised charge was concluded to be 0.22 C .

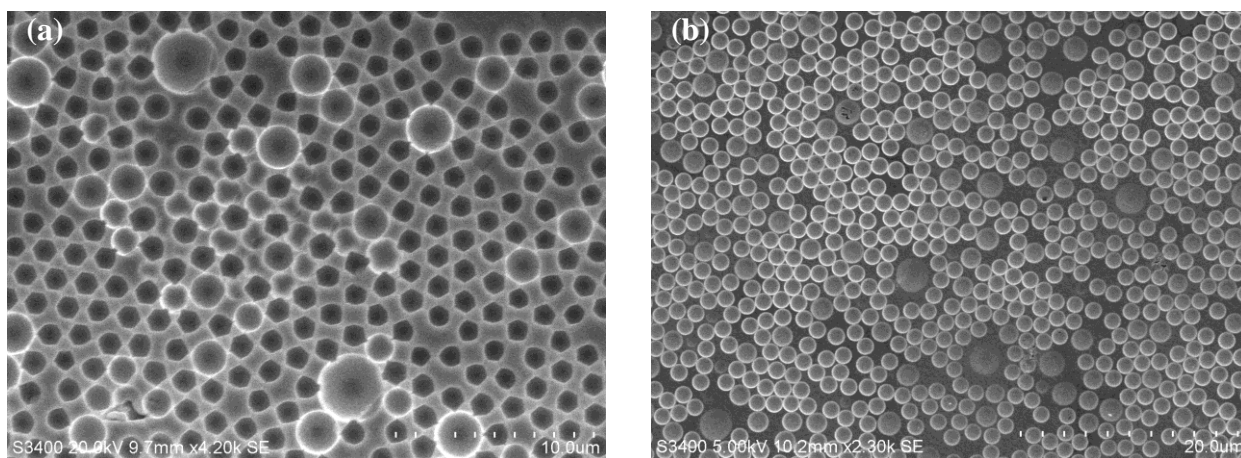


Figure 2.7: Optimisation of the charge used for the deposition of gold to produce $1.6 \mu\text{m}$ cavities (a) -0.9 V , 0.4 C ($\times 4.2\text{k}$ magnification) (b) -0.9 V , 0.22 C ($\times 2.3\text{k}$ magnification). All images were collected using identical conditions at 5.00kV accelerating voltage.

Optimisation of the potential was then examined initially for 1.6 μm cavities; the quantity of charge passed and the applied potential influence the rate of gold deposition and thus the depth to which the gold deposited around the spheres. Figure 2.8 represents two images of substrates prepared at two different voltages; at (a) -1.0 V, where the surface was rough and had a flaky appearance due to the gold depositing at too fast a rate and (b) -0.85 V, where the array had a smoother appearance and the cavities were well defined. The optimised voltage was determined as -0.85 V.

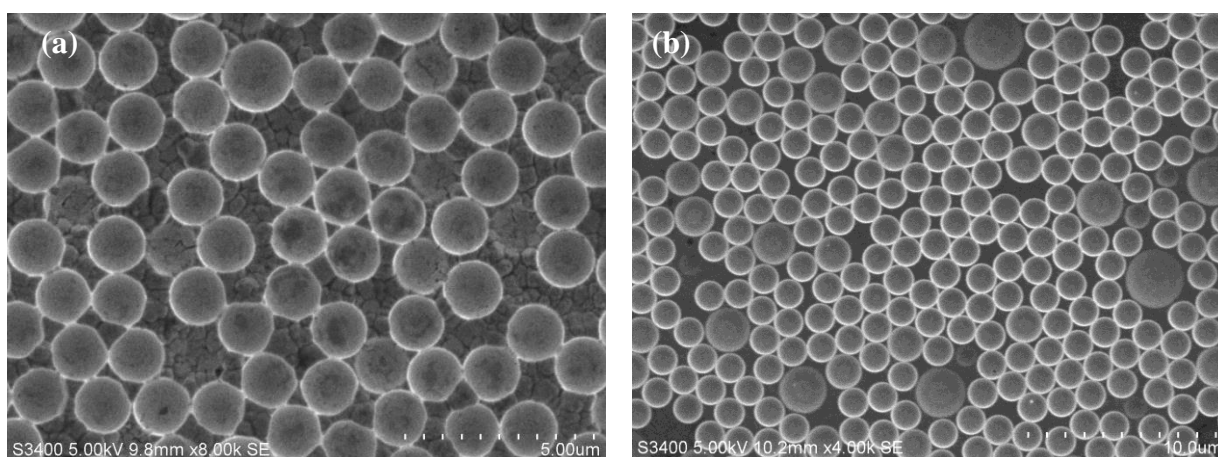


Figure 2.8: Optimisation of the potential used for the deposition of gold to produce 1.6 μm cavities (a) -1.0 V, 0.22 C (x8.00k magnification) (b) -0.85 V, 0.22 C (x4.00k magnification). All images were collected using identical conditions at 5.00kV accelerating voltage.

As can be seen from Figure 2.7 (b), the cavities were not very compact; there was a relatively large amount of planar top surface areas. To optimise the packing of the cavities, the sphere deposition solution was modified: 1 % solution of spheres was prepared in deionised water, 1 % solution of spheres was prepared in deionised water after washing the spheres by centrifugation and 1 % solution of spheres was prepared in 0.1 % SDS. Using 0.1 % SDS, Figure 2.9 (a) showed that the spheres were too compact and clustered as they were overlapping with each other. Figure 2.9 (b) presents the results when the spheres were washed by centrifugation, the spheres were less compact and more dispersed after dropcasting. The optimised sphere solution was found to be a 1 % solution in deionised water, which gave well packed cavity electrodes with relatively low defect density.

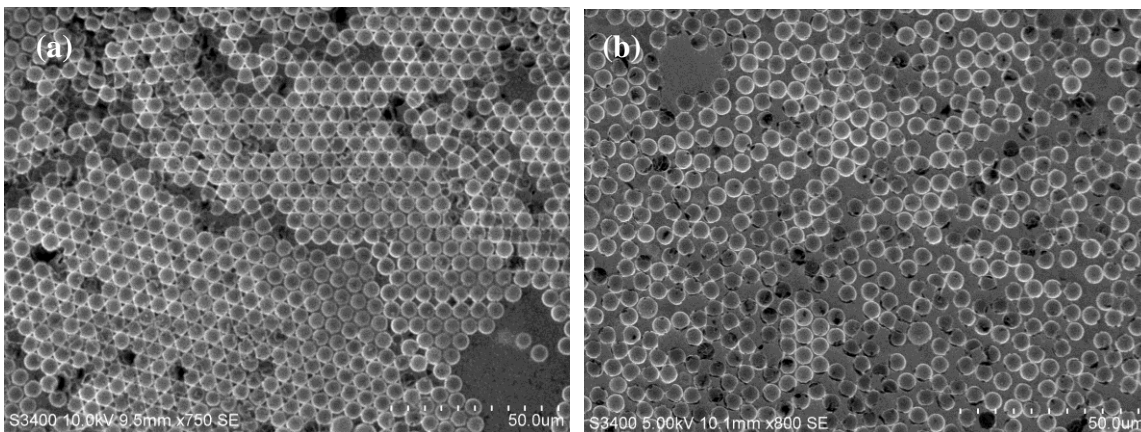


Figure 2.9: Optimisation of the potential used for the deposition of gold to produce 1.6 μm cavities (a) PS spheres prepared in 0.1 % SDS solution, -0.85 V, 0.22 C (x750 magnification) (b) PS spheres washed by centrifugation, -0.85 V, 0.22 C (x800 magnification). All images were collected using identical conditions at 5.00kV accelerating voltage.

Applying the above optimised protocol to the $2.88 \pm 0.28 \mu\text{m}$ PS spheres, it was found that, as shown in Figure 2.10 below, the packing density and defectiveness was far superior and more reproducible for the larger spheres and so this array size was used throughout the rest of the thesis, where the $2.88 \pm 0.28 \mu\text{m}$ spheres were dissolved in a 1 % solution of deionised water and gold was deposited electrically at a - 0.95 V potential and a charge of 0.7 C.

2.2.2 Characterisation of Gold Cavity Arrays

SEM was used to characterise the structure and topology of the fabricated arrays.

$2.80 \pm 0.04 \mu\text{m}$ gold cavity arrays were fabricated by gold electrodeposition as described in section 2.2.3. THF was used to remove the spheres, and in this instance there was a 2-mercaptoetanol modification on the array, the structure of the cavities was assessed by SEM imaging (Figure 2.10). The images show that the deposition method produced compact, well ordered arrays of uniform depth and diameter over a 1 cm^2 area after dissolution of the spheres in THF. The SEM images in Figure 2.10 confirm the diameter of the cavities to be $2.80 \pm 0.04 \mu\text{m}$ (where $2.80 \mu\text{m}$ is the average of 6 measurements and 0.04 is the standard deviation). These images illustrate that the gold electro-deposition technique implemented produced uniform areas of compact, closely packed $2.80 \pm 0.04 \mu\text{m}$ microcavity arrays.

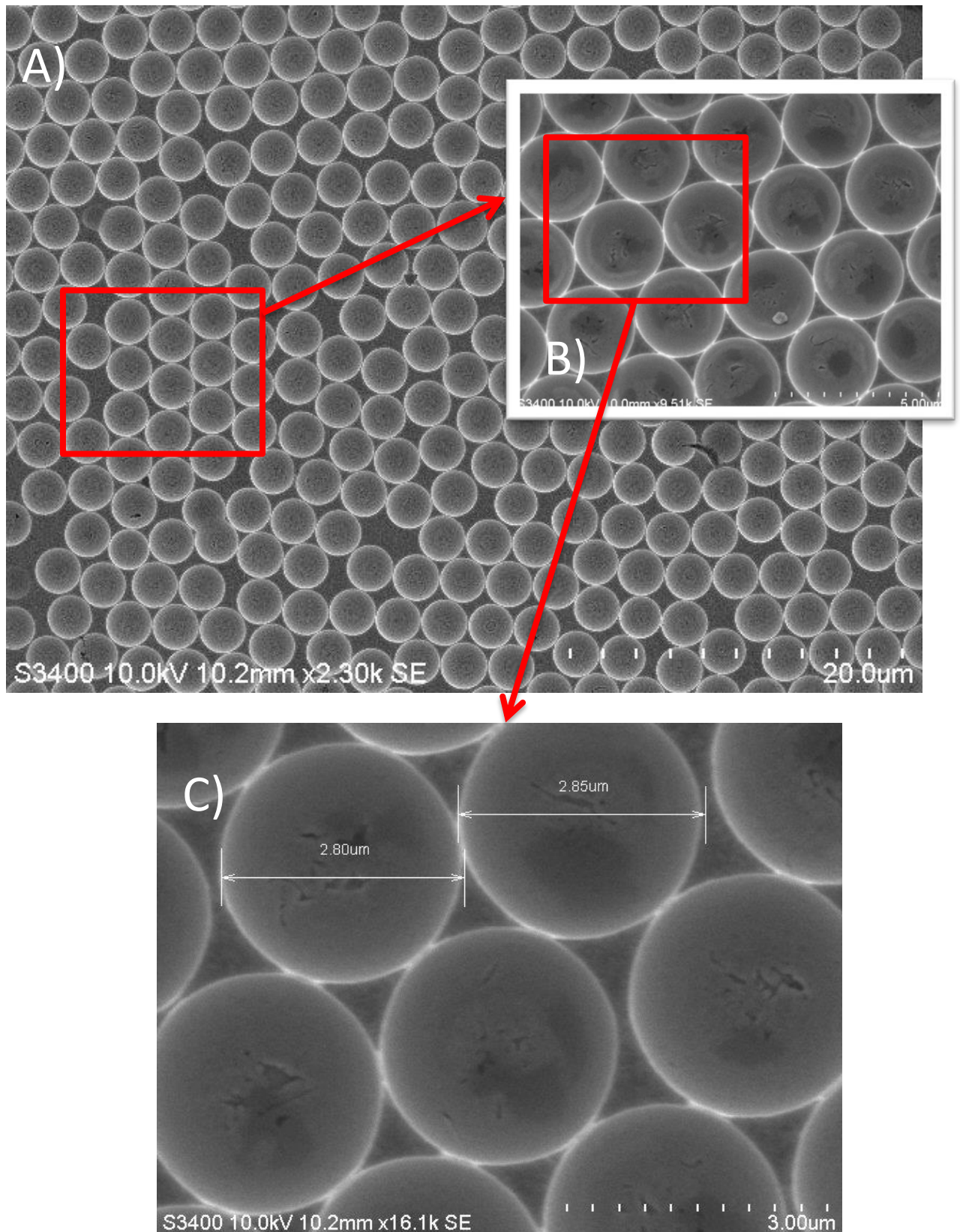


Figure 2.10 A) SEM image of an ordered structure of gold micro-cavity arrays, $2.80 \pm 0.04 \mu\text{m}$ in diameter, prepared by polystyrene sphere lithography on gold wafers followed by electrodeposition of gold and sonication in THF to remove the spheres (x2.3k

magnification) B) SEM images showing enlarged sections of the cavity arrays (x9.51k magnification) and C) A further enlarged SEM image of the microcavities (x16.1k magnification). All images were collected using identical conditions at 5.00kV accelerating voltage.

Images were collected at relatively low incident electron energy of 5 kV to ensure that the top surface of the array was imaged to allow an estimate to be made of the relative area of the array, including cavity and planar surfaces. Using an SEM image of a partial area of the array, the dimensions of the area in focus were extracted. This area value does not incorporate the area of each cavity. Therefore, to calculate the total surface area of the array, the total circular areas needed to be subtracted from this value and subsequently the hemispherical area given by the cavities had to be added. The total circle area under analysis was calculated by the number of cavities by the average radius squared, accurately measured by Image J software:

$$A = \pi r^2$$

Equation 2.1

The SA of all cavities in an SEM image was obtained using the equation of a hemisphere:

$$A = 2\pi r^2$$

Equation 2.2

Where A is the surface area of hemisphere and r is the radius. The actual SA was then calculated as follows:

$$\text{Actual } A = (\text{Total rectangular } A - \text{total circular } A) + \text{total hemispherical } A$$

Equation 2.3

Where total rectangular A is the area of the SEM image, total circular area is the area of the apertures of the cavities and total hemispherical area is the sum of the SA of all the

cavities within the image. As this value now only reflects the total surface of the array visible in the SEM image, this value had to be representative of the total array, which was fabricated to be 1 cm². This was extended by 1 cm² to obtain the factor that the total SA calculated had to be multiplied by to represent the whole array. Table 2.1 shows the calculated results across three arrays which had a calculated SA of 1.77 ± 0.03 cm².

Table 2.1: SA of three MSLBs determined using SEM.

Sample	SA (cm²)
1	1.74
2	1.78
3	1.79
Average	1.77 ± 0.03

This approach of calculating array SA contains a number of assumptions as a small area of the total array is assumed to reflect the total MSLB and calculating the area of the cavities is not a true hemisphere as the gold is electrodeposited above the equator. This calculation does also not consider any nanoscale roughness of the gold on the surface.

To obtain the electroactive area cyclic Voltammetry was used. A voltammetric scan rate study shows a linear relation of reversible electrochemical reaction of ferrocyanide, [Fe(CN)₆]⁴⁻, on gold microcavities and this was used in combination with the Randles-Sevick equation to obtain the surface area:

$$i_p = 2.69 \times 10^5 n^3 A D^{\frac{1}{2}} C v^{\frac{1}{2}}$$

Equation 2.4

where i_p = peak current (A), n = electron stoichiometry, A = electrode area (cm²), D = diffusion coefficient (cm²/s), C = concentration (mol/cm³) and v = scan rate (V/s).

Figure 2.11 and 2.12 below show the results when the MSLB was analysed by CV. Using the value from the linear regression, the Randles- Sevcik equation was then employed to calculate the SA, which is illustrated in Table 2.2.

$$A = \frac{2.69 \times 10^5 n^{\frac{3}{2}} D^{\frac{1}{2}} C v^{\frac{1}{2}}}{i_p}$$

Equation 2.5

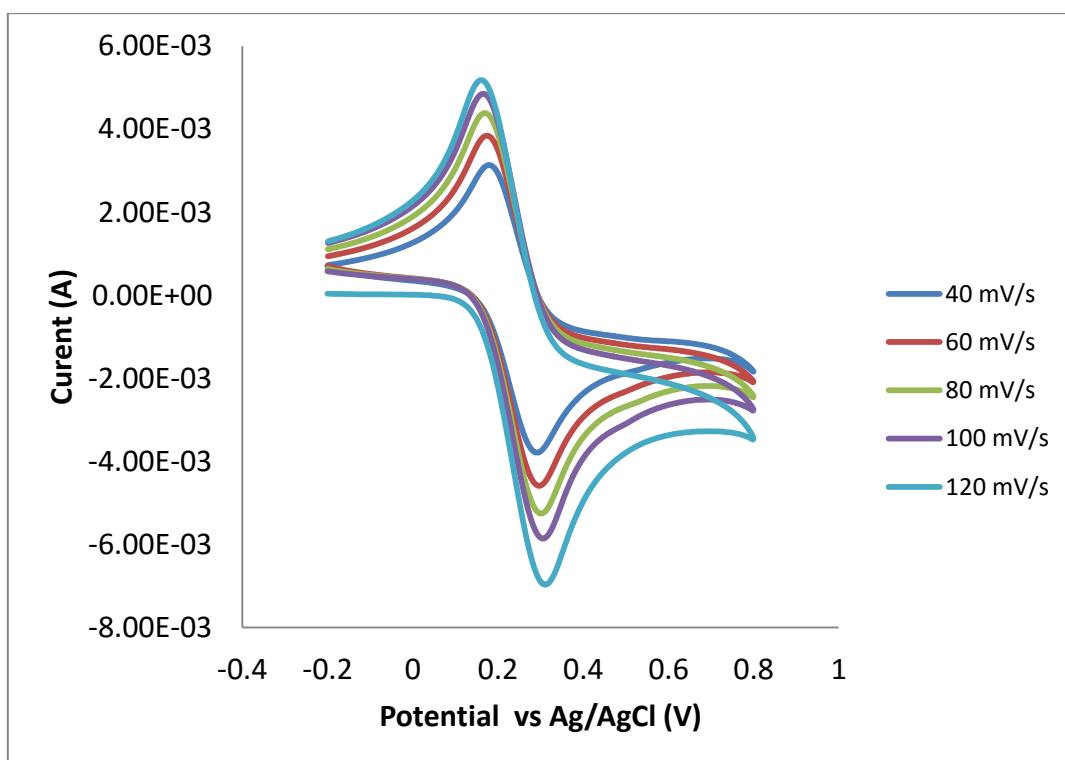


Figure 2.11: CV of gold MSLB, $2.80 \pm 0.04 \mu\text{m}$ in ferrocyanide.

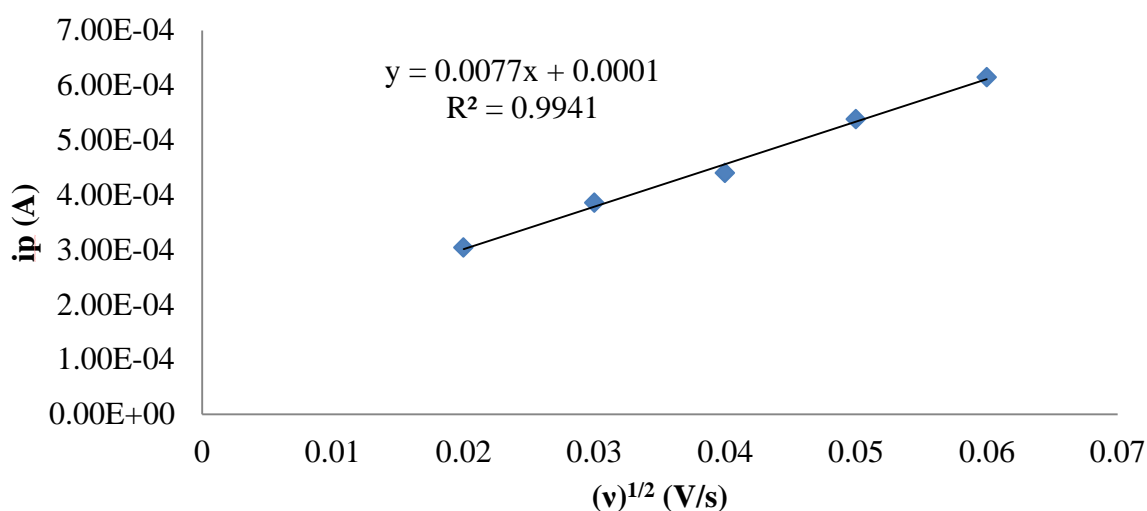


Figure 2.12: Determination of the S.A of gold micro cavities using C.V.

The SA was determined to be $2.93 \pm 0.54 \text{ cm}^2$ which is greater than the SEM calculated value. This value is a realistic SA as CV it takes into account the defects on the surface, variation in cavity size and also nanoscale roughness.

Table 2.2: Electroactive SA determined using CV/ Randles- Sevcik fit.

Sample	SA (cm^2)
1	2.57
2	2.66
3	3.55
Average:	2.93 ± 0.54

Following surface modification of the gold cavity arrays with 2-mercaptoethanol the water contact angle was measured to assess the hydrophilicity of the substrate. Each of the three SAMs explored are expected forming a close packed layer but with varying chain length. In each case the thiol is terminated by an alcohol, which should render the surface hydrophilic and facilitate DOPC spanning monolayer formation by ensuring the correct orientation of the amphiphilic lipid molecules onto the substrate.

Figures 2.13 and 2.14 show water contact angle goniometry at an unmodified gold $2.80 \pm 0.04 \mu\text{m}$ array and one which is modified with 2-mercaptoethanol. Comparing the two figures visually, it is evident that the shape of the water droplet changes in each condition. Figure 2.13 shows the unmodified gold array has a water contact angle of 90.02° whereas Figure 2.14 mercaptoethanol treated gold array shows a lower value of 60.69° . It is clear that the array modified with a thiol molecule terminating in an alcohol group renders a surface which is due to stronger adhesive forces with the liquid water molecules to the –OH group, additionally seen by the larger base width, 4.7052 mm (Figure 2.13) relative 4.2109 mm (Figure 2.14) as the drop has a greater surface area interacting with the substrate.

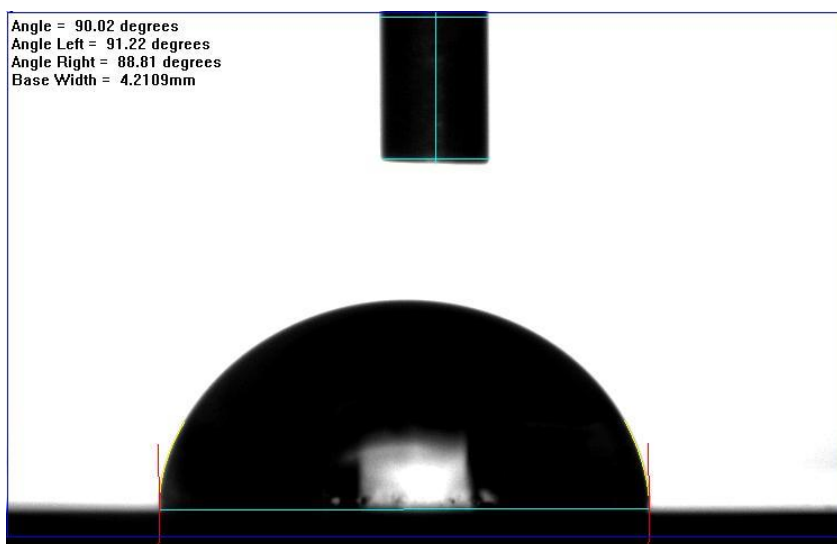


Figure 2.13: Water contact angle measurement for unmodified gold $2.80 \pm 0.04 \mu\text{m}$ cavity array.

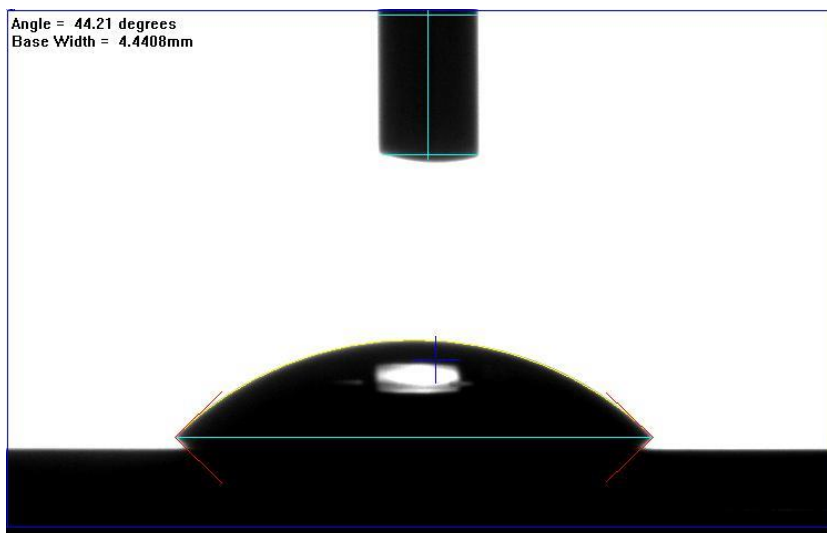


Figure 2.14: Water contact angle measurement for 2-mercaptoethanol modified gold $2.80 \pm 0.04 \mu\text{m}$ cavity array.

Contact angles vary from high values of $80 - 120^\circ$ (hydrophobic) to low contact angles of $10 - 80^\circ$ (hydrophilic). A summary table presenting the averaged water contact angle of the surface with and without 2-mercaptoethanol modification is presented in Table 2.3. In this instance, these results reflect unfilled cavities. An average water contact angle of $85.56 \pm 1.14^\circ$ for the unmodified gold surface indicates that this was modestly hydrophobic. As expected, following 2-mercaptoethanol SAM formation, the hydrophobicity of the surface decreased and the newly modified substrate rendered itself as hydrophilic with a water contact angle of $45.70 \pm 2.11^\circ$.

Table 2.3: Water contact angle measurements for unmodified gold alone and 2-mercaptoethanol for $2.80 \pm 0.04 \mu\text{m}$ diameter cavity arrays. $N = 3$ in all cases.

Surface Modification	$2.80 \pm 0.04 \mu\text{m}$ diameter Cavity Array Water Contact Angle ($^\circ$)
Unmodified gold	85.56 ± 1.14
2-Mercaptoethanol	45.70 ± 2.11

In order to fill smaller cavities, the array must be sonicated in the solution for at least 30 mins (Jose, 2011). In Table 2.4, the cavities were previously filled with 0.01 M PBS buffer pH 7.4 and the contact angle was measured again. For unmodified gold, the angle increases when the cavities are filled to an angle of $94.83 \pm 0.62^\circ$, but in the case of 2-

mercaptoethanol modification, which is used in our work, the angle is $61.37 \pm 0.96^\circ$. The similarity in the values suggests the cavities are filling in the water contact angle experiments.

Table 2.4: Water contact angle measurements for unmodified gold alone and 2-mercaptoethanol for $2.80 \pm 0.04 \mu\text{m}$ diameter cavity arrays which are pre-sonicated in buffer solution. $N = 3$ in all cases.

Surface Modification	$2.80 \pm 0.04 \mu\text{m}$ diameter Cavity Array Water Contact Angle ($^\circ$)
Unmodified gold	94.83 ± 0.62
2-Mercaptoethanol	61.37 ± 0.96

2.2.3 Characterisation of Lipid Bilayer

Bilayers were formed and successfully spanned across the cavities. This was confirmed by FLCS, shown in Figure 2.15, courtesy of Dr Sivaramakrishnan Ramadurai. Using two different probes, Atto655-DOPE and β -BODIPY-C5-HPC, the diffusion coefficients were determined to be 11.7 ± 0.8 and $14.35 \pm 1.52 \mu\text{m}^2/\text{s}$ respectively.

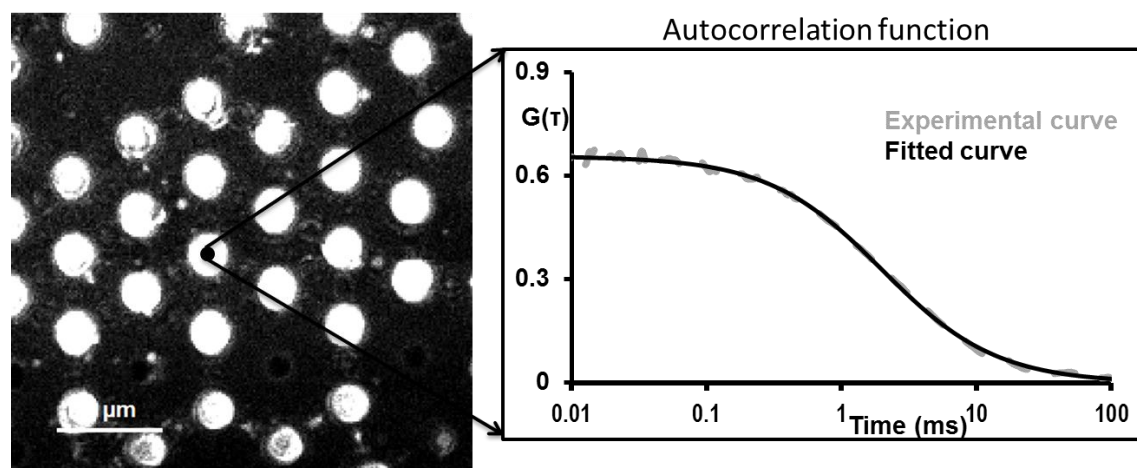


Figure 2.15: Representative of back reflectance image of the microcavity made from PDMS. The white spherical part represents the buffer filled cavities and the dark part represents the planar and non-filled PDMS cavities. The cavity sizes are $2.5 \pm 0.5 \mu\text{m}$. The DOPC lipid bilayer was formed on these microcavities by Langmuir-Blodgett technique and vesicles disruption method. The black spot on the microcavity was the

graphical representation of the observation volume, where the fluorescence molecules fluctuation over the time was measured using FLCS. On the right hand side is a typical FLCS curve obtained after normalising the fluctuation signal and fluorescence lifetime signature to calculated true autocorrelation curve. The grey dash line represent experimental curve and black solid line correspond to 2D-fitting model, which yield the diffusion time and number of molecules in the observation volume.

An important issue in applying these model membranes to electrochemical impedance spectroscopy is the stability of the bilayers and the stability of their EIS signal over time in the absence of perturbation. EIS was therefore explored also to investigate the stability of the DOPC bilayer over time in contact with PBS at pH 7.4. This data is shown in Figure 2.16 and reveals that the impedance response does not alter significantly over the 300 minutes, the experiment was run. This temporal window was examined as it is sufficient time to conduct all experiments in Chapter 3 and 4. These results confirm that the bilayer shows good stability and the membrane resistance is reported numerically in Tables 2.5 and 2.6 below.

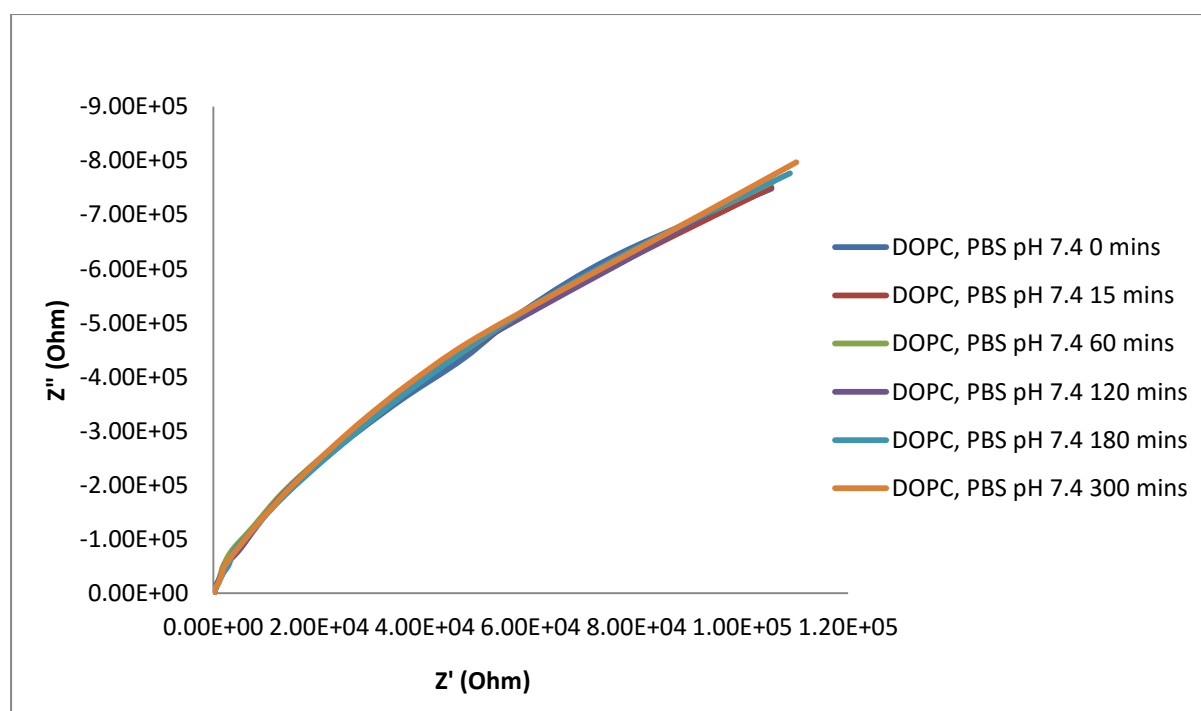


Figure 2.16: DOPC Stability in PBS Buffer, pH 7.4 Nyquist plot depicting a time study of DOPC bilayer suspended across $2.80 \pm 0.04 \mu\text{m}$ cavities in a 0.01 M PBS solution (pH 7.4): frequency range 0.1 MHz to 10 mHz.

Table 2.5 shows the real resistance values and it can be seen that membrane resistance value varies between substrates, 12.20 ± 0.54 and $17.09 \pm 0.87 \text{ M}\Omega \text{ cm}^3$ respectively. Variation in resistance from substrate to substrate is expected because of variations in the surface structure/area. Alternatively, Table 2.6 shows the relative change. This is a more useful representation of the bilayer as it compares membrane resistance change rather than absolute value which are substrate dependent. The variation in actual values is due to substrate differences encompassing number of PS deposited, roughness of the surface and surface area of the array. These are factors which will be addressed in Chapter 5.

Table 2.5: Stability of the bilayer in PBS buffer at pH 7.4. Results represented depict real resistance values obtained.

Minutes	N=1 ($\text{M}\Omega \text{ cm}^2$)	N=2 ($\text{M}\Omega \text{ cm}^2$)
15	11.25	16.12
45	12.31	17.29
75	12.42	17.17
105	12.25	16.26
135	12.54	17.02
165	11.57	16.09
195	12.28	16.76
225	11.66	18.75
255	12.83	18.22
285	12.89	17.26

Average	12.20 ± 0.54	17.09 ± 0.87
----------------	--------------	--------------

Table 2.6: Stability of the bilayer in PBS buffer at pH 7.4. Results represented depict change (Δ) recorded following drug addition, relative to bilayer prior to drug interaction.

Minutes	$\Delta_{\text{DOPC Bilayer}}$ N=1 ($\text{M}\Omega \text{ cm}^2$)	$\Delta_{\text{DOPC Bilayer}}$ N=2 ($\text{M}\Omega \text{ cm}^2$)
45	1.05	1.17
75	1.17	1.05
105	1.00	0.15
135	1.29	0.91
165	0.32	-0.03
195	1.03	0.64
225	0.41	2.64
255	1.58	2.11
285	1.64	1.14
315	1.05	1.17
$\Delta_{\text{DOPC Bilayer}}$ Mean ($\text{M}\Omega \text{ CM}^2$)	1.05 ± 0.45	1.09 ± 0.85

From Tables 2.5 and 2.6, it is evident that Δ_{Bilayer} changes to a very small extent over time in the absence of perturbation this allows us to define a standard deviation for measurement. This ensures its stability and potential as an alternative model cell membrane as lengthy analysis is possible.

2.3 Conclusions

Chapter 2 examined the fabrication and surface modification of a $2.80 \pm 0.04 \mu\text{m}$ gold cavity array. The topological and electrochemical area of the arrays were determined and the effect of surface modification on the wettability of the substrates was explored. This work demonstrated that a DOPC bilayer is spanned across its surface between two aqueous environments. FLCS confirms the bilayer's formation and confirmed that the bilayer is fluid and spanning across the pores and EIS illustrate the bilayer shows excellent stability over the experimental time-span. All substrates in Chapters 3 and 4 were fabricated according to this chapter unless otherwise stated.

2.4 References

Jose, B. 2011. *Biomimetic Photonic Nanocavity Arrays*. PhD thesis, Dublin City University.

Biolin Scientific 2014. *Langmuir, langmuir-blodgett and langmuir-schaefer technologies* [Online]. Available from: <http://www.biolinscientific.com/ksvnima/technologies/?card=KT1> [Accessed 04 August 2015].

Dongqing, L. 2008. *Encyclopedia of Microfluidics and Nanofluidics*. Springer Science & Business Media.

Gentle, I. and Barnes, G. 2005. *Interfacial science: an introduction*. 1st ed. Oxford; New York: Oxford University Press.

Mallon, C.T., Jose, Bincy, Forster, R.J. and Keyes, T.E., 2010. Protein nanopatterning and release from gold nano-cavity arrays. *Chemical Communications*, 46, pp. 106–108.

Purdue University, 2014. *Scanning Electron Microscope* [Online]. Available from: <https://www.purdue.edu/ehps/rem/rs/sem.htm> [Accessed 25 July 2015].

Chapter 3: EIS Study of Drug Interactions with Lipid Membrane

3.0 Introduction

During drug design the therapeutic agent is programmed to travel to its site of action within the organism by two principle factors: (a) lipophilicity, which permits the drug to cross membranes and (b) molecular structures, that mark it specific to its site of action, i.e. frequently a drug targets a single protein but has the ability to permeate the whole organism e.g. through the blood stream. Irrespective of the drugs purpose, it must typically cross numerous membrane structures within the organism following its administration. Current tools used to predict drug membrane interaction and ultimately permeability range from Log P and D to PAMPA assays. The former are crude and yield unreliable predictions of drug toxicity and PAMPA, although more advanced using lipids, does not exploit true membrane bilayer structures. This chapter describes the application of a biomimetic microcavity array supported lipid bilayer systems as a model of the cell membrane, as an alternative and far more biomimetic means of assessing drug plasma membrane interactions. Herein, $2.80 \pm 0.04 \mu\text{m}$ diameter gold nanopore arrays were used whose surfaces, were chemically modified (molecular self-assembly) to render them hydrophilic and assemble lipid bilayers using Langmuir Blodgett to form the initial monolayer and vesicle disruption to create the final bilayer structure.

Following its administration, whatever its effect be it pain relief, instigated by morphine, or cell death, initiated by penicillin a drug must cross multiple membrane boundaries within the host organism, depending on the location of the target. The lipid bilayer

presents a semi-permeable fatty barrier between the cell's exterior and interior surroundings and although there are a number of transport proteins types incorporated into the real membrane, most drug manufacturers are interested in promoting passive diffusion of drugs across the membrane.

In general, drugs that interact with the cell membrane do so via binding. e.g., electrostatic or by intercalation and then passive diffusion across the membrane. These interactions will perturb the lipid structure and its packing to varying degrees. It has been proposed for example that general anaesthetics work by altering the structure and conducting properties of cell membranes directly by interacting with the lipids within (Patrick 2005). Darvas et al. (2012) investigated this by studying the effect of four general anaesthetic molecules, chloroform, halothane, diethyl ether and enflurane on a dipalmitoylphosphatidylcholine (DPPC) membrane and concluded that the anaesthetics induced lateral expansion of the membrane and also increased local disorder in the lipid tails adjacent to the anaesthetic molecules. Anaesthetics are not the only class of drugs that affect the membrane properties of an organism. Often the impact of a drug targeted to a pathogen is through membrane disruption, for example, amphotericin B is an antifungal agent used to treat athlete's foot topically and works against life-threatening fungal diseases systemically (Patrick 2005). Its mode of action is via disruption of the cell wall of the fungi, where it builds tunnel like structures or pores through the bilayer, causing it to become more permeable which results in cell death (de Ghellinck et al. 2015, Yamamoto et al. , Kamiński et al. 2015). Additionally Valinomycin and Gramicidin are two antibiotics that permeate the bilayer where they act as ion channels within the cell membrane (Patrick 2005, Becucci et al. 2008, Rose and Jenkins 2007).

3.0.1 Log P and Log D Values

Understanding drug-membrane interaction is important both to understand permeability and also assess potential toxicity. The hydrophobic character of a drug provides insight into how easily it will passively cross the cell membrane. (Patrick 2005). Currently, the pharmaceutical industries rely heavily on a drugs log P value to predict how drug or cosmetic molecules will interact with the lipid membranes. The log P value is a partition coefficient between immiscible phases (organic and aqueous). It is measured by testing

the un-ionised drug's relative distribution in an n-octanol/water mixture and the numerical value is obtained by the following equation:

$$\log P = \log \left(\frac{[\text{Unionised drug}]_{\text{Octanol}}}{[\text{Unionised drug}]_{\text{Aqueous}}} \right)$$

Equation 3.1

Log P is typically plotted against the drug's biological activity, which is expressed as 1/C (where C is the concentration of the drug required which elicits its desired response in a living organism), to observe if there is a relationship between these two properties (Patrick 2005). This method is significant in estimating effective doses and also confirms that increasing hydrophobicity of drugs aids the crossing of the cell membrane. General anaesthetics are the best examples of drugs with high hydrophobicity as they function by dissolving into the neuronal membrane and thereby influence nerve conduction and membrane structure (Hille 2001). This implies that log P values should be a good indicator of a general anaesthetics efficacy, and correspondingly log P values close to 2 should be attained for drugs such as the anaesthetics, which are specifically targeted to intercalate into the cell membrane (Patrick 2005).

Log D, the distribution coefficient is very similar to log P, the partition coefficient. It too is a ratio of a compound between two phases but it differs in that log P refers to the concentration of an unionised compound whereas log D is the ratio of the sum of the concentrations of all forms of the compound, both ionised and unionised in the organic and aqueous phases. As it relates to charged and neutral forms, it is heavily dependent on pH. Therefore, a buffer is used in the aqueous phase to maintain the pH at a specific value. The pH must therefore be specified when the log D value is quoted. A pH value of 7.4 is usually selected as this is the physiological pH value of blood serum. The distribution coefficient is expressed in Equation 3.2:

$$\log D = \log \left(\frac{[\text{Unionised drug}]_{\text{Octanol}} + [\text{Ionised drug}]_{\text{Octanol}}}{[\text{Unionised drug}]_{\text{Aqueous}} + [\text{Ionised drug}]_{\text{Aqueous}}} \right)$$

Equation 3.2

Although widely used, partition coefficients and distribution coefficients are crude and generally inaccurate models. They do not consider a number of key interactions between molecule and membrane and are typically poor predictors of membrane permeability and very poor predictors of toxicity.

3.0.2 Cell-based Methods

Whereas log P and D are typically used as a starting point for predicting drug uptake, cell-based methods are often the second line of pre-clinical assessment employed to assess and predict in vitro permeability assessment. The commonly used model is the epithelial cell layer permeability barrier of the small intestine that drug or pharmaceutical compounds encounter as they pass through the human body (Di and Kerns 2010). A cell line from human colon carcinoma (Caco-2) is utilised as it is immortal and models multiple mechanisms for permeability; for instance it resembles the morphology of the human gastrointestinal (GI) epithelial cells through microvilli and caco-2 cells additionally express cell membrane transporters on their apical surface (Di and Kerns 2010). Other cell lines are also used such as the Madin Darby Canine Kidney (MDCK) cell line which has been employed actively in the prediction of passive drug permeability (Di and Kerns 2010). To implement the cell-based method, industries utilise a device termed the cell culture insert, where cells are plated onto the insert where they settle onto a support composed of porous filters. The cells are left to incubate and grow to confluence over a period of 21 days and consequently cover the surface (preferably as a monolayer) of the filter support (Di and Kerns 2010). It is vital that there is full coverage, otherwise the drug compound can leak directly through the filter via gaps in the cell monolayer which distort the analytical results. The drug under analysis is added above the cell monolayer into the cell culture insert and this is termed the apical region. The basal compartment represents the concentration of drug that successfully diffused across the membrane and the filter. LCMS is often used to quantify and quantitate the drug and its concentration that successfully partitioned across the cell membrane assay.

Cell based methods have the advantage in that they represent real biological cell lines, specifically those in the endothelial region. However, critically this technique does not provide insight into the nature of the membrane interaction nor give an indication as to any damage the drugs invoke on the membranes themselves. The cell culture often contains very heterogeneous cells and it is a very lengthy and expensive analysis with the requirement of cell culture, which itself is prone to error including cell death, formation of multilayers rather than a monolayer and also incomplete surface coverage.

3.0.3 PAMPA

The most advanced lipid model adopted by industry is PAMPA. PAMPA is an abbreviation for parallel artificial membrane permeability assay which utilises a synthetic membrane of phospholipids solubilised in a long-chain hydrocarbon such as dodecane, which is impregnated into a polymer membrane (Di and Kerns 2010). The drug of interest is diluted in aqueous buffer and is placed in a 96-well plate. 'Donor' is the term then applied to each of these wells which are filled with the diluted compound. The next step is the application of a 96-well filter plate that is placed on top of the donor wells, with the porous filter on the bottom, placed in contact with the aqueous buffer (Di and Kerns 2010). The artificial barrier is then formed in the holes of the filter by the addition of a few millilitres of a phospholipid solution where subsequently, blank buffer is placed inside the filter plate wells, termed an 'acceptor'. The final PAMPA can be described as a sandwich of the donor 96-well plate, containing the diluted drug under analysis, and the acceptor 96-well filter plate containing blank aqueous buffer, separated by an artificial barrier of phospholipids. This assay is maintained at constant humidity and temperature and of a time that is dictated by the laboratory's protocol and the permeability of the drug, generally within the interval of 1 and 18 hours (Di and Kerns 2010). Following incubation, samples are taken from the donor and acceptor wells and can be analysed for drug concentration using a variety of techniques such as liquid chromatography mass spectrometry (LC/MS), liquid chromatography ultraviolet (LC/UV) or an instrument that analyses the UV of the plates directly. Di and Kerns (2010) also specify that a standard can be used to quantitate the concentration of the drug in the donor cells by using unused donor solution where subsequently permeability (often coined effective permeability, P_e) can be calculated. This method is more biomimetic than the Log P and Log D techniques

as it assesses artificial barrier crossing, and it is less time consuming and expensive than the cell based approaches. However, PAMPA does not use a lipid bilayer for its analysis and only measures passive diffusion across a lipid impregnated polymer layer. It does not provide any insight into the effect that a drug may have on a lipid bilayer structure and it is very weakly biomimetic.

3.1 Effect of Drug Binding

The effect that drug binding has on the cell membrane is a significant factor to human health as it may have adverse side effects when significant and possible irreversible damage is caused. Kaplowitz (2004) discussed how approximately one half of all acute liver failure cases are caused by drug-induced hepatotoxicity where the parent drug or the metabolites can directly affect the cell's biochemistry. Greater than 1000 drugs have been implicated with most screened out during preclinical development but there are those that are not detected until it has been administered to a patient in a clinical situation. Doxorubicin is an effective anticancer drug used in chemotherapy to treat tumours however it is accompanied by a dose-dependent cardiotoxicity side effect (Deavall et al. 2012). This drug has numerous impacts on cardiac tissue. In relation to membranes, this drug peroxidises lipids which results in cell damage. Chronic effects of doxorubicin can lead to fatal congestive heart failure (Deavall et al. 2012). A membrane model with a truly biomimetic lipid bilayer structure, which is capable of quantitatively reporting on perturbation of the bilayer structure, would be very effective both as a membrane transport model, but in particular to predict such risk.

This chapter reports a preliminary study of MSLBs as alternative models to report on binding and perturbation of drug on the cell membrane. It is more biomimetic than the Log P and Log D approaches because it uses a genuine lipid bilayer and it is anticipated to be more accurate than the cell based and PAMPA techniques as clear drug/membrane interaction is realised. Additionally, MSLBs offer the opportunity to study a wide variety

of membrane compositions spanning very simple to complex, as will be described in the next chapter, including asymmetric bilayers, which is the form that many biological bilayers take.

3.1.1 Ibuprofen and Diclofenac

Ibuprofen and diclofenac were studied in this programme as they represent two drug members of the nonsteroidal anti-inflammatory drug (NSAID) classification. Ibuprofen is a well-known, widely-administered and well-researched NSAID with its principle application in the treatment of rheumatic diseases and in pain relief, stiffness, inflammation, fever reduction, and aches originating in the head and muscles (Ng, Gani and Dam-Johansen 2006). It is estimated that ibuprofen has been received worldwide by over 100 million patients and its availability now spans across 100 countries (Busson 1986). Ibuprofen has the IUPAC name of 2-(4-Isobutyl-phenyl)-propionic acid and is a colourless, crystalline solid with a melting point of 350 K (Ng, Gani and Dam-Johansen 2006).

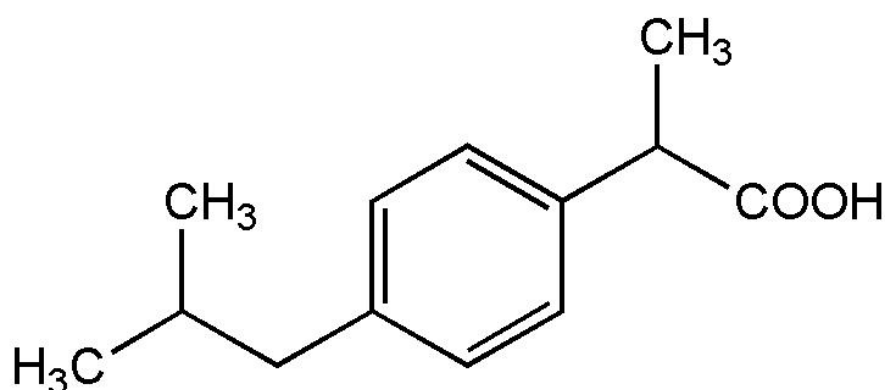


Figure 3.1: Ibuprofen molecular structure (Ng, Gani and Dam-Johansen 2006).

Ibuprofen has been available for use since the early 1970's yet today, though interestingly, research is still conducted into the nature of its permeability. Cilurzo et al. (2010) conducted a study into the effect of drug chirality on the permeability of ibuprofen using a transdermal permeation approach on human skin, followed by HPLC to ascertain

drug concentration that successfully permeated. This research concluded by illustrating the role chirality can play in permeation; however it failed to investigate how both forms of the drug affected the cell membrane itself. Similarly Levis, Lane and Corrigan (2003) investigated ibuprofen's permeability but focused on buffer media composition and how this affected the drug's solubility and subsequently, permeability. Levis, Lane and Corrigan (2003) focused on the permeability coefficient by utilising male Wistar rats and applying the gut perfusion method followed by blood analysis. Conclusions were made into how various factors must be considered when trying to ascertain permeability coefficients medium such as pH, buffer capacity and osmolarity. Again, the nature of the drugs interaction with the cellular membrane was not addressed. Dua et al. (2006) aimed to address this deficit by using electrochemical impedance spectroscopy to investigate the ibuprofen/bilayer interaction with a planar lipid membrane a supported surface of a glassy carbon electrode. It was reported that with increasing concentration, the bilayer was defected. In this study, the ibuprofen was dissolved in NaOH and the molarity of the administered drug was not stated. Furthermore, no controls were reported on the impact of the solution on their model membrane system.

Diclofenac is also a member of the NSAID and is estimated to be the most widely used within that family of pharmaceutical compounds (Lemke and Williams 2012). It has medicinal applications in areas of anti-inflammatory, antipyretic and analgesic. It was introduced onto the markets at a later stage than ibuprofen with its introduction to the United States occurring in 1989 (Lemke and Williams 2012).

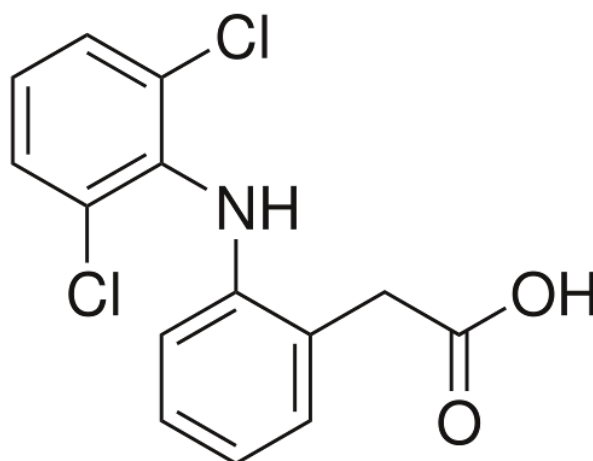


Figure 3.2: Diclofenac molecular structure (Lemke and Williams 2012).

Membrane permeability studies of diclofenac were conducted by Aldwaikat and Alarjah (2015) who were also interested in skin permeability, similar to Cilurzo et al. (2010), where they used ultrasound to assess if this could promote the permeability of diclofenac, which they found it did. Similar to many permeability reports, the state or condition of the membrane is not considered. Talele, Choudhary and Kishore (2016) examined the use of surfactants in drug delivery, applied to diclofenac to understand and quantitate partitioning of diclofenac micelles using isothermal titration calorimetry. They concluded that diclofenac mainly interacts electrostatically with the cationic tetradecyltrimethylammonium bromide (TTAB) micelles at the surface and that isothermal titration calorimetry is a useful technique that provides insight into the energetics of drug interactions with delivery media and target sites (Talele, Choudhary and Kishore 2016).

Currently, there is no method applied that accurately interrogates drug/membrane interactions in a robust, relatively quick and stable manner in truly biomimetic membrane models. The use of microcavity supported lipid bilayers aims to address this deficit and provide a solution to how membrane/drug interactions can be investigated. Additionally, using cell only methods leads to further complexities and also less variation

as typically only one cell line or type of cell could be investigated. The model presented in this study is a simple, single lipid membrane model but illustrates the potential for further studies where composition can be varied with enhanced complexity without the need of onerous cell culture. This chapter applies the $2.80 \pm 0.04 \mu\text{m}$ gold MSLB fabricated in Chapter 2 (Figure 2.6) as a biomimetic model the cell membrane to compare the impact of two NSIAD drugs; diclofenac and ibuprofen, to report on their different interactions with the cell membrane by electrochemical impedance spectroscopy.

3.2 Materials and Methods

3.2.1 Materials

Materials were described in to Chapter 2, section 2.2.1. Ibuprofen sodium salt, diclofenac sodium salt, sodium chloride, 6-Mercapto-1-heaxanol ($\geq 97\%$) and 11-Mercapto-1-undecanol ($\geq 97\%$) were all purchased from Sigma Aldrich, Ireland.

3.2.2 Experimental Equipment

As per Chapter 2, section 2.2.2.

3.2.3 Methods

As per Chapter 2, section 2.2.3. All methods were conducted at room temperature, 20 °C.

3.2.3.1 Preparation of Ibuprofen and Diclofenac Stock Solutions

Ibuprofen and diclofenac were both prepared for introduction into the bilayer contacting solution in the same manner. The former, ibuprofen was dissolved in deionised water to prepare a 150 mM stock solution. This stock was used to prepare a second stock of 4 mM. Similarly, the latter drug, diclofenac, was prepared in an identical manner except the solvent used was methanol because of the poor solubility of this drug in water.

The two drug stocks were then used in the EIS experiments by introducing them to the contacting buffer solution. The drug was added so that the final concentrations in the aqueous contacting solutions were: 1, 5, 20, 40, 100, 400, 1000 and 4000 μM . These were prepared by adding the required stock solution volume into the electrochemical cell to yield a final volume in the EIS cell of 20 mL 0.01 M PBS buffer, pH 7.4.

3.2.3.2 EIS

The EIS measurements were carried out in a standard three electrode electrochemical cell. Ag/AgCl (sat. KCl) was used as the reference electrode; the microcavity, with suspended bilayer, was the working electrode; and a platinum mesh wire was employed as the counter electrode. The Ag/AgCl (Sat KCl) reference electrode was placed in a salt bridge to prevent chloride ion contamination. A potential of 0 V versus Ag/AgCl was applied by a Model 660 CH electrochemical workstation. After stabilisation of the MSLB, determined by 3 repeat EIS measurements where the response did not change, the electrochemical impedance spectroscopy measurements were carried out in the frequency range 0.1 MHz to 10 mHz. Data acquisition was performed by CHI 660 Electrochemical Workstation and analysed using ZView software.

3.3 Results and Discussions

Schreier, Malheiros and de Paula (2000) reviewed and focused on amphiphilic drug interactions (non-steroidal anti-inflammatory drugs fall under this umbrella) with the cell membranes and how this leads to shape changes, vesiculation, membrane disruption and solubilisation from a physicochemical perspective. Ibuprofen and diclofenac were both mentioned in this review as they are known to create drug containing mixed micelles from liposomal dispersions. Schreier, Malheiros and de Paula (2000) conclude by acknowledging the fact that regardless of the surface active drug's membrane activity mechanism or self-association properties, they do exert effects at the molecular level when they interact with cell membranes. The following results provide an alternative technique to investigate the membrane-drug interactions.

2.80 ± 0.04 micron DOPC modified arrays were prepared and characterized according to Chapter 2.

3.3.1 EIS Analysis of Drug Interaction

The application of the bilayer supported microcavity arrays to evaluate the impact of two representative NSAIDs; ibuprofen and diclofenac on a DOPC bilayer was examined. This was conducted by Electrochemical Impedance Spectroscopy (EIS) which was enabled by the gold arrays, which behave as the working electrode in the experimental set up.

3.3.1.1 Ibuprofen

The ibuprofen sodium salt in PBS buffer was introduced to the contacting solution of a DOPC bilayer suspended across 2.80 ± 0.04 μm cavities filled with PBS buffer at pH 7.4. Figure 3.3 shows a representative impedance response across a single MSLB substrate to varying concentrations of ibuprofen: at 1, 5, 10, 40, 100, 1000 and 4000 μM respectively. The larger concentration of 4 mM was selected based on research on ibuprofen conducted by Alsop et al. (2015). A lot of research is focused on high concentration of drugs however, as drugs are administered in various doses, it is important to a range of different concentrations. This is what makes our technique appealing in that a wide variety of concentration ranges can be used that can be lower or higher than the physiological range.

In each case, the drug was titrated into the contacting solution and allowed to equilibrate for 2 minutes after each drug concentration increase before EIS was measured. This time was selected as initial control experiments showed no difference in EIS response when equilibration times were extended.

Changes to EIS in response to drug administration, where they occurred, were essentially immediate for both Ibuprofen and Diclofenac. Each measurement at each drug concentration was measured in triplicate. There was no variation in response over these triplicate measurements again, confirming equilibrium between the drug and membrane occurred quickly. Each EIS measurement was 15 mins and the repeat measurement was taken directly after. Then after the highest concentration had been introduced, allowed to equilibrate, and EIS measured in triplicate, the lipid bilayer was washed through 2 times with PBS buffer to clear any remaining drug from the contacting solution. This was carried out to assess the reversibility of drug binding. In a separate EIS experiment it was confirmed that “washing” the bilayer in this way had no measureable impact on the bilayer impedance.

The EIS data is presented here as a Nyquist plot where the sum of the real, Z_{re+} , and imaginary, Z_{im} components represent the complex impedance. This complex impedance response originates from the resistance and capacitance of the cell. As the plot shifts towards Z_{im} (y axis), this indicates that there is an increase in the impedance of the bilayer. Similarly, a graphical shift towards Z_{re} (x axis) implies that the bilayer capacitance has reduced. In lipid bilayer systems, this is typically attributable to the bilayer becoming , permeable or leaky, i.e. less resistive. A similar response was reported by Sugihara et al. (2012) where the resistivity of a DMPC supported lipid bilayer decreased when the pore-forming peptide, melittin, interacted with it.

Figure 3.3 below shows the EIS responses to a DOPC bilayer suspended across the gold microcavity array. The response was measured for 300 minutes to ensure stability. This time is sufficient to analyse the various concentrations of the selected drug and the membrane’s response.

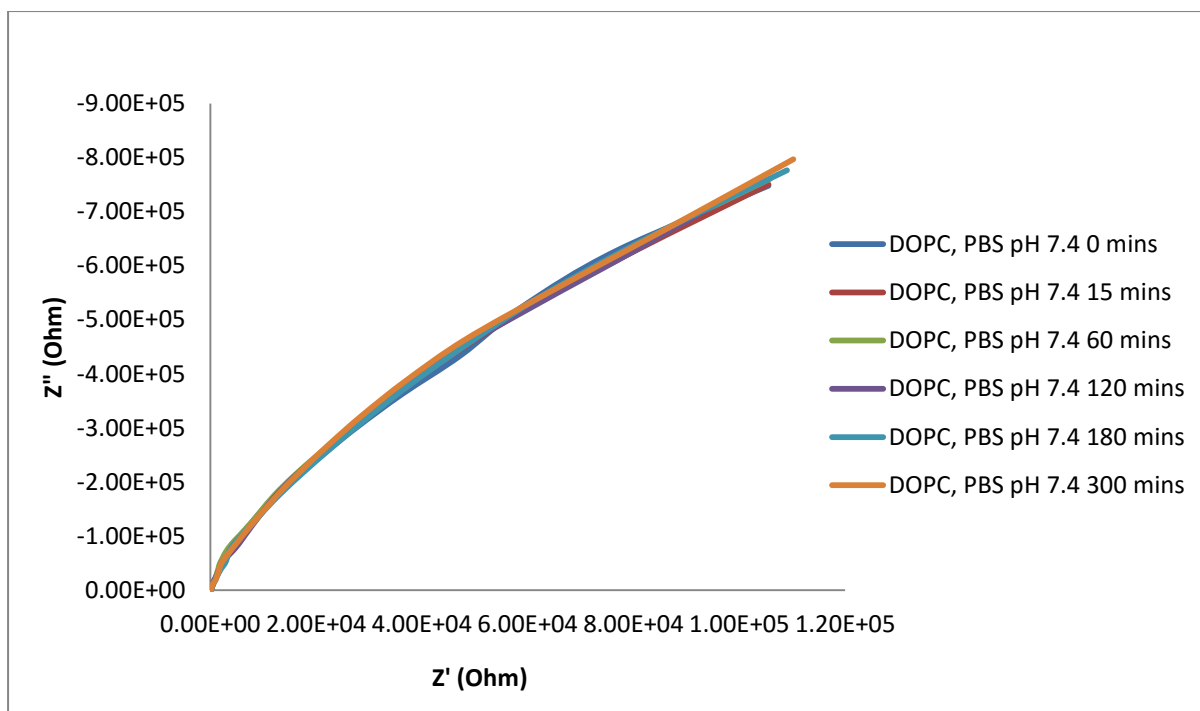


Figure 3.3: DOPC Stability in PBS Buffer, pH 7.4 Nyquist plot depicting a time study of DOPC bilayer suspended across $2.80 \pm 0.04 \mu\text{m}$ cavities in a 0.01 M PBS solution (pH 7.4): frequency range 0.1 MHz to 10 mHz.

Graphical representations of impedance are useful in highlighting the effect ibuprofen has, however for more quantitative insights into the resistance values of the lipid bilayer were extracted using the equivalent circuit model (ECM) shown in Figure 3.4. The ECM model applied to the AC impedance data obtained represents the MSLB system through the following parameters:

- Resistance of the solution (R_{sol})
- Capacitance of the bilayer (CPE_{bl})
- Resistance of the bilayer (R_{bl})
- Resistance of the cavities (R_{cav})
- Capacitance of the double layer (CPE_{dl})

The circuit consists of the solution resistance (R_{sol}) in series with a resistor and capacitor in parallel, which corresponds to the 2-mercaptoethanol layer/lipid bilayer on the electrode surface (R_{bl} , C_{bl}). The circuit also contains a component for the resistance of the micro cavities (R_{cav}), and the double layer capacitance

(Cdl). The circuit uses Constant Phase Elements (CPE) instead of pure capacitors to account for surface defects on both the electrode surface and the lipid bilayer. The impedance of a CPE is given by $Z_{CPE} = Q^{-1}(j\omega)^{-\alpha}$ where Q is the magnitude of the capacitance of the CPE, ω is the angular frequency, and α is a real number between 1 and 0 (the closer α gets to 1 the more ideal the capacitive behaviour of the CPE).

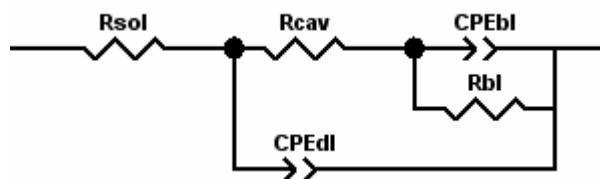


Figure 3.4: ECM model used to fit AC impedance data.

As varying concentrations of drugs were titrated to the contacting electrolyte solution, it is expected that R_{sol} values may change depending on the nature of the drug, e.g. its charge but everything else remains static. Both ibuprofen and diclofenac are negatively charged. R_{cav} is expected that this would not vary within a sample as there are no changes occurring in this component of the electrical system. CPE_{bl} and R_{bl} are connected in parallel. The membrane acts as an impermeable and insulating medium in biological cells as both the intracellular and extracellular environments contain various concentrations of ionic salt solutions permitted by the membrane. Similarly in the biomimetic MSLB, there is an external and internal environment of PBS buffer separated by a semi-permeable phospholipid bilayer. Essentially, this insulating bilayer is separating two ionic phases and is hence acting as a capacitor.

The AC impedance data was fitted to the ECM model given in Figure 3.4 and the results are plotted below in Table 3.1. The real resistance values of the membrane obtained at each concentration across separately prepared gold MSLBs are presented as examples of absolute variation of the resistance values for the substrates. Table 3.1 shows the real resistance values and Table 3.2 depicts the relative change of a stable bilayer. These values illustrate that the bilayers resistivity will alter moderately between samples which

is due to sample sample variation. Within sample, the average resistivities for the three samples are -0.76 ± 0.44 , 0.36 ± 0.14 and 0.37 ± 0.27 respectively. The first result is an outlier and focusing on the second two responses it can be concluded that the bilayer's resistivity increases within the 300 minutes but by applying standard deviation to our data, it can be concluded that this change is due to the fluctuation of the lipid molecules as it is suspended between the two aqueous environments.

Table 3.1: Stability of the bilayer in PBS buffer at pH 7.4 in same time period as ibuprofen drug experiment. Results represented depict real resistance values obtained.

Minutes	N=1 (MΩ)	N=2 (MΩ)	N=3 (MΩ)
15	5.89	3.84	5.50
45	4.74	4.20	5.90
75	5.60	4.24	5.86
105	4.69	4.18	5.55
135	5.75	4.28	5.81
165	5.45	3.95	5.49
195	4.69	4.19	5.72
225	5.60	3.98	6.40
255	5.04	4.38	6.22
285	5.52	4.40	5.89

Table 3.2: Stability of the bilayer in PBS buffer at pH 7.4 in same time period as ibuprofen drug experiment. Results represented depict change (Δ) recorded following drug addition, relative to bilayer prior to drug interaction.

Minutes	$\Delta_{\text{DOPC Bilayer}}$ N=1 (MΩ)	$\Delta_{\text{DOPC Bilayer}}$ N=2 (MΩ)	$\Delta_{\text{DOPC Bilayer}}$ N=3 (MΩ)
45	-1.15	0.35	0.40
75	-0.29	0.40	0.36
105	-1.20	0.33	0.05
135	-0.14	0.44	0.31
165	-0.44	0.11	-0.01
195	-1.21	0.35	0.22
225	-0.29	0.14	0.90
255	-0.85	0.53	0.72
285	-0.37	0.56	0.39
315	-1.15	0.35	0.40
$\Delta_{\text{DOPC Bilayer}}$ Mean (MΩ)	-0.76 ± 0.44	0.36 ± 0.14	0.37 ± 0.27

From the above data in Tables 3.1 and 3.2 respectively, it is evident that Δ_{Bilayer} changes to a very small extent over time in the absence of perturbation this allows us to define a standard deviation for measurement. The remaining data will illustrate the mean change of the bilayer relative to the initial stable measurement in PBS buffer. The average SD across multiple substrates is used here but this is a gross overestimation of error.

Visually examining the EIS curves, it is evident that ibuprofen does not have a very large impact on bilayer impedance, as illustrated in Figure 3.5. Nonetheless, compared with the DOPC bilayer alone over time (Figure 2.16 in Chapter 2) there is a measureable systematic increase in overall impedance with increasing drug concentration. This suggests that this drug is not penetrating through the bilayer which would be expected to be characterised by disrupting lateral lipid interactions, thus increasing porosity which

would cause a decrease in resistance, instead the small resistance increase suggests that the drug is adsorbing onto the bilayer.

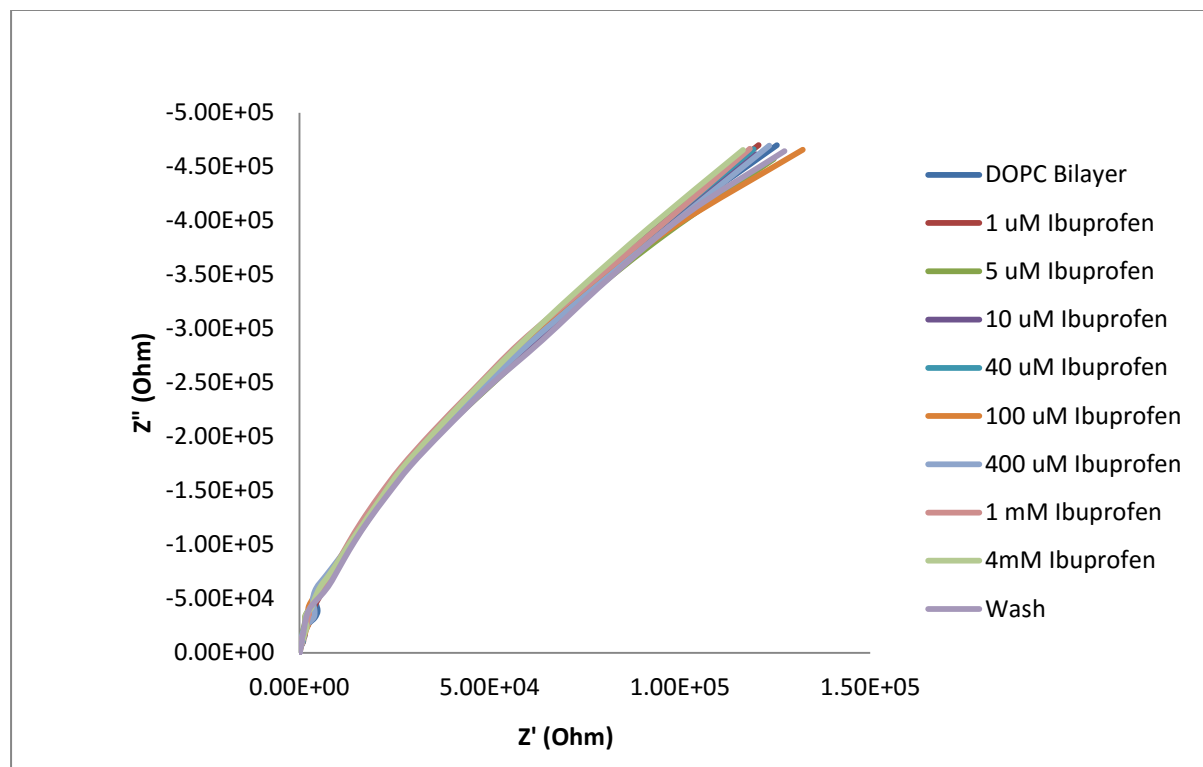


Figure 3.5: Nyquist plot titration of ibuprofen into contacting solution at a DOPC bilayer suspended across $2.80 \pm 0.04 \mu\text{m}$ cavities in a 0.01 M PBS solution (pH 7.4): frequency range 0.1 MHz to 10 mHz.

Table 3.3: Effect of ibuprofen on the resistance of a bilayer at increasing concentrations. Results represented depict real resistance values obtained. The data shown here represent that collected from two independently prepared and studied gold cavity array substrates.

Ibuprofen Concentration	N=1 (MΩ)	N=2 (MΩ)
DOPC Bilayer	7.33	11.25
1 uM	7.53	12.31
5 uM	7.30	12.42
10 uM	7.85	12.25
40 uM	7.91	12.54
100 uM	7.65	11.57
400 uM	7.79	12.28
1 mM	8.85	11.66
4 mM	8.94	12.83
Wash	9.11	12.89

It is evident from comparing resistance values from fitting across two substrate in Table 3.3, that the initial resistance values range from substrate to substrate. This is unsurprising and can be attributed as described, to numerous factors: including the uniformity of cavity packing, variations in substrate area, coverage of lipid bilayer, microscale roughness of gold substrate etc. Therefore, in comparing data across several substrates, the relative changes in bilayer resistance are reported rather than absolute values as shown in Table 3.4. It is evident from the data, and of course consistent with the EIS plots shown above, that ibuprofen induces a small but significant increase in bilayer resistance with increasing drug concentration. Such an increase suggests thickening of the bilayer.

This is attributed to deposition of ibuprofen at the membrane exterior interface, but in such manner that it is not penetrating the bilayer (which would be expected to decrease resistance). Our observations are consistent with results reported by Manrique-Moreno et al. (2009) who investigated ibuprofen with DMPC lipids and identified that it most

strongly interacted with the polar headgroups than other NSAIDs used in the study, including diclofenac. Similarly, Manrique-Moreno et al. (2011) used x-ray diffraction and differential scanning calorimetry (DSC) data to show that ibuprofen binds to DMPC multilayers and located in the polar head region but did not significantly affect the organisation of the hydrocarbon chains of the lipids.

Table 3.4: Effect of ibuprofen on the resistance of a bilayer at increasing concentrations. Results represented depict change (Δ) recorded following drug addition, relative to bilayer prior to drug interaction.

Ibuprofen Concentration	Mean ($M\Omega\text{ cm}^2$)
1 μM	$0.62 \pm 0.02\%$
5 μM	$0.56 \pm 0.02\%$
10 μM	$0.76 \pm 0.03\%$
40 μM	$0.94 \pm 0.04\%$
100 μM	$0.32 \pm 0.01\%$
400 μM	$0.76 \pm 0.03\%$
1 mM	$0.97 \pm 0.04\%$
4 mM	$1.58 \pm 0.06\%$
Wash	$1.70 \pm 0.07\%$

Dr Sivaramakrishnan Ramadurai carried out FCS experiments on PDMS substrates to investigate how ibuprofen impacted the diffusion of the lipids within the bilayer. The data is shown in Appendix 1, but to summarize: two different probes, Atto655-DOPE and β -BODIPY-C5-HPC were used to assess how ibuprofen, ranging from 0 – 1000 μM , affected the diffusion of the bilayer. Using the Atto655-DOPE probe, diffusion at 0 and 1000 μM was 11.7 ± 0.8 and $11.27 \pm 1.2\ \mu\text{m}^2/\text{s}$ respectively and using the β -BODIPY-C5-HPC probe, diffusion decreased from 14.35 ± 1.52 to $11.00 \pm 1.15\ \mu\text{m}^2/\text{s}$ respectively. These results comply with the EIS response as the Atto655-DOPE probe shows that the lipid diffusion does not alter significantly when increasing concentrations of ibuprofen are added to the membrane, and the β -BODIPY-C5-HPC probe shows a decrease in diffusion, indicating the ibuprofen is adding to the bilayer.

3.3.1.2 Diclofenac

The second NSAID Diclofenac was then studied in an identical manner at a microcavity supported DOPC bilayer. Figure 3.6 shows the impedance response at a gold MSLB to titration of concentrations of the drug: 1, 5, 10, 40, 100, 1000 and 4000 μM respectively. These concentrations were chosen in keeping with the ibuprofen drug study and again, encompass a physiologically relevant range.

At the end of the experiment after titration of the largest concentration of diclofenac, a 0.01 M PBS blank buffer (pH 7.4) solution (4 ml) was washed across the membrane to remove any unbound drug and to examine if impedance changes were reversible. From visual inspection of the EIS response, Figure 3.6, it is evident that diclofenac interacts in a much more intimate way with the bilayer. In contrast to Ibuprofen the impedance is decreasing with increasing concentration of Diclofenac at the DOPC membrane. It is also clear that the magnitude of the impedance changes is significantly greater, with a large response following the first addition of diclofenac at a concentration of 1 μM .

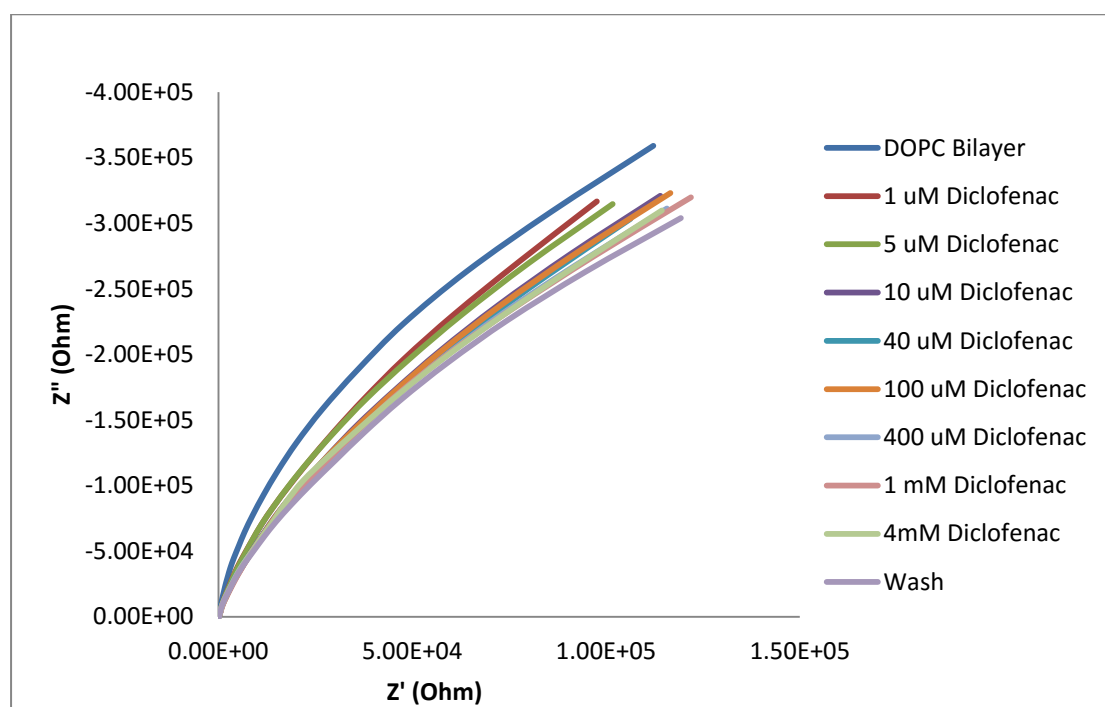


Figure 3.6: Nyquist plot of different concentrations of diclofenac and its effect on DOPC bilayer suspended across $2.80 \pm 0.04 \mu\text{m}$ cavities in a 0.01 M PBS solution (pH 7.4): frequency range 0.1 MHz to 10 mHz.

The EIS response is quantified by fitting the data to the same ECM model as described earlier. The results are plotted below in Table 3.5 which shows the average real resistance values of the membrane obtained at each concentration across a range of three samples. The relative change is shown in the last column and is evident that this change is significant when compared to the results obtained from the ibuprofen EIS analysis.

Table 3.5: Effect of diclofenac on the resistance of a bilayer at increasing concentrations. Results represented depict change (Δ) recorded following drug addition, relative to bilayer prior to drug interaction. The data shown here represent that collected from three independently prepared and studied gold cavity array substrates.

Diclofenac Concentration	$\Delta_{\text{DOPC Bilayer}}$ Mean (MΩ)
1 μM	-31.12 \pm 1.24%
5 μM	-35.83 \pm 1.43%
10 μM	-38.53 \pm 1.54%
40 μM	-38.79 \pm 1.55%
100 μM	-40.49 \pm 1.62%
400 μM	-40.67 \pm 1.63%
1 mM	-40.81 \pm 1.63%
4 mM	-41.52 \pm 1.66%
Wash	-42.72 \pm 1.71%

The resistance change is much larger in magnitude and is illustrated in the graph, Figure 3.7. This data shows that after the initial addition of the diclofenac, a decrease in membrane resistance is observed instantaneously. Interestingly, the plot suggests that saturation binding of diclofenac is occurring at approximately 5 μmol .

Decreasing resistance indicates the bilayer is becoming less well-packed, and leaky. Our observations are consistent results reported by Moreno et al. (2009) where they showed that diclofenac interacts with a DMPC bilayer where phase separation of the hydrocarbon

chains was observed resulting in diclofenac-rich and diclofenac-poor phases, with destabilisation of the bilayer reported at increasing concentrations. Kaur and Sanyal (2010) used diclofenacs interactions with the membrane as a chemopreventative approach to initial stages of colon cancer induced by 1,2-dimethylhydrazine as diclofenac induced permeabilisation of the mitochondrial membrane and released cytochrome c and subsequently induced apoptosis

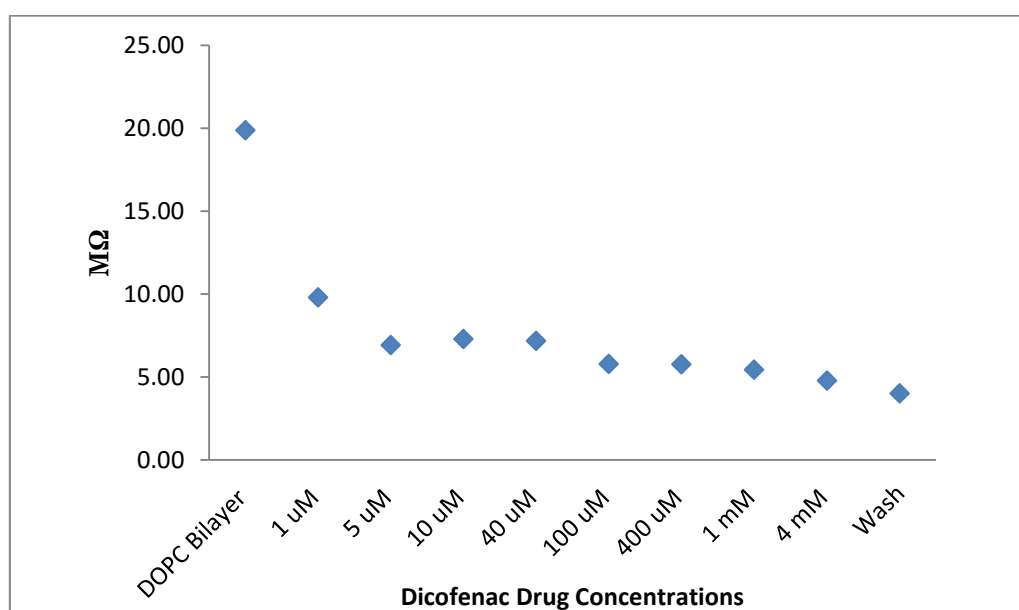


Figure 3.7: Effect of diclofenac on the resistance of a bilayer at increasing concentrations.

As diclofenac was prepared in a methanol solvent, a control was conducted to ensure that the membrane resistance change was due to the interaction with the drug, diclofenac with the membrane and not due to membrane disruption by methanol. Organic solvent, is frequently used in cell imaging to permeablise membranes, and is thought at concentrations in the range of 3 to 5% V/V to cause membrane scrambling, however the final alcohol concentrations used here are below this level (Patra et al., 2006). This is confirmed where the DOPC EIS was measured over a range of methanol volumes added to the 0.01 M PBS electrochemical cell (v/v %) which corresponded to the methanol concentration used here. Figure 3.8 shows methanol has an initial response causing the membrane resistance to decrease, the magnitude of this response is the same over 15

minutes, but following this initial interaction, it is evident that any subsequent additions do not impose a large resistance change. These results confirm that the change in resistance observed numerically in Figure 3.7 is due to the mechanism by which diclofenac interacts with the DOPC membrane.

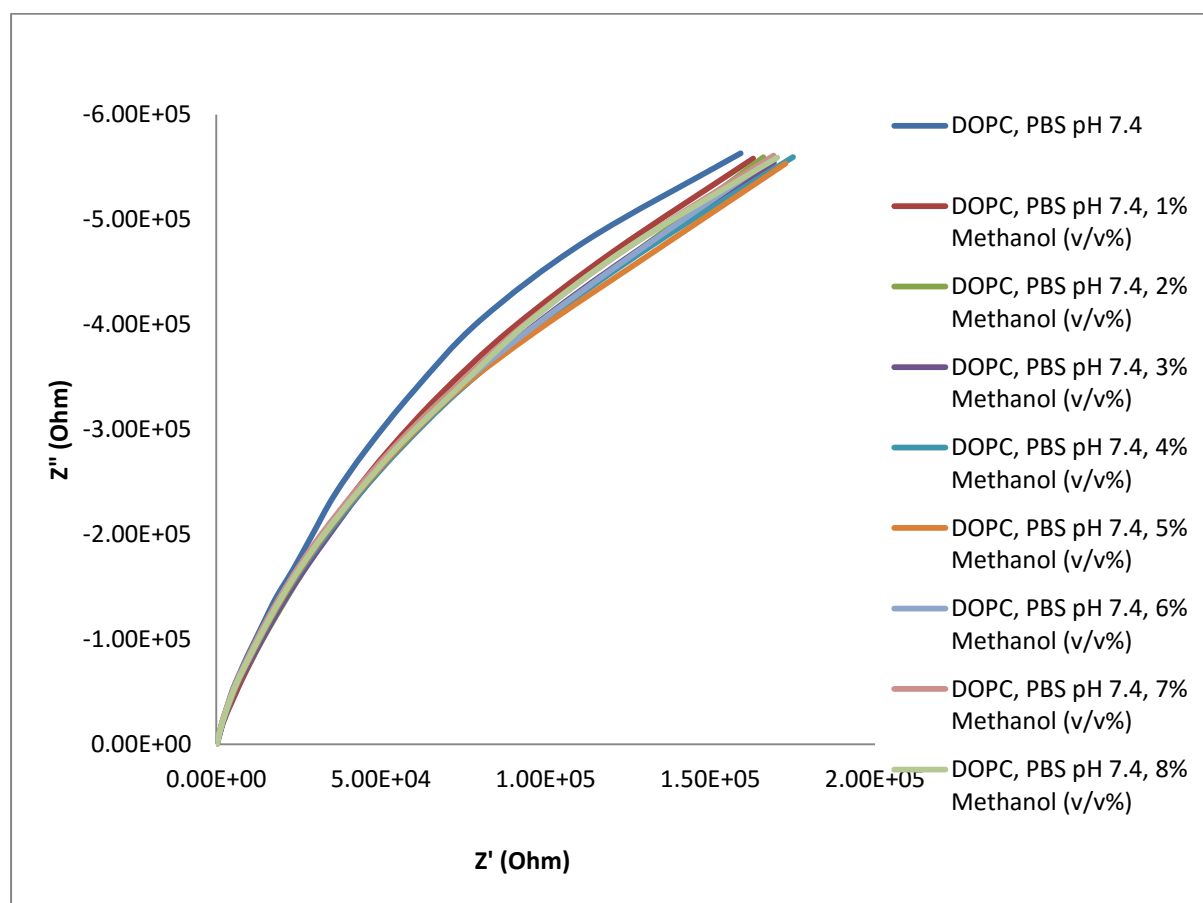


Figure 3.8: Nyquist plot of different v/v % values of methanol additions to 0.01 M PBS solution (pH 7.4) and its effect on DOPC bilayer suspended across $2.80 \pm 0.04 \mu\text{m}$ cavities in a: frequency range 0.1 MHz to 10 mHz.

The fitted resistance values in Table 3.6 show the magnitude of resistance decrease at the bilayer. Importantly, the relative change caused by diclofenac dissolved in nearly an order of magnitude larger than for methanol alone.

Table 3.6: Effect of the solvent methanol on the resistance of the bilayer at increasing volumes.

Methanol Volume/Volume % (V/V %)	$\Delta_{\text{DOPC Bilayer}}$ Mean (M Ω)
1 %	-5.36 \pm 0.21%
2 %	-5.83 \pm 0.23%
3 %	-5.33 \pm 0.21%
4 %	-5.13 \pm 0.21%
5 %	-4.89 \pm 0.20%
6 %	-5.04 \pm 0.20%
7 %	-4.98 \pm 0.20%
8 %	-4.66 \pm 0.19%

This is also represented in graph format in Figure 3.9 and it again illustrates the large change in resistance is due to the diclofenacs interaction with the DOPC bilayer. The initial response is impacted slightly by the methanol but after this, the change is relatively small.

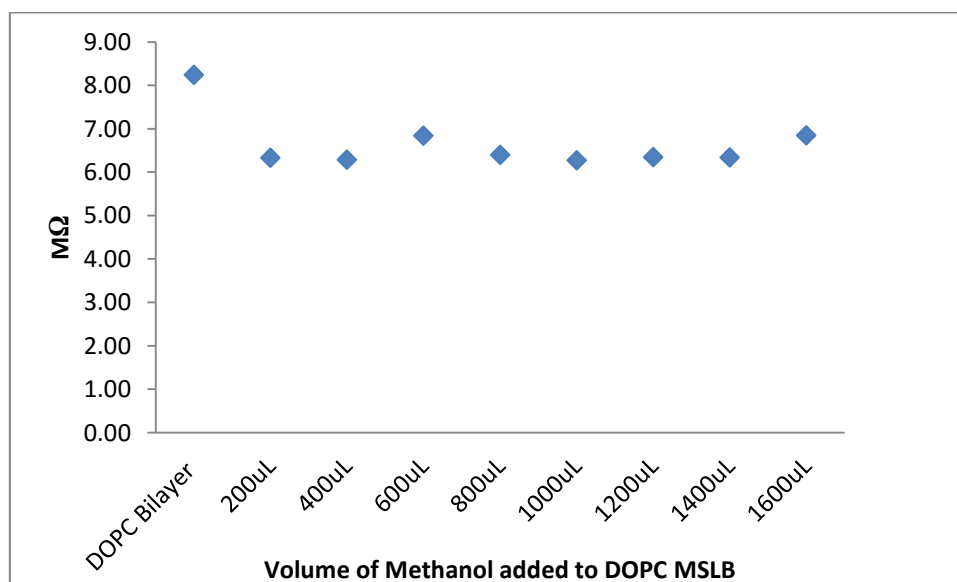


Figure 3.9: Effect of increasing volumes of methanol on DOPC MSLB.

To ensure that diclofenac binding had equilibrated within the time-scale of the studies above, the time-course of EIS was followed following addition of 100 μM to the contacting buffer solution. Figure 3.10 shows this study and confirms that beyond the initial 30 minutes there is no further change in the EIS signal. This is further confirmed by reference to fitted data shown in Table 3.7. This data confirms that during a single titration, both the fundamental EIS signal is stable and that drug membrane interaction equilibrates within the 15 minutes equilibration time applied to each measurement. Interestingly, and consistent with the proposed penetration of diclofenac into the layer compared with ibuprofen surface adsorption, diclofenac takes about 15 minutes to equilibrate, whereas ibuprofen induced in the EIS changes are instantaneous.

The stability of the EIS signal is again notable, showing the temporal stability of these MSLBs.

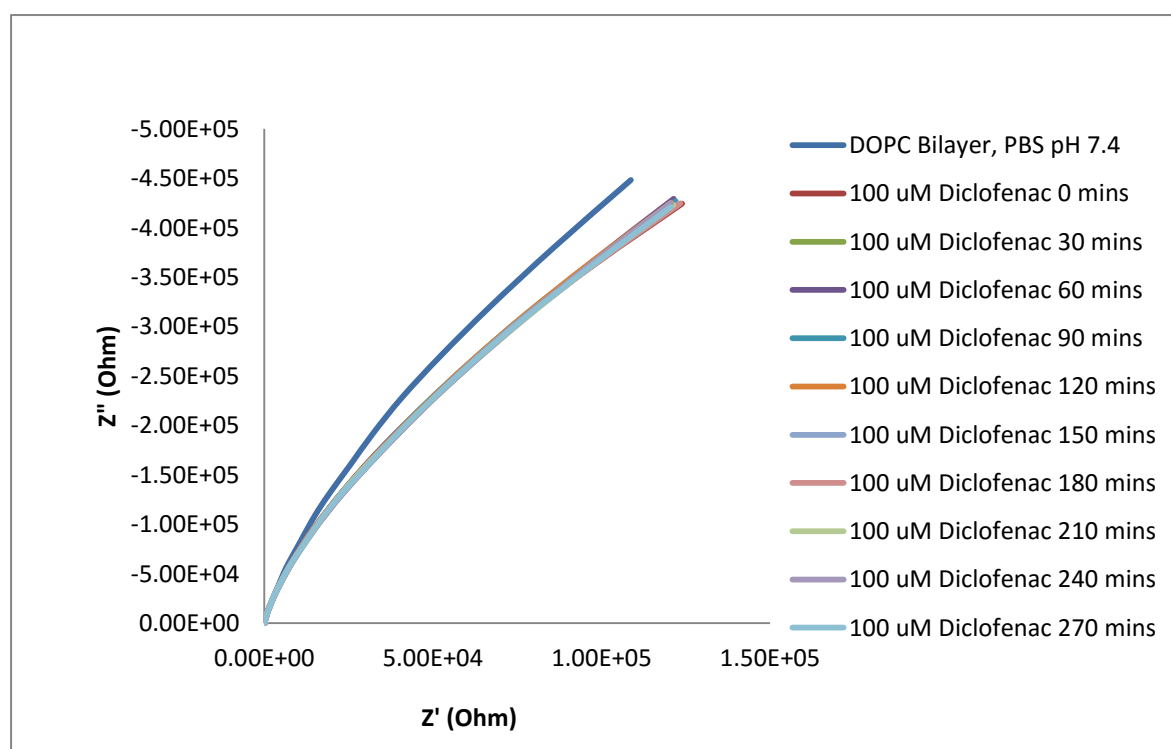


Figure 3.10: Nyquist plot of 100 μM concentration of diclofenac and its effect on DOPC bilayer suspended across $2.80 \pm 0.04 \mu\text{m}$ cavities in a 0.01 M PBS solution (pH 7.4) over time: frequency range 0.1 MHz to 10 mHz.

Table 3.7: Diclofenac control investigating stability of response after interaction.

100 μM Diclofenac	$\Delta_{\text{DOPC Bilayer}}$ Mean (MΩ)
0 mins	-38.71 \pm 1.55%
30 mins	-38.21 \pm 1.53%
60 mins	-39.73 \pm 1.59%
90 mins	-40.20 \pm 1.61%
120 mins	-39.99 \pm 1.60%
150 mins	-39.00 \pm 1.56%
180 mins	-39.50 \pm 1.58%
210 mins	-38.03 \pm 1.52%
240 mins	-39.29 \pm 1.57%
270 mins	-39.17 \pm 1.57%

Additionally, Dr Sivaramakrishnan Ramadurai carried out FCS experiments on PDMS substrates to investigate how diclofenac impacted the diffusion of the lipids within the bilayer when it was introduced to the external solution. The data is shown in Appendix 1, but to summarize: using the Atto655-DOPE probe, diffusion at 0 and 1000 μ M increased from 11.7 ± 0.8 to $41.5 \pm 8.0 \mu\text{m}^2/\text{s}$ respectively and using the β -BODIPY-C5-HPC probe, diffusion decreased from 14.35 ± 1.52 to $10.00 \pm 0.9 \mu\text{m}^2/\text{s}$ respectively. These results comply with the EIS response as the Atto655-DOPE probe shows that the lipid diffusion increase significantly when increasing concentrations of diclofenac are added to the membrane. This data complies with the change observed in EIS. As EIS showed a decrease in membrane resistance, FCS showed an increase in lipid diffusion implying that the membrane had been disturbed and became increasingly leaky.

It has been shown through x-ray diffraction studies of diclofenac with human erythrocytes that diclofenac reduces order in the membrane structure and this study is consistent with this picture (Suwalsky et al. 2010). The reduction in membrane resistance indicates the membrane is becoming more ion permeable, which is likely to be due to formation of nanoscale defects in the layer induced by the drug. Manrique-Moreno et al. (2009)

carried out a detailed study on the IR spectroscopy and calorimetry of NSAIDs; ibuprofen, diclofenac, and naproxen on aqueous suspensions of dimyristoylphosphatidylcholine (DMPC). They concluded that these drugs interacted with the phosphate region within the headgroup of the lipid but also noted that they reduced chain-chain interactions in the lipid tails, which they described as a fluidization effect. They noted that a phase separation is observed, inducing the formation of a NSAID-rich and a NSAID-poor phase which was particularly pronounced for diclofenac, although they noted that FRET did not show internalisation of the drugs into the lipid bilayer. This is the first study to our knowledge of EIS as a means of studying NSAIDs-lipid bilayer interactions.

The advantage of EIS is that it is sensitive but also directly reflects the packing of the lipid or deposition of a thicker film. Our results indicate that ibuprofen does not intercalate strongly in the hydrophobic membrane region, but thickens the bilayer film, most likely by binding electrostatically at membrane surface as noted by Manrique-Moreno et al. 2009. Conversely, EIS data on diclofenac shows strong evidence for intercalation and its penetration into the layer with, in contrast to ibuprofen, a reduction in membrane resistance associated with a decrease in order and permeability/leakiness of the layer.

3.3.2 Enhancing the Ibuprofen EIS response

The impact of Ibuprofen on the MSLB impedance was small. As described it is believed that this is because it binds only at the membrane surface, thickening rather than disrupting the film. The research then focused on trying to amplify the EIS response so that even small changes, which reflect such binding, could be seen more clearly. A very significant advantage of using the cavity arrays is that they offer the opportunity to fill the cavities with a solution which is dissimilar to the contacting solution at the bilayer distal leaflet. Using this approach an ionic gradient was used by introducing 0.01 M PBS, pH 7.4 within the cavities and 600 mM NaCl 0.01 M PBS, pH 7.5 in the external environment (within the electrochemical cell). The Nernst potential mathematically expresses the equilibrium potential for a single ion species in an environment where there are unequal concentrations in two compartments which are separated by a thin membrane:

$$E = \left[\frac{RT}{zF} \right] \ln\{C(out)/C(in)\}$$

Equation 3.3

Where E is the potential, R is the gas constant, T is the actual temperature, z is the number of charges on the ionic species, F is the Faraday constant and C is the concentration: 'C(out)' refers the extracellular concentration and 'C(in)' refers to the intracellular concentration. Therefore, by employing an ionic gradient, this sets up a membrane potential across the impermeable bilayer.

This membrane potential can then only be dissipated when the membrane becomes increasingly leaky. This dissipation of the membrane potential would then induce an increased change in the interfacial membrane resistance compared to a membrane at equilibration. In other words, by creating a larger membrane capacitance, this creates the potential for larger changes in film resistance and hence amplifying response. Figure 3.11 shows a representative EIS response of a DOPC MSLB with the above ionic gradient and the impact of the addition of ibuprofen in an identical method as done previously on the EIS data. The first EIS measurements show the stability of this new MSLB format. There is a little more drift in EIS signal over time than observed in the absence of the gradient, however, interestingly, unlike the ionically equilibrated membranes the EIS undergoes a dramatic change on introduction of ibuprofen with a significant decrease in membrane impedance.

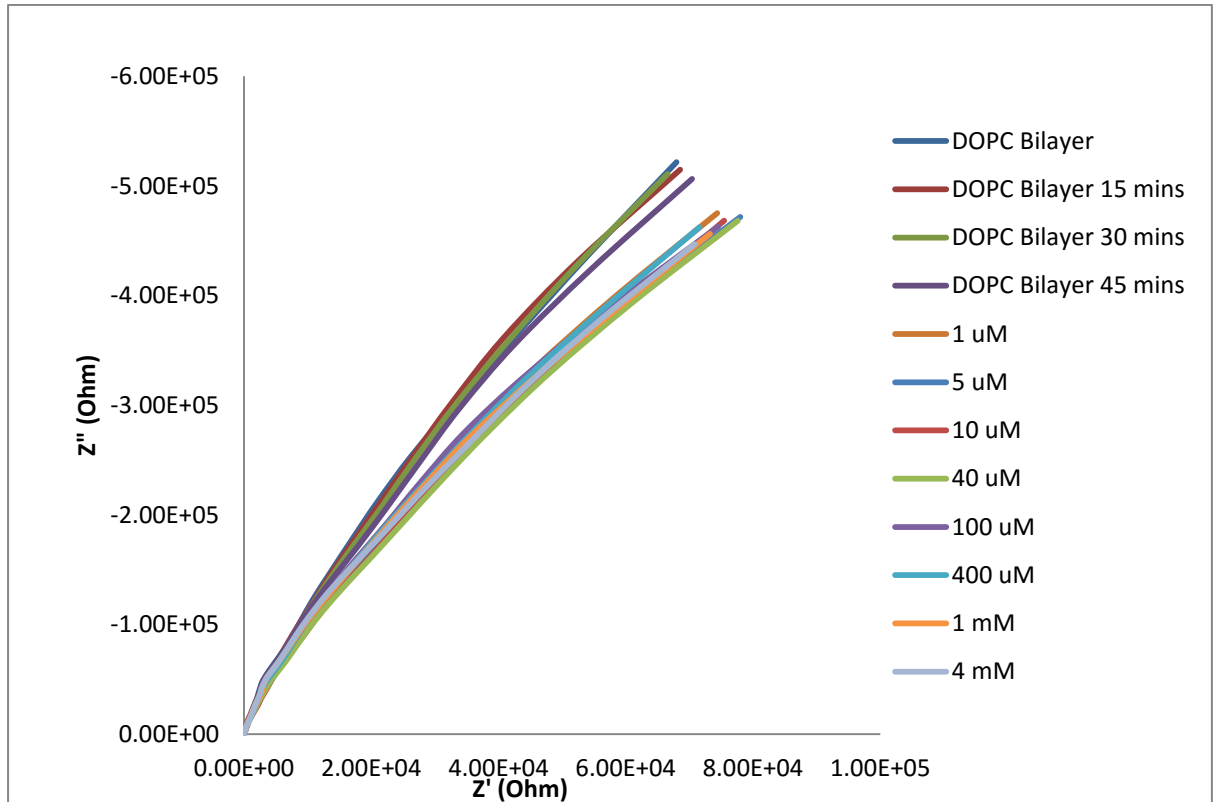


Figure 3.11: Nyquist plot of various concentrations of ibuprofen and its effect on a DOPC bilayer suspended across $2.80 \pm 0.04 \mu\text{m}$ cavities in a 0.01 M PBS solution ($\text{pH } 7.4$) with 0.6 M NaCl over time: frequency range 0.1 MHz to 10 mHz .

This initial data indicated that as soon as ibuprofen is added to the MSLB, there is a decrease in resistance of the bilayer which then remains relatively constant, even with the addition of increasing concentration. To assess whether this was simply a stability issue relating to the ionic gradient the EIS of DOPC bilayer in this ionic gradient environment was monitored over time. Figure 3.12 shows a representative experiment..

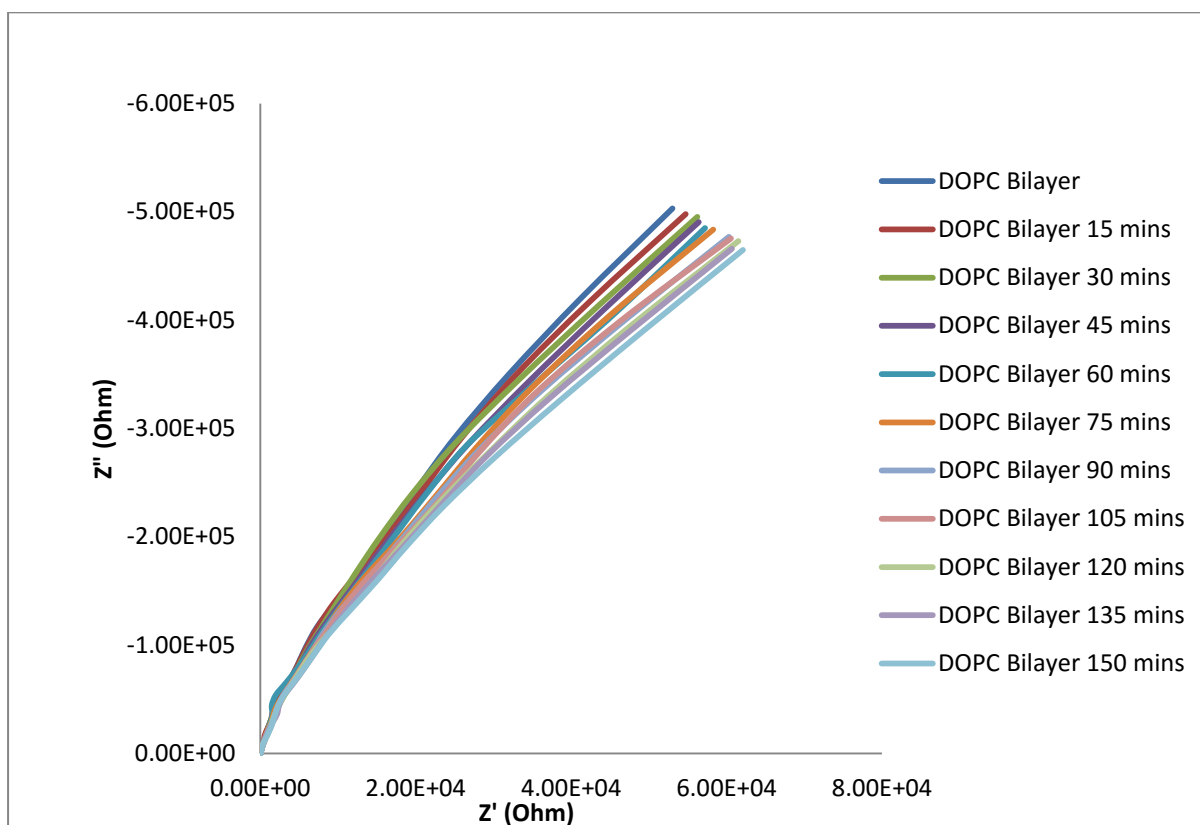


Figure 3.12: Nyquist plot of stabilisation of a DOPC bilayer suspended across $2.80 \pm 0.04 \mu\text{m}$ cavities in a 0.01 M PBS solution (pH 7.4) with 0.6 M NaCl over time: frequency range 0.1 MHz to 10 mHz.

Figure 3.12 shows that the MSLB is less stable in the ionic gradient as the EIS response shows a consistent decrease over time. This may be due to some loss of the gradient between the external and inner cavity environments over time perhaps due to loss of suspended bilayer over some pores. Using this information a rest time was implemented to allow the MSLB to stabilise before the addition of the drug.

The addition of ibuprofen to the MSLB using an ionic gradient was repeated when the bilayer had stabilised (Figure 3.13).

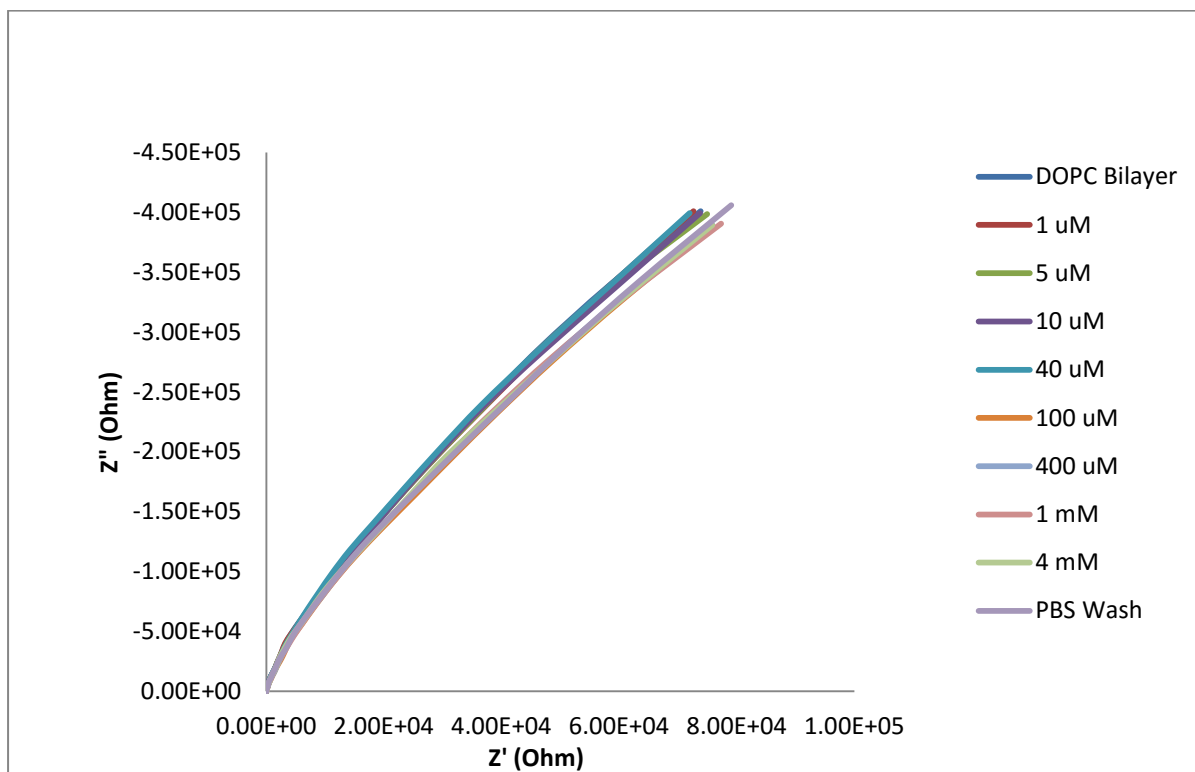


Figure 3.13: Nyquist plot of various concentrations of ibuprofen and its effect on a DOPC bilayer suspended across $2.80 \pm 0.04 \mu\text{m}$ cavities which was allowed to stabilise in a 0.01 M PBS solution ($\text{pH } 7.4$) with 0.6 M NaCl over time: frequency range 0.1 MHz to 10 mHz .

On implementation of a 180 minutes rest period it was found, as shown in Figure 3.13, that ibuprofen did not alter the bilayer as significantly as initially noted, therefore at least some of the change is ascribed to the bilayer stability.

3.3.3 Improving the stability of the EIS response

It was investigated if further improvements to the stability of the arrays with ion gradients could be achieved in the MSLB by increasing the chain length of the mercapto-alcohol group used to create the hydrophilic surface. This approach highlights one of the other advantages of the MSLB; Because of the templating mode of preparation, it is possible to selectively modify the substrate so that SAMS are prepared only at the top surface of the array. SAM absorption to gold surfaces is a simple technique to modify and functionalise the array. 2-mercapto-ethanol was the SAM system used in the above studies; however in

the following two investigations the impact of modifying the top surface of the array with, 6-mercaptohexanol and 11-mercaptoundecanol on the ibuprofen was investigated.

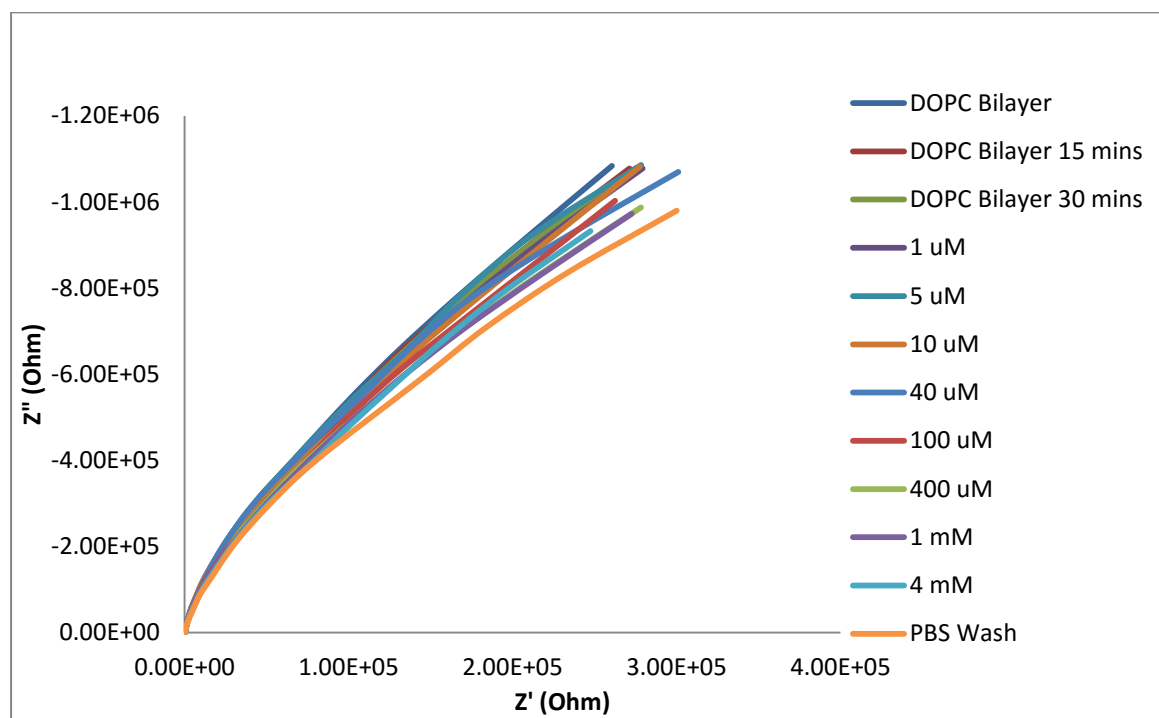


Figure 3.14: Nyquist plot of various concentrations of ibuprofen and its effect on a DOPC bilayer suspended across $2.80 \pm 0.04 \mu\text{m}$ gold cavities which were surface modified with 11-mercapto-undecanol in a 0.01 M PBS solution (pH 7.4) with 0.6 M NaCl over time: frequency range 0.1 MHz to 10 mHz.

Figure 3.14 illustrates the EIS response when 11-mercaptoundecanol replaces 2-mercaptoethanol as the SAM. This EIS response is one that is unstable as there are greater fluctuations in response. These changes are not consistent as they increase and decrease irregularly. This implies that using 11-mercaptoundecanol is a more unstable option as a SAM. The reason for the poor stability is unclear, but would seem to indicate that the bilayer is less stable suspended at these long chain lengths. One explanation may be that the water meniscus is prevented from contacting properly with the bilayer because of the hydrophobic chains of the monolayer at the top surface causing deformation and reduced stability of the bilayer across the pores.

If this was the case, then a shorter chain length alkane should improve bilayer stability. With this in mind, an intermediate chain length using of 6-mercapto-hexanol was investigated. Figure 3.15, shows a response that is stable and is similar to that of 2-mercaptoethanol. The comparison between the two SAMs is difficult to represent visually in the graph, however EIS fitting provides useful insights (Table 3.8).

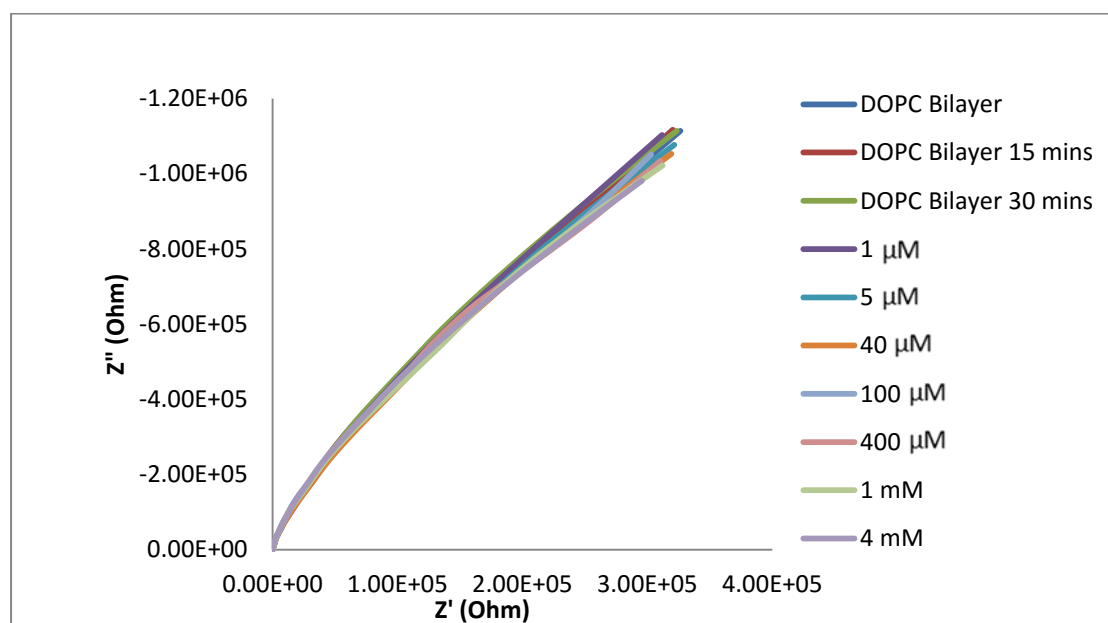


Figure 3.15: Nyquist plot of titration of ibuprofen into the MSLB contacting solution (concentration indicates final concentration in the solution) and its effect on EIS of a DOPC bilayer suspended across $2.80 \pm 0.04 \mu\text{m}$ gold cavities top surface modified with 6-mercapto-hexanol in a 0.01 M PBS solution (pH 7.4) with 0.6 M NaCl over time: frequency range 0.1 MHz to 10 mHz.

Table 3.8: Effect of using 6-mercapto-hexanol as a surface modifier to improve the MSLB model.

Ibuprofen Concentration	$\Delta_{\text{DOPC Bilayer}}$ Mean (MΩ)
1 μM	0.11 \pm 0.09
5 μM	0.13 \pm 0.06
10 μM	-0.32 \pm 0.02
40 μM	-0.37 \pm 0.07
100 μM	-0.17 \pm 0.15
400 μM	-0.67 \pm 0.09
1 mM	-0.74 \pm 0.01
4 mM	-0.62 \pm 0.07
Wash	-0.87 \pm 0.09

6-mercaptohexanol appears to be a superior top surface modifier to either 2-mercaptoethanol or 11-mercaptoundecanol for bilayer measurements incorporating ionic gradients. In the presence of 6-mercaptohexanol the bilayers were more stable, resulting in a lower percentage deviation. This is an encouraging as it provides a small but significant advancement to the MSLB, as the sensitivity as now been improved by changing two of the components of the model: ionic gradient and surface modifier.

3.4 Conclusions

To conclude, MSLBs pose a unique, electrochemical alternative to investigate the affect that various drugs have when they permeate through the membrane. This is a much needed technique in current pharmaceutical research as currently a substantial amount of money and time is being investigated into improving drug permeability.

Aqueous filled microcavity supported lipid bilayers were prepared at uniform 2.80 ± 0.04 μm diameter gold micropore array electrodes. The impact of introducing ibuprofen and diclofenac over a range of concentrations on the resistance of the DOPC film was compared. Ibuprofen caused an increase in the electrochemical resistance of the lipid bilayers which is in keeping with literature reports which discuss how ibuprofen interacts with the hydrophilic head groups of the bilayer. Conversely, diclofenac caused a decrease in membrane resistance. The magnitude of the change caused by diclofenac was much greater than that of the ibuprofen, as it interacts with the hydrophobic tails of the lipids. Control experiments were conducted for both drugs and these conclude that the changes observed in the membranes resistance are due to the NSAIDs used in the study. These changes were irreversible after washing.

Latter experiments focused on the improvement of the MSLB by investigating the stability of a DOPC bilayer when an ionic gradient was applied and when various alcoholthiols were used as SAMs. These experiments demonstrated that 6-mercaptohexanol appears to be a superior top surface modifier to either 2-mercaptoethanol or 11-mercaptopundecanol for bilayer measurements incorporating ionic gradients. Overall the MSLB platform is expected to be useful in providing valuable insights into the fundamental behaviour of lipid membranes and the influence of agents on their structure and molecular membrane permeability. The value of these models crosses a range of sectors including pharmaceuticals and cosmetics.

3.5 References

Aldwaikat, M. and Alarjah, M. 2015. Investigating the sonophoresis effect on the permeation of diclofenac sodium using 3D skin equivalent *Ultrasonics Sonochemistry*, 22pp.580-587.

Alsop, R.J., Armstrong, C.L., Magbool, A., Topozini, L., Dies, H. and Rheinstädter, M.C. 2015. Cholesterol expels ibuprofen from the hydrophobic membrane core and stabilizes lamellar phases in lipid membranes containing ibuprofen. *Soft Matter*, 11(24), pp. 4756-4767.

Becucci, L., Innocenti, M., Salvietti, E., Rindi, A., Pasquini, I., Vassalli, M., Foresti, M.L. and Guidelli, R. 2008. Potassium ion transport by gramicidin and valinomycin across a Ag(111)-supported tethered bilayer lipid membrane. *Electrochimica Acta*, 53(22), pp.6372-6379.

Busson, M. 1986. Update on ibuprofen: Review article. *Journal of International Medical Research*, 14(2), pp.53-62.

Cilurzo, F., Alberti, E., Minghetti, P., Gennari, C.G.M., Casiraghi, A. and Montanari, L. 2010. Effect of drug chirality on the skin permeability of ibuprofen. *International Journal of Pharmaceutics*, 386(1-2), pp.71-76.

Darvas, M., Hoang, P.N., Picaud, S., Sega, M. and Jedlovszky, P. 2012. Anesthetic molecules embedded in a lipid membrane: A computer simulation study. *Physical Chemistry Chemical Physics*, 14(37), pp.12956-12969.

de Ghellinck, A., Fragneto, G., Laux, V., Haertlein, M., Jouhet, J., Sferrazza, M. and Wacklin, H. 2015. Lipid polyunsaturation determines the extent of membrane structural changes induced by amphotericin B in *pichia pastoris* yeast. *Biochimica Et Biophysica Acta (BBA) - Biomembranes*, 1848(10, Part A), pp.2317-2325.

Deavall, D.G., Martin, E.A., Horner, J.M. and Roberts, R. 2012. Drug-induced oxidative stress and toxicity. *Journal of Toxicology*, 2012

Di, L. and Kerns, E.H. 2010. *Drug-like Properties: Concepts, Structure Design and Methods: from ADME to Toxicity Optimization*. Academic Press.

Dua, L., Liua, X., Huang, W. and Wang, E. 2006. A study on the interaction between ibuprofen and bilayer lipid membrane *Electrochimica Acta*, 51(26), pp.5754-5760.

Hille, B. 2001. *Ion channels of excitable membranes*. Sinauer Sunderland, MA.

Kamiński, D.M., Pocięcha, D., Górecka, E. and Gagoś, M. 2015. The influence of amphotericin B on the molecular organization and structural properties of DPPC lipid membranes modified by sterols. *Journal of Molecular Structure*, 1082, pp.7-11.

Kaplowitz, N. 2004. Drug-induced liver injury. *Clinical Infectious Diseases : An Official Publication of the Infectious Diseases Society of America*, 38 Suppl 2pp.S44-8.

Lemke, T.L. and Williams, D.A. 2012. *Foye's Principles of Medicinal Chemistry*. Lippincott Williams & Wilkins.

Levis, K.A., Lane, M.E. and Corrigan, O.I. 2003. Effect of buffer media composition on the solubility and effective permeability coefficient of ibuprofen *International Journal of Pharmaceutics*, 253(1-2), pp.49-59.

Manrique-Moreno, M., Garidel, P., Suwalsky, M., Howe, J. and Brandenburg, K. 2009. • The membrane-activity of Ibuprofen, Diclofenac, and Naproxen: A physico-chemical study with lecithin phospholipids. *Biochimica et Biophysica Acta (BBA) - Biomembranes*, 1788(6), pp.1296-1303.

Manrique-Moreno, M., Villena, F., Sotomayor, C.P., Edwards, A.M., Muñoz, M.A. and Garidel, P. 2011. Human cells and cell membrane molecular models are affected in vitro by the nonsteroidal anti-inflammatory drug ibuprofen. *Biochimica et Biophysica Acta (BBA) - Biomembranes*, 1808(11), pp. 2656-2664.

Ng, K.M., Gani, R. and Dam-Johansen, K. 2006. *Chemical Product Design: Towards a Perspective through Case Studies: Towards a Perspective through Case Studies*. Elsevier.

Patra, M., Salonen, E., Terama, E., Vattulainen, I., Faller, R., Lee, B.W., Holopainen, J. and Karttunen, M. 2006. Under the Influence of Alcohol: The Effect of Ethanol and Methanol on Lipid Bilayers. *Biophysical Journal*, 90(4), pp. 1121-1135.

Patrick, G.L. 2005. *An Introduction to Medicinal Chemistry*. 3rd ed. New York, United States: Oxford University Press.

Rose, L. and Jenkins, A.T.A. 2007. The effect of the ionophore valinomycin on biomimetic solid supported lipid DPPTE/EPC membranes. *Bioelectrochemistry*, 70(2), pp.387-398.

Schreier, S., Malheiros, V.P. and de Paula, E. 2000. Surface active drugs: self-association and interaction with membranes and surfactants. Physicochemical and biological aspects. *Biochimica et Biophysica Acta* 1508, pp. 210-234.

Suwalsky, M., Manrique, M., Villena, F. and Sotomayer, C.P. 2010. Phospholipid Bilayers as Molecular Models for Drug-Cell Membrana Interactions. The Case of the Antiinflammatory Drug iclofenac. *Macromolecular Symposia*, 296(1), pp. 436-445.

Talele, P., Choudhary, S. and Kishore, N. 2016. Understanding thermodynamics of drug partitioning in micelles and delivery to proteins: Studies with naproxen, diclofenac sodium, tetradecyltrimethylammonium bromide, and bovine serum albumin *The Journal of Chemical Thermodynamics*, 92pp.182-190.

Yamamoto, T., Umegawa, Y., Tsuchikawa, H., Matsumori, N., Hanashima, S., Murata, M., Haser, R., Rawlings, B.J. and Caffrey, P. 2015. Role of polyol moiety of amphotericin B in ion channel formation and sterol selectivity in bilayer membrane. *Bioorganic & Medicinal Chemistry*, 23(17), pp. 5782-5788.

4.0 Introduction

Gangliosides (GSLs) comprise an oligosaccharide (sugar) and lipid (ceramide) tail and reside within the outer leaflet of all cell-membranes. Despite their wide prevalence in mammalian cells, the extent of the role that the GSL association with their partner galectin (protein) receptor plays in signalling, infection, immune response, cancer and reproduction is only recently being fully realised.

Upon GSL binding to galectin (lectin), the pair oligomerise to form an ordered network or lattice within the cell membrane. The structure of this oligomerisation is controlled by galectin identity and, it is suspected, by lipid membrane composition. This 2-dimensional self-assembly is the cornerstone of GSL-galectin signalling. To date, this interaction has yet to be studied systematically outside of cell models, primarily because of the limitations of cell membrane models. A model is required which is both highly fluidic to allow diffusion driven assembly but also which can be used to build asymmetric bilayers. Liposomes for example enable the former but not the latter and SLBs the latter but not the former. The microcavity array supported lipid bilayers enable both. Herein, the relative impact of interaction of galectin 1, 3 and recombinant galectin 3 (truncated) (Galectin-1, Galectin-3 or Galectin-3t) with GM1 on the packing and structure of a DOPC bilayer using Electrochemical Impedance Spectroscopy is reported.

4.1 Glycobiology

Glycobiology is a term first coined in 1988 by Rademacher, Parekh and Dwek to address the combination of carbohydrate chemistry and biochemistry with an emphasis on understanding the cellular and molecular biology of glycans (Varki et al. 1999). Glycobiology has numerous applications in research, biomedicine and biotechnology in areas of carbohydrate chemistry, glycan-modifying proteins and their enzymology and also glycans and their function in complex biological systems.

Carbohydrates have biological roles in interactions between cells and the external matrix and it is becoming increasingly clear that they are critical components in the assembly of complex multicellular organs and organisms whereas previously they were only viewed as having roles in structure and energy production. Glycans are compounds comprising of a large number of covalently attached sugars (monosaccharides) or sugar chains (oligosaccharides) that are linked glycosidically with biological roles spanning from subtle functions to roles that are crucial in the organism's development, growth, functioning, or survival (Varki, Cummings and Esko 2009). A glycosidic linkage links a hydroxyl group of one monosaccharide to another residue. These linkages can be α linkages or β linkages depending on the relationship between the anomeric carbon (stereocenter) and the oxygen. Glycans can be compounds that are free-standing but most are located on the outer surface of cell membranes as secreted macromolecules to function in the development of complex multicellular organisms. (Varki, Cummings and Esko 2009). Glycans and their various forms are shown in Figure 4.1.

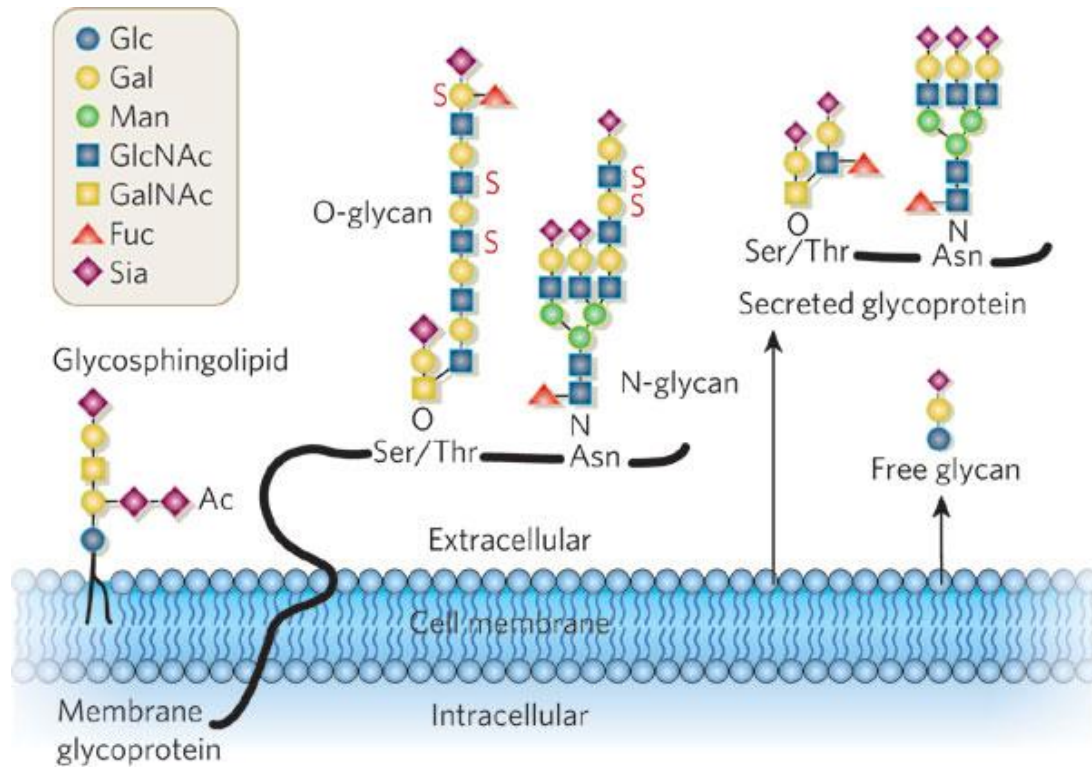


Figure 4.1: Illustration depicting a variety of glycan molecules embedded within the plasma membrane, which are located in an ideal position that is critical to the development and function of complex multicellular organisms by acting as mediators between a wide variety of events in cell-cell, cell-matrix, and cell-molecule interactions (Varki 2007).

Based on the diversity of glycans, there are hundreds of different ganglioside structures which are defined by the ceramide and the sugars attached to it as illustrated in Table 4.1, which depicts the structures of the most common eukaryote gangliosides.

Table 4.1: Gangliosides most commonly found in eukaryotes with structures, commonly used abbreviations and IUPAC-IUB nomenclature (Cantù et al. 2011).

Oligosaccharide chain core structure	Trivial abbreviation	IUPAC-IUB nomenclature
β -Galactin-(1-1)-Cer	GM4	Neu5AcGalactinCer
β -Galactin-(1-4)- β -Glc-(1-1)-Cer	GM3	II ³ Neu5AcLacCer
	GD3	II ³ (Neu5Ac) ₂ LacCer
	O-acetyl-GD3	II ³ [Neu5,9Ac ₂ -(2-8)-Neu5Ac]LacCer
β -GalactinNAc-(1-4)- β -Galactin-(1-4)- β -Glc-(1-1)-Cer	GM2	II ³ Neu5AcGg ₃ Cer
	GD2	II ³ (Neu5Ac) ₂ Gg ₃ Cer
β -Galactin-(1-3)- β -GalactinNAc-(1-4)- β -Galactin-(1-4)- β -Glc-(1-1)-Cer	GM1	II ³ Neu5AcGg ₄ Cer
	GM1b	IV ³ Neu5AcGg ₄ Cer
	Fuc-GM1	IV ² α FucII ³ Neu5AcGg ₄ Cer
	GD1a	IV ³ Neu5AcII ³ Neu5AcGg ₄ Cer
	GD1 α	IV ³ Neu5AcIII ⁶ Neu5AcGg ₄ Cer
	GD1b	II ³ (Neu5Ac) ₂ Gg ₄ Cer
	GD1b-lactone	II ³ [Neu5Ac-(2-8,1-9)-Neu5Ac]Gg ₄ Cer
	Fuc-GD1b	IV ² α FucII ³ Neu5Ac ₂ Gg ₄ Cer
	GT1a	IV ³ (Neu5Ac) ₂ II ³ Neu5AcGg ₄ Cer
	GT1b	IV ³ Neu5AcII ³ (Neu5Ac) ₂ Gg ₄ Cer
	O-Acetyl-GT1b	IV ³ Neu5AcII ³ [Neu5,9Ac ₂ -(2-8)-Neu5Ac]Gg ₄ Cer
	GT1c	II ³ (Neu5Ac) ₃ Gg ₄ Cer
	Chol-1 α -a	IV ³ Neu5AcIII ⁶ Neu5AcII ³ Neu5AcGg ₄ Cer
	Chol-1 β	III ⁶ Neu5AcII ³ (Neu5Ac) ₂ Gg ₄ Cer
	GT1 α	IV ³ Neu5AcIII ⁶ (Neu5Ac) ₂ Gg ₄ Cer
	GQ1b	IV ³ (Neu5Ac) ₂ II ³ (Neu5Ac) ₂ Gg ₄ Cer
	GQ1c	IV ³ Neu5AcII ³ (Neu5Ac) ₃ Gg ₄ Cer
	GQ1 α	IV ³ (Neu5Ac) ₂ III ⁶ (Neu5Ac) ₂ Gg ₄ Cer
	Chol-1 α -b	IV ³ Neu5AcIII ⁶ Neu5AcII ³ (Neu5Ac) ₂ Gg ₄ Cer
	GP1c	IV ³ (Neu5Ac) ₂ II ³ (Neu5Ac) ₃ Gg ₄ Cer
β -GalactinNAc-(1-4)- β -Galactin-(1-3)- β -GalactinNAc-(1-4)- β -Galactin-(1-4)- β -Glc-(1-1)-Cer	GalectinNAc-GM1	II ³ Neu5AcGg ₅ Cer
	GalectinNAc-GD1a	IV ³ Neu5AcII ³ Neu5AcGg ₅ Cer

Gangliosides are the major glycans on nerve cells and are sialic-bearing glycosphingolipids (GSLs) (Lopez and Schnaar 2009). Glycosphingolipids have a similar structure to phospholipids with the exception that in glycosphingolipids, the head group is a variety of sugars joined to form a carbohydrate chain either straight or branching, which function in protection, inhibition of GSL synthesis and others where a specific GSL has a specific role (Mader 2001, Schnaar, Suzuki and Stanley 2009, Lingwood 2011).

The lipid portion is a ceramide chain which is responsible for the ganglioside insertion in the lipid bilayer and is composed of a long chain amino alcohol, 2-amino-1,3-dihydroxy-octadec-4-ene, linked by an amide bond with a fatty acyl chain, otherwise termed sphingosine (Roisen et al. 1981). These gangliosides are located in the plasma membrane, typically anchored in the outer leaflet where the long saturated hydrocarbon chains of ceramide cause the formation of lipid rafts (microdomains within the membrane incorporating other sphingolipids, cholesterol and selected signalling molecules) as the gangliosides partition laterally (Lopez and Schnaar 2009). The lipid moiety, ceramide, is composed of a long chain amino alcohol (sphingosine) with an amide linkage to a fatty acid and this results in lipid structural diversity as the ceramide structures vary in length, hydroxylation and saturation of both the sphingosine and fatty acid moieties (Schnaar, Suzuki and Stanley 2009). This range of ceramide variations impacts the attached glycan's presentation on the membrane surface, adding diversity; however, major classifications in structure and function have been assigned to the glycans.

There are two categories of which the biological functions can be divided into: (1) the glycan's structural and modulatory properties and (2) the glycan's specific recognition by other molecules, aptly termed glycan-binding proteins (GBPs or lectins), which is itself further subdivided into two categories of (1) intrinsic lectins, recognising glycans from the same organism and (2) extrinsic lectins, which conduct the opposite role of recognising glycans from a different organism, illustrated in Figure 4.2 (Varki and Lowe 2009).

Biological Roles of Glycans

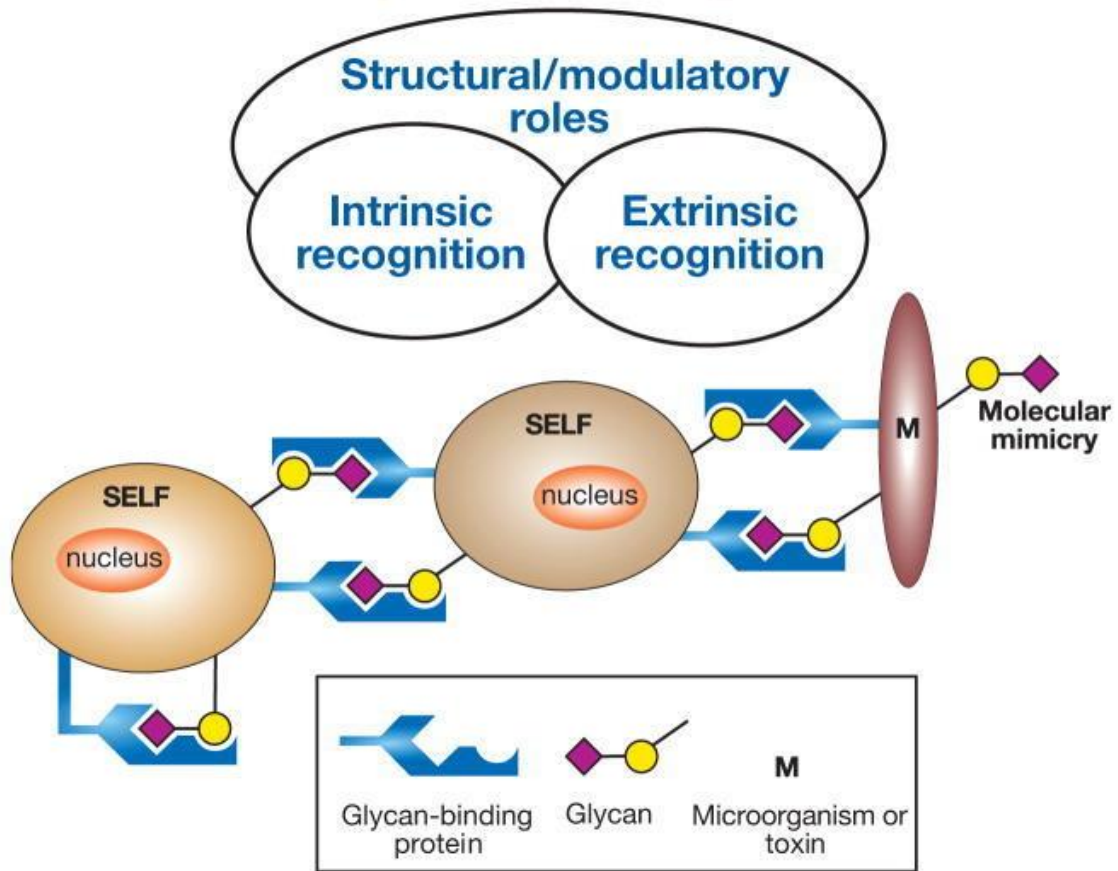
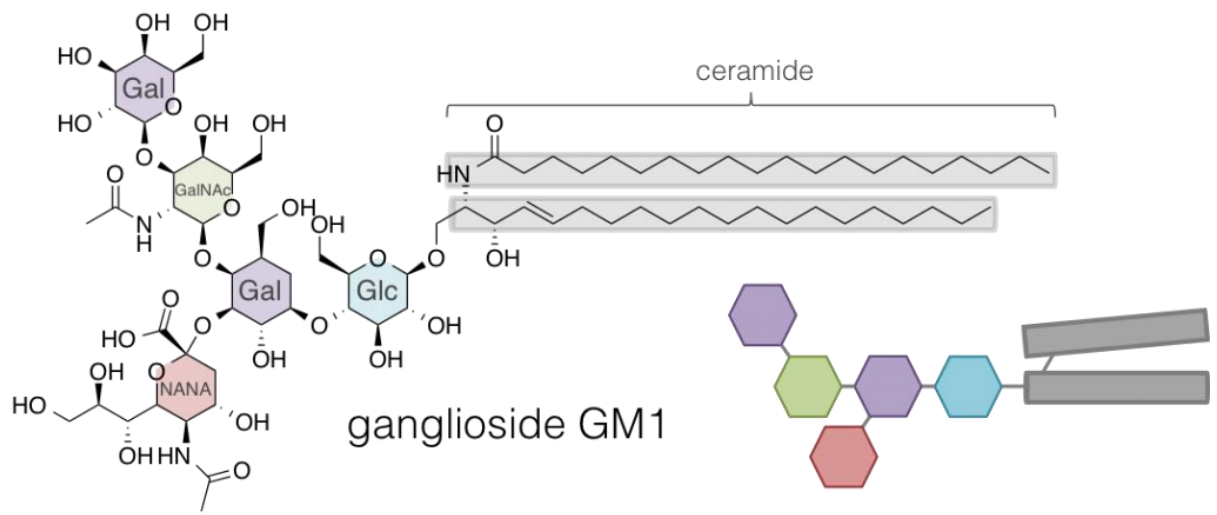
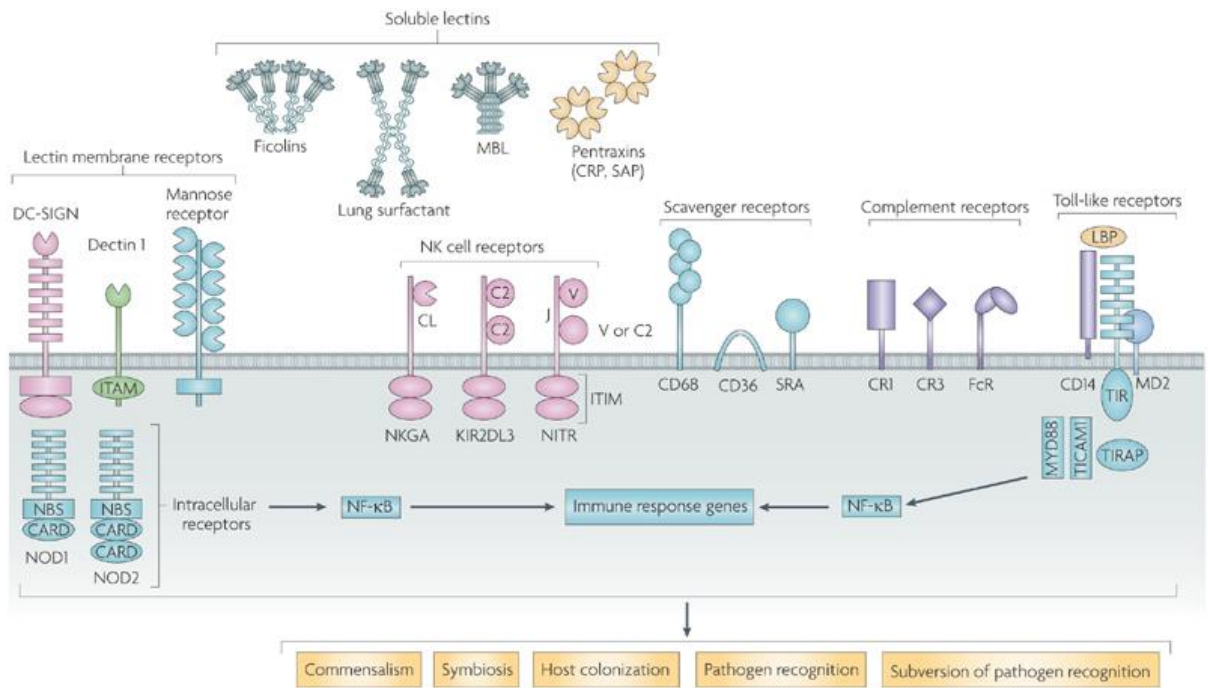
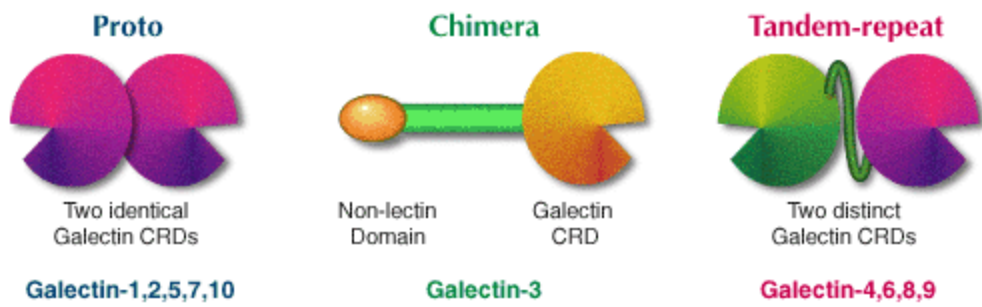


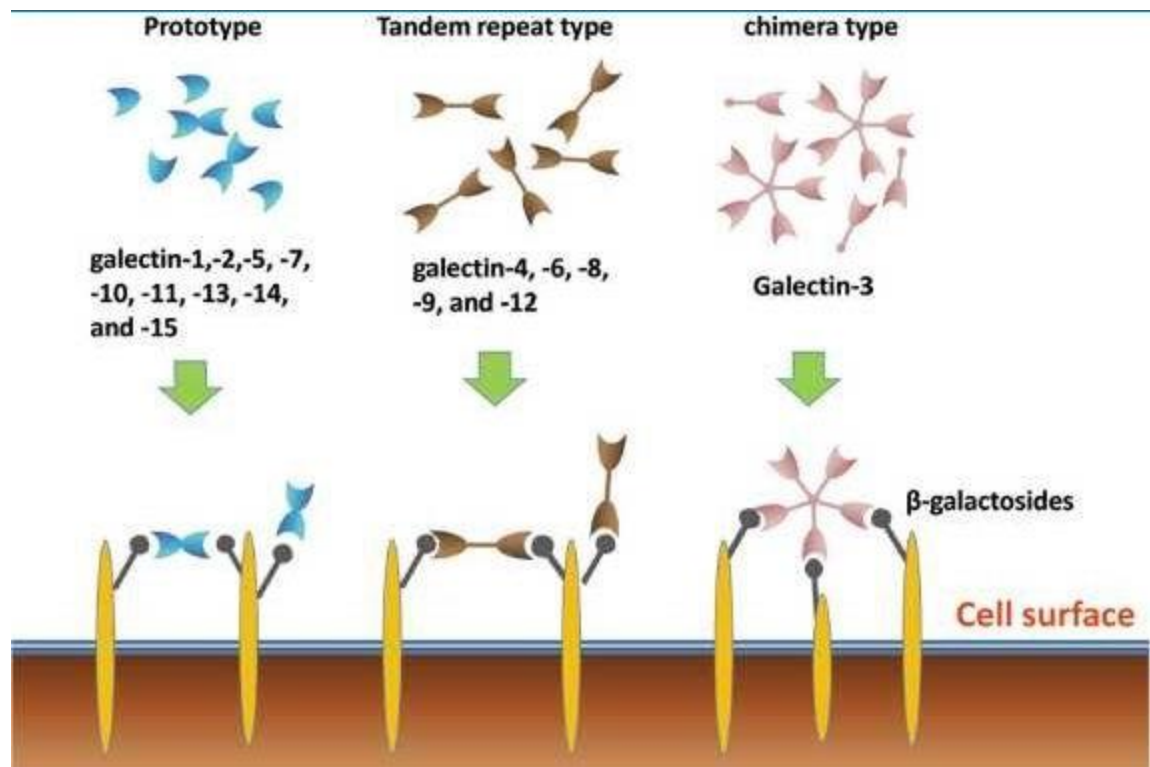
Figure 4.2: Glycan classification whereby glycans have a structural/modulatory role and also a recognition role. This illustration further emphasises this subdivision into intrinsic and extrinsic recognition with intrinsic recognition mediating cell-cell interactions originating from the same organism and extrinsic recognition where lectins bind to pathogenic microbial adhesions, agglutinins or toxins (Varki and Lowe 2009)

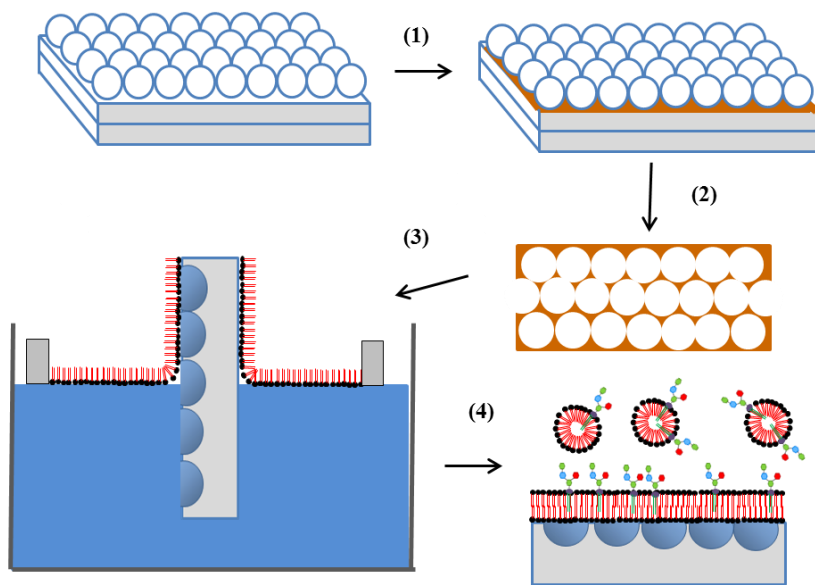


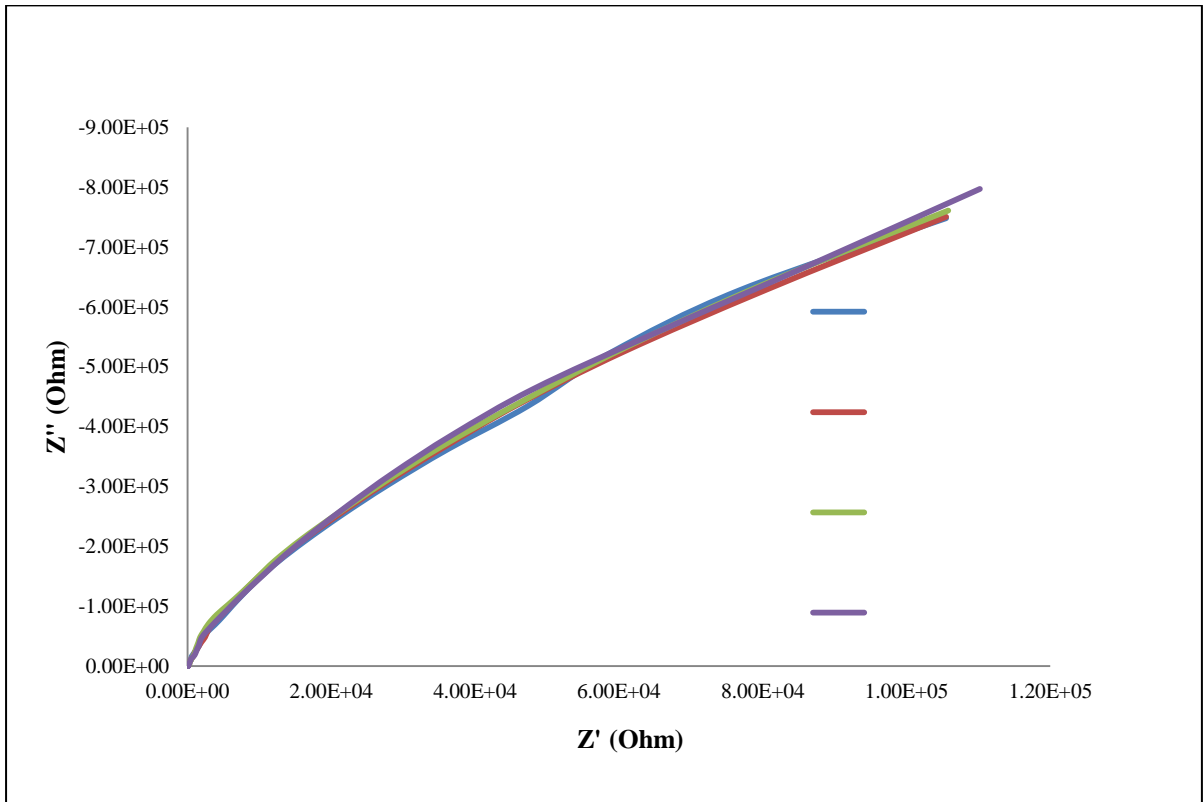


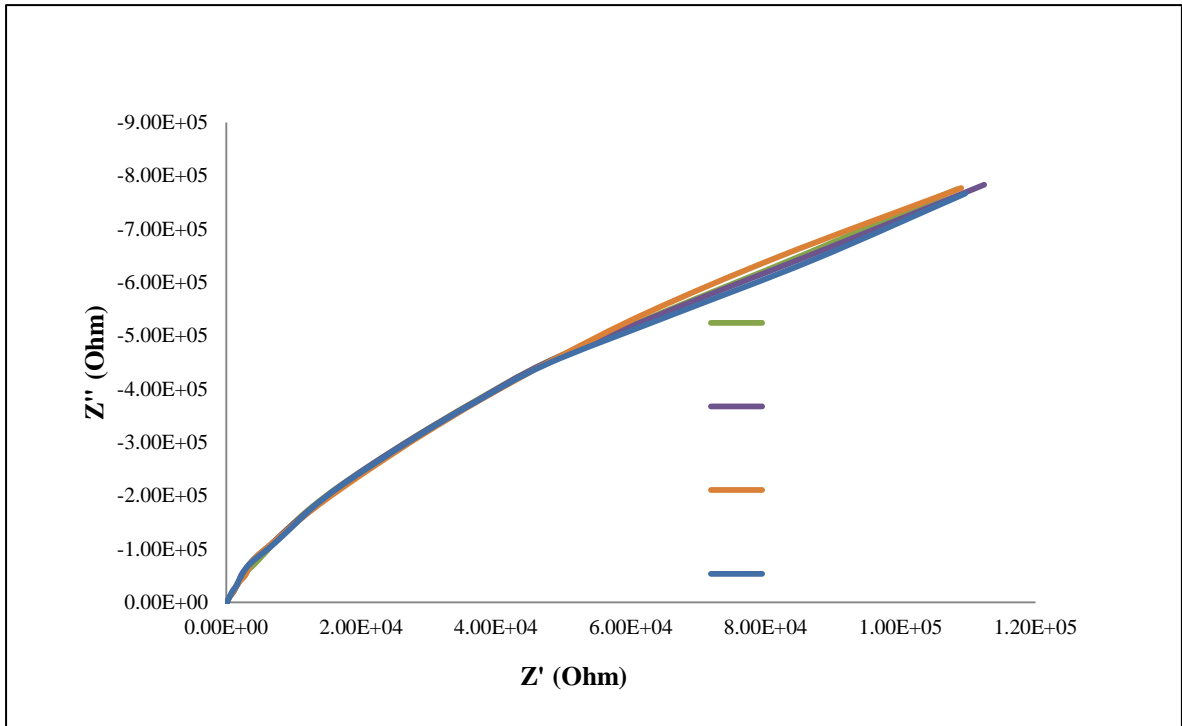
Three Architectural Types of Galectin

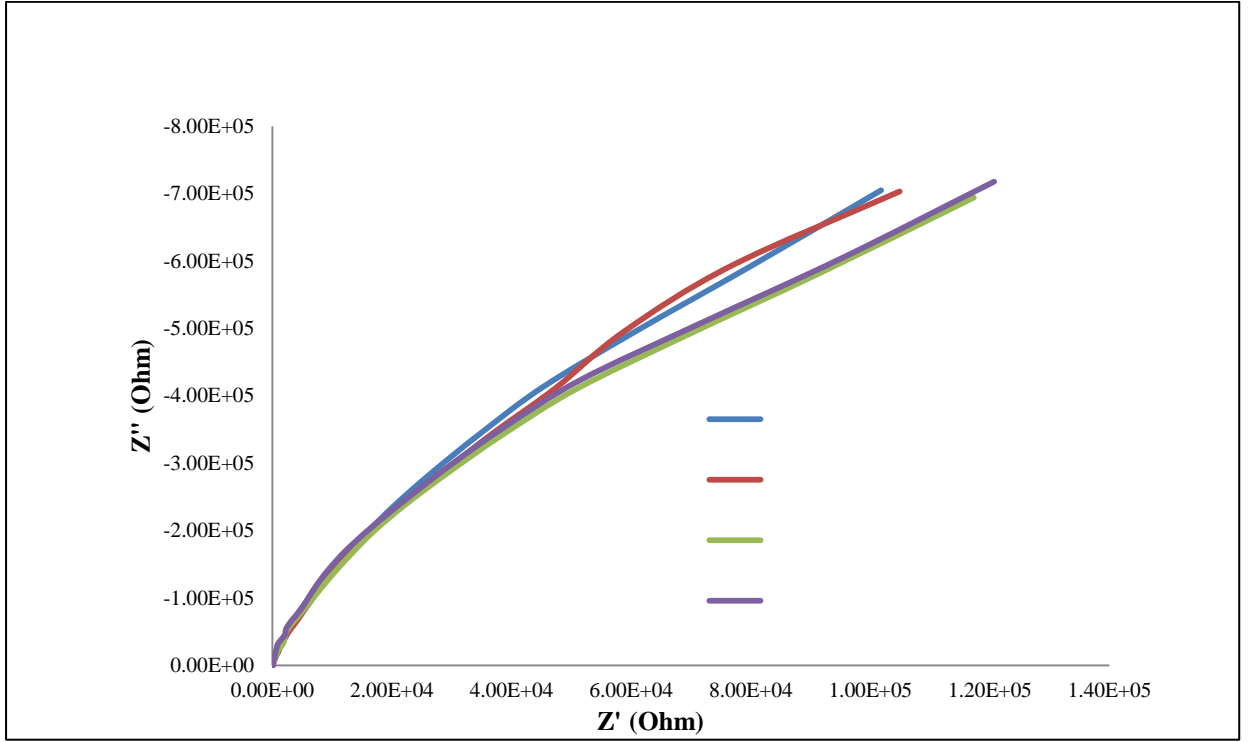


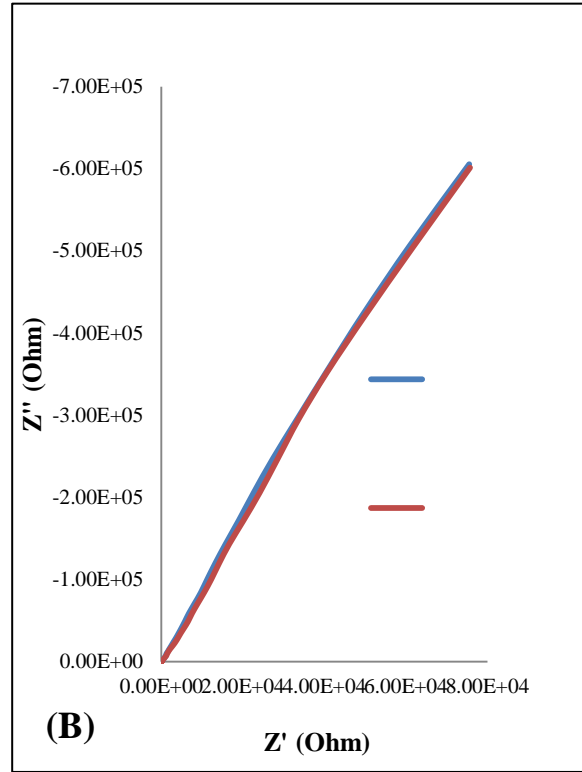
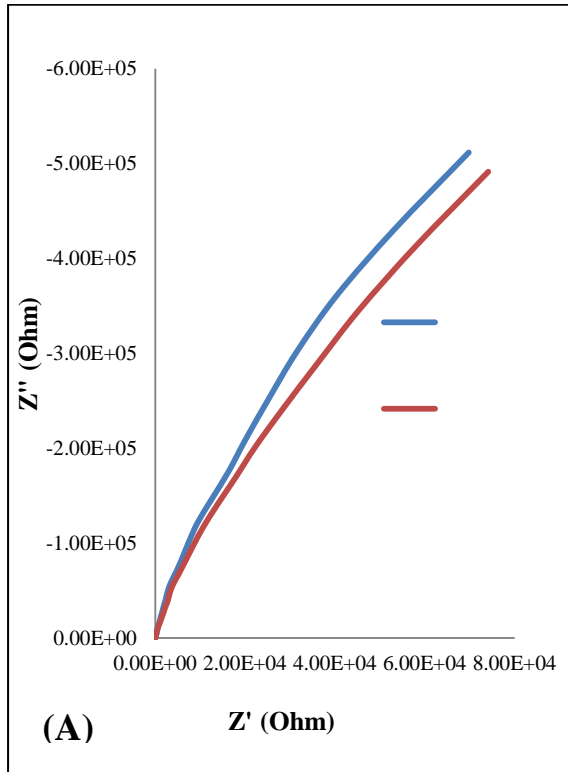


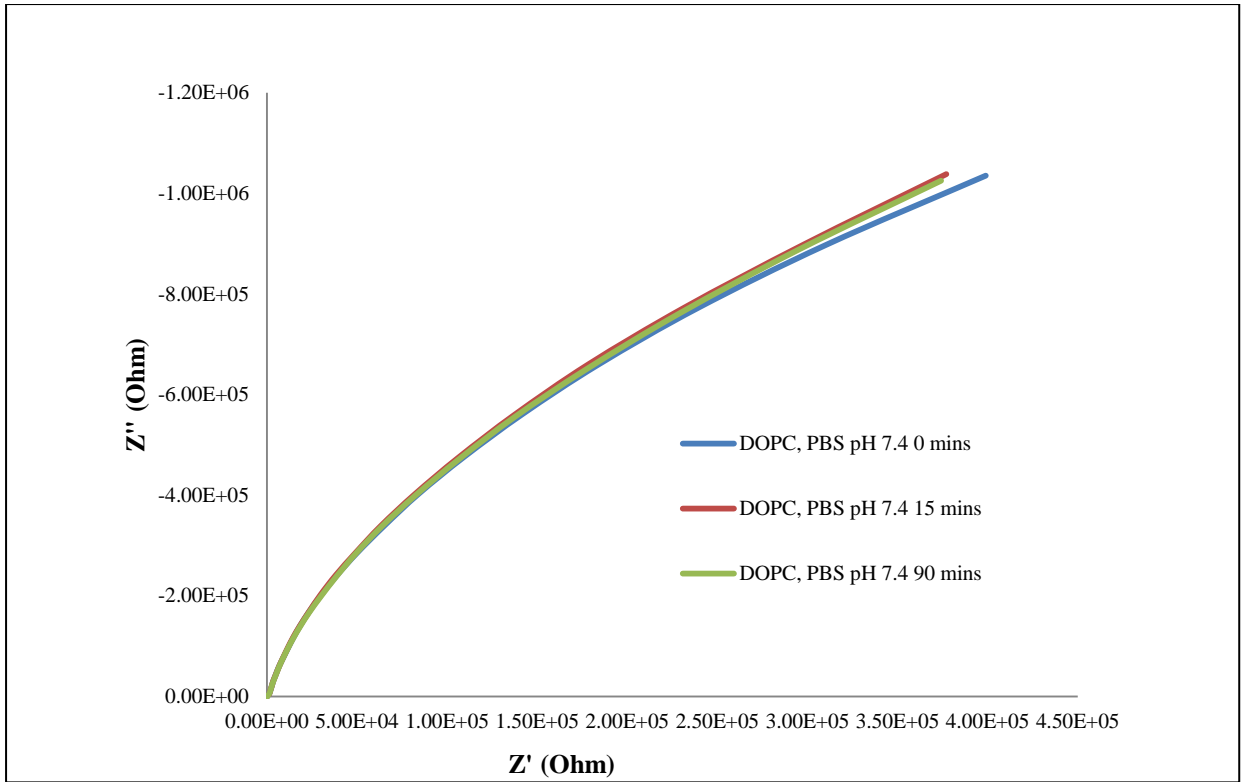


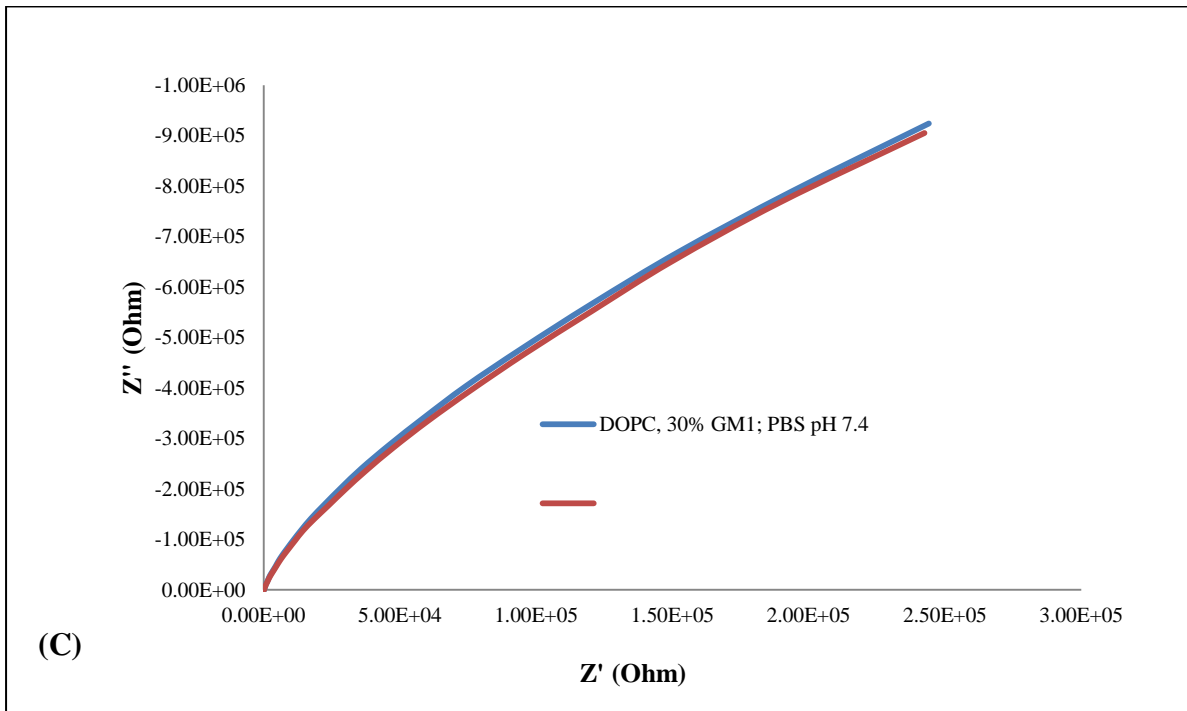
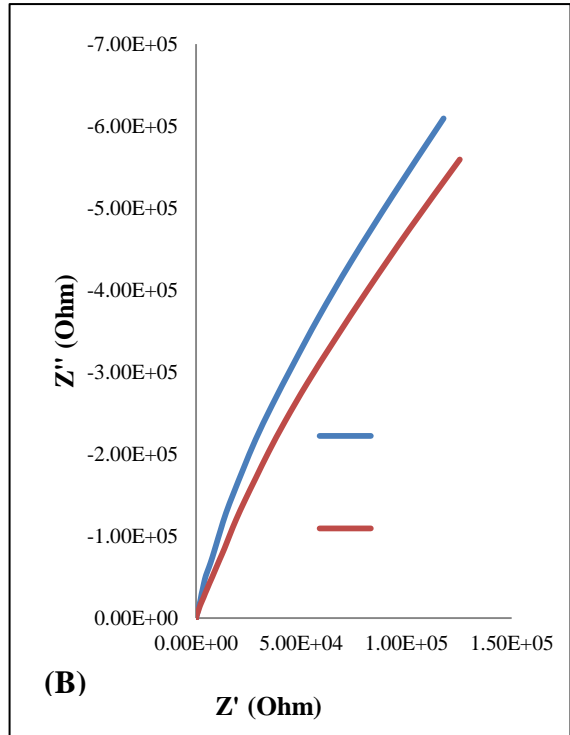
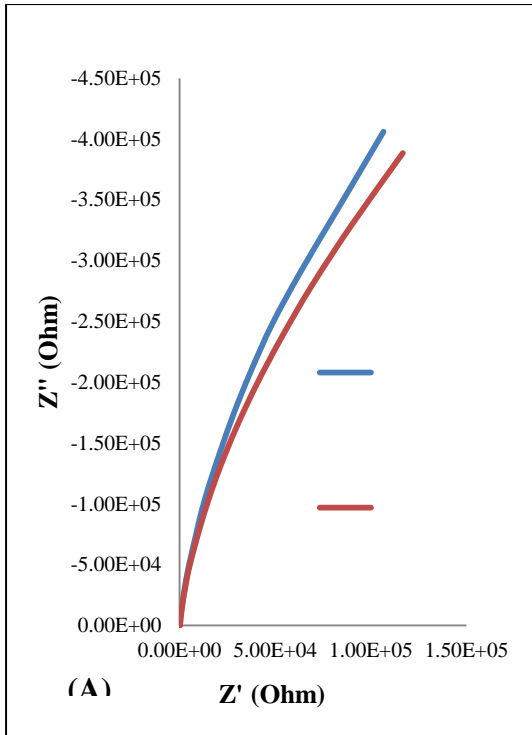


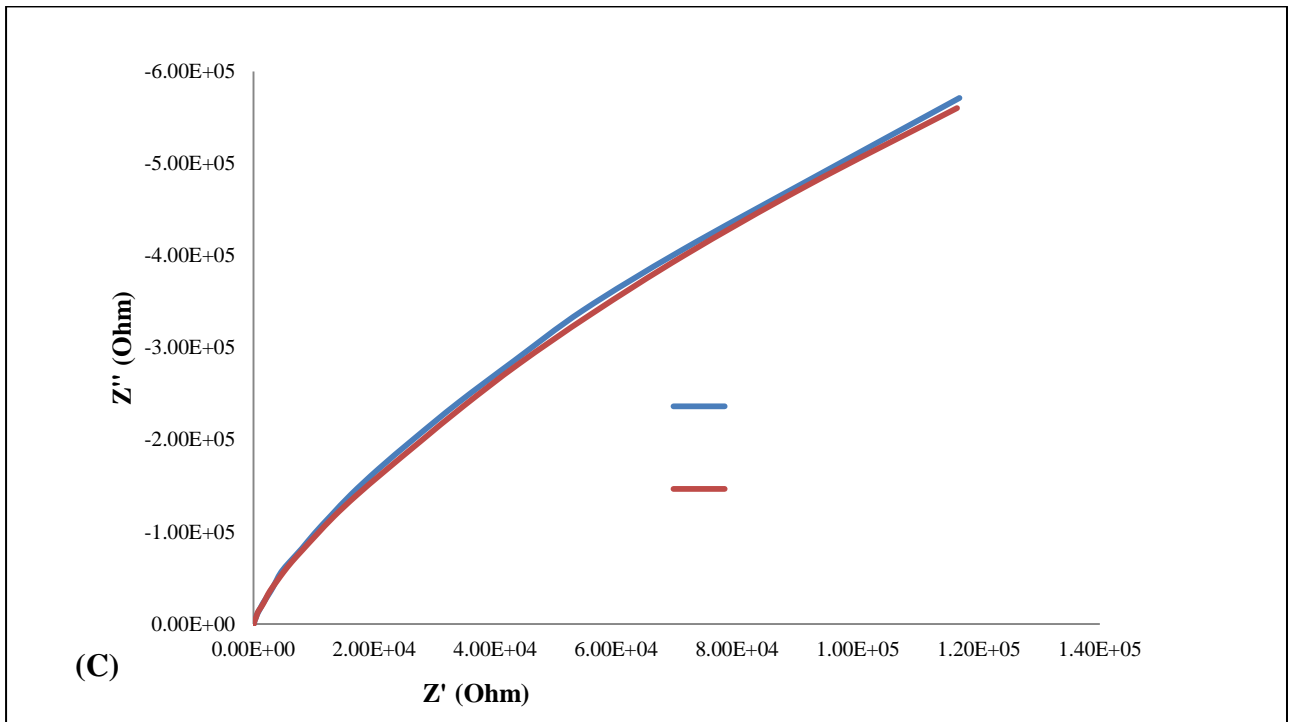
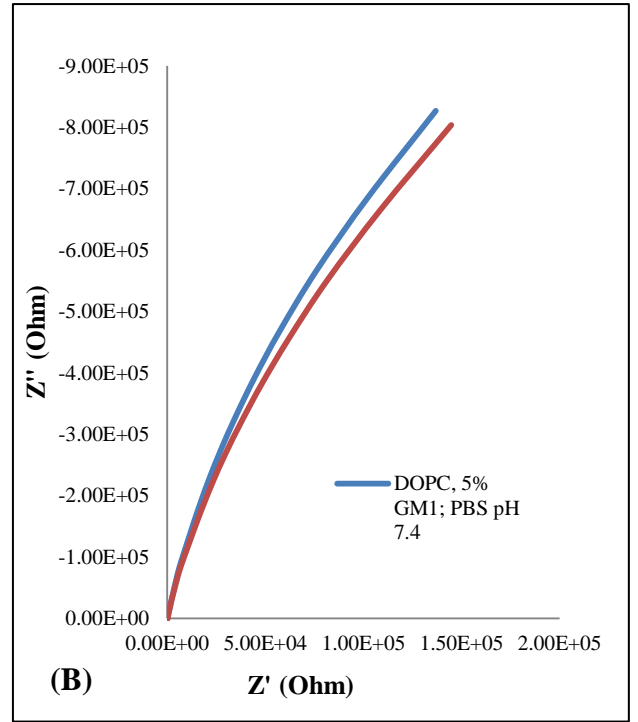
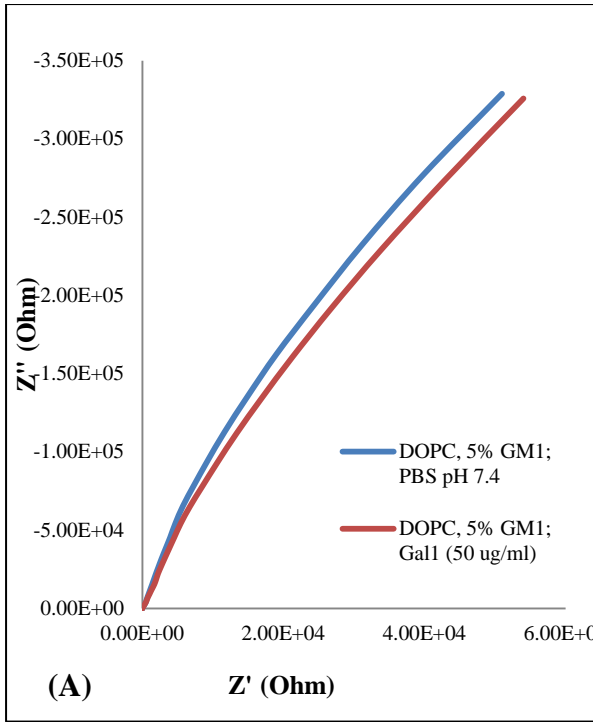


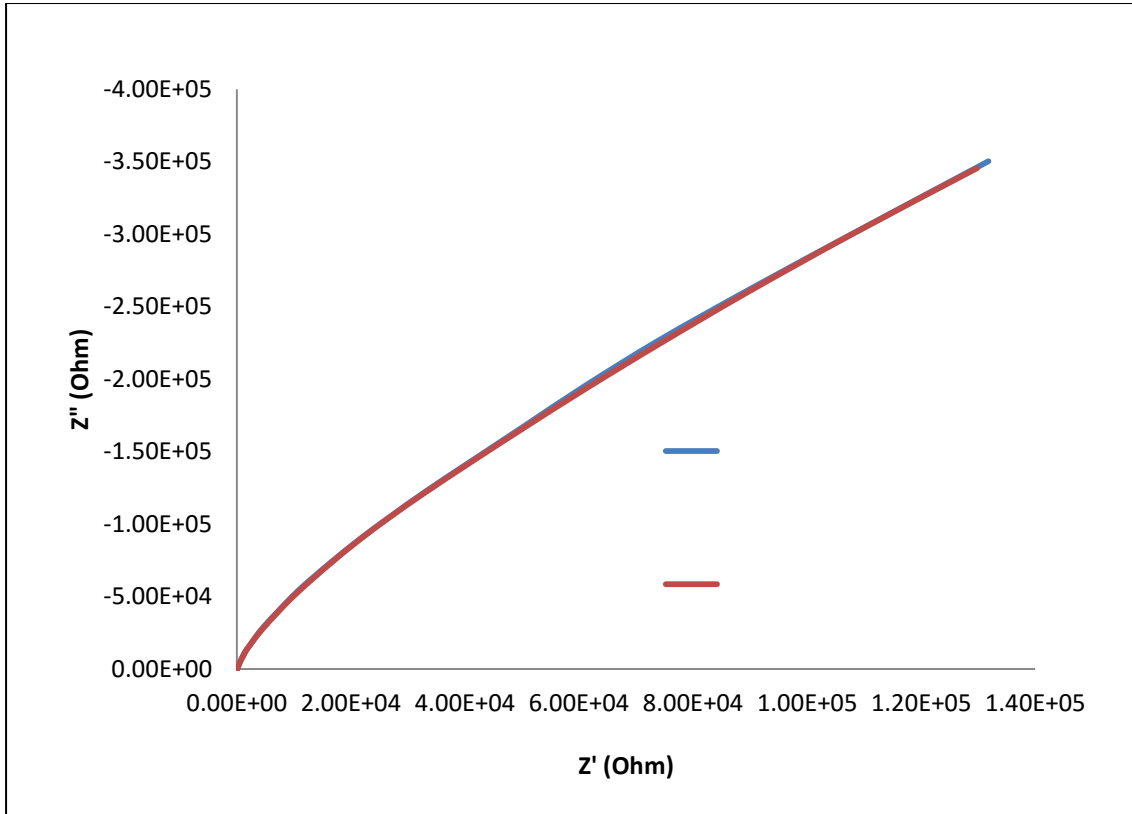


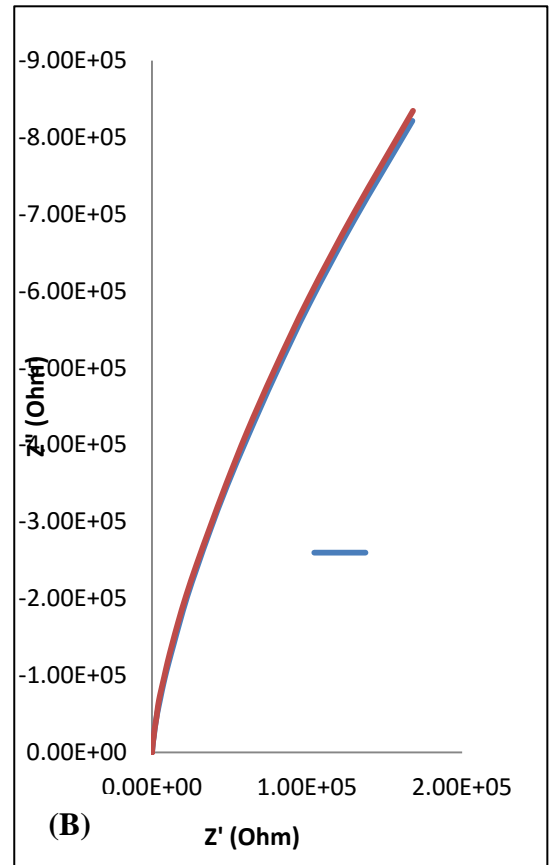
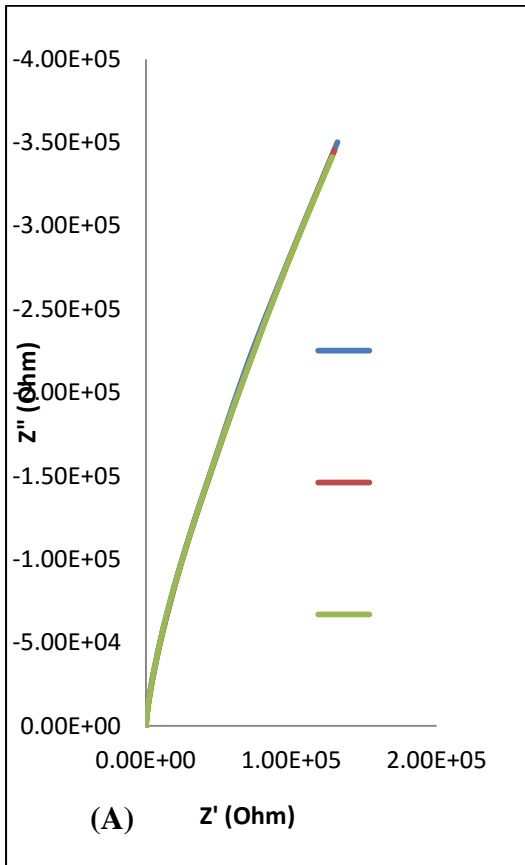


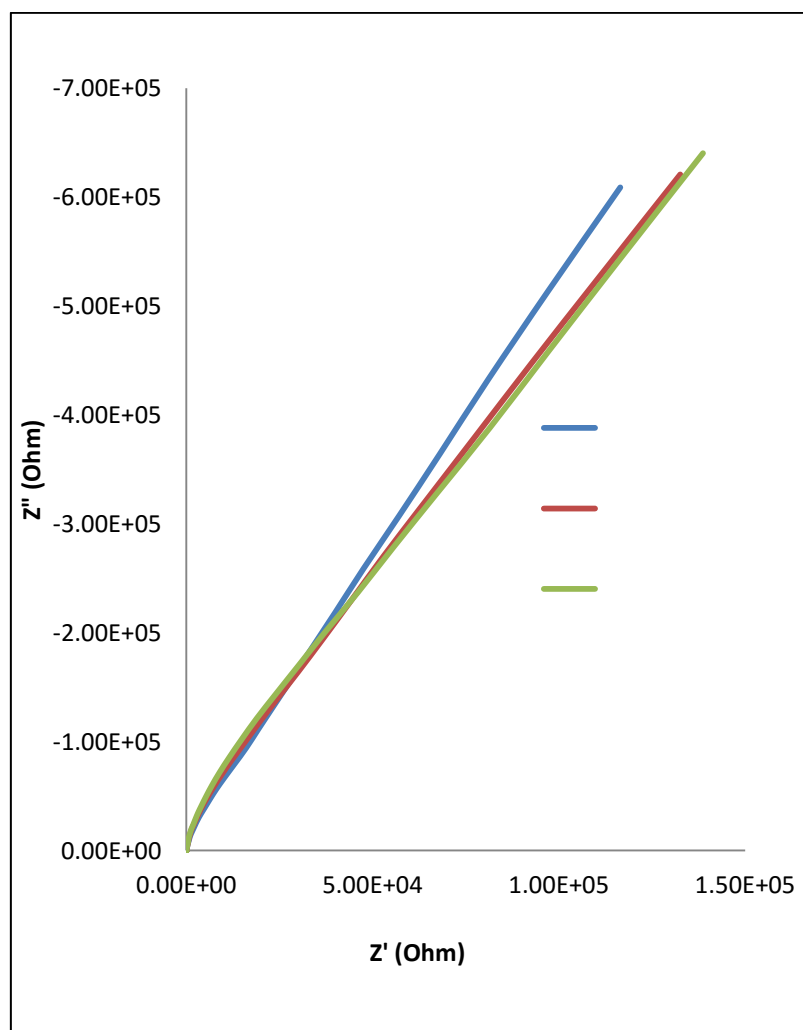


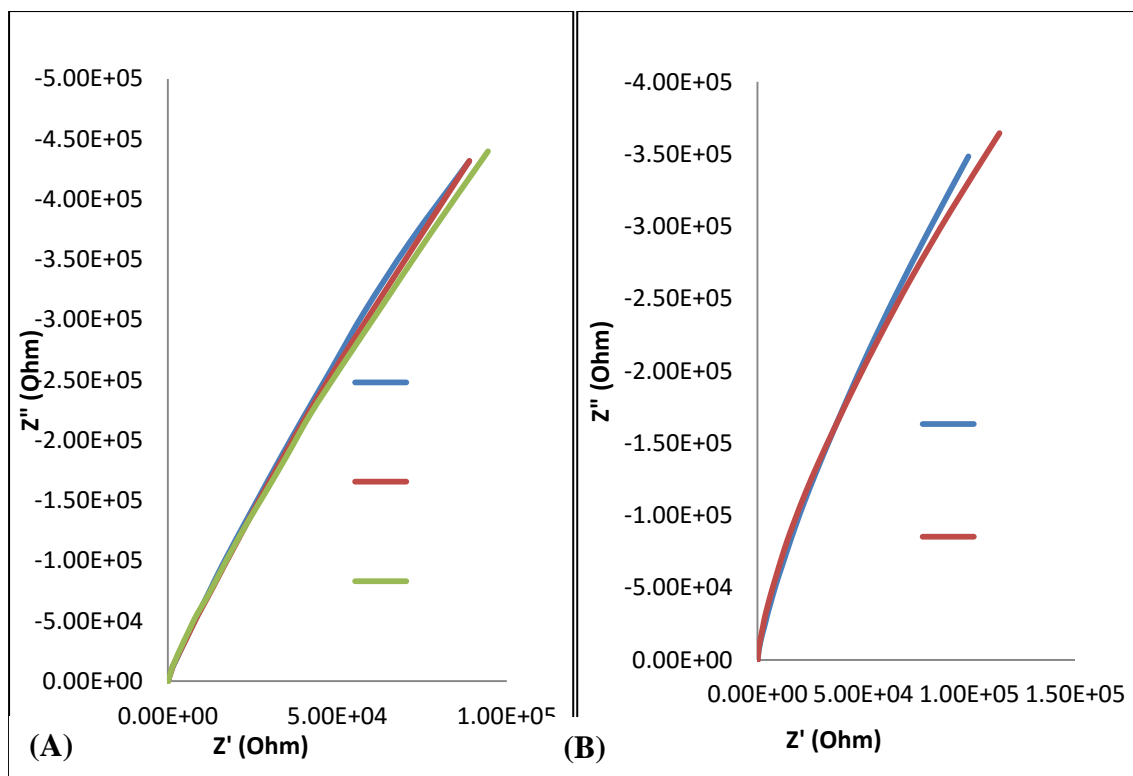


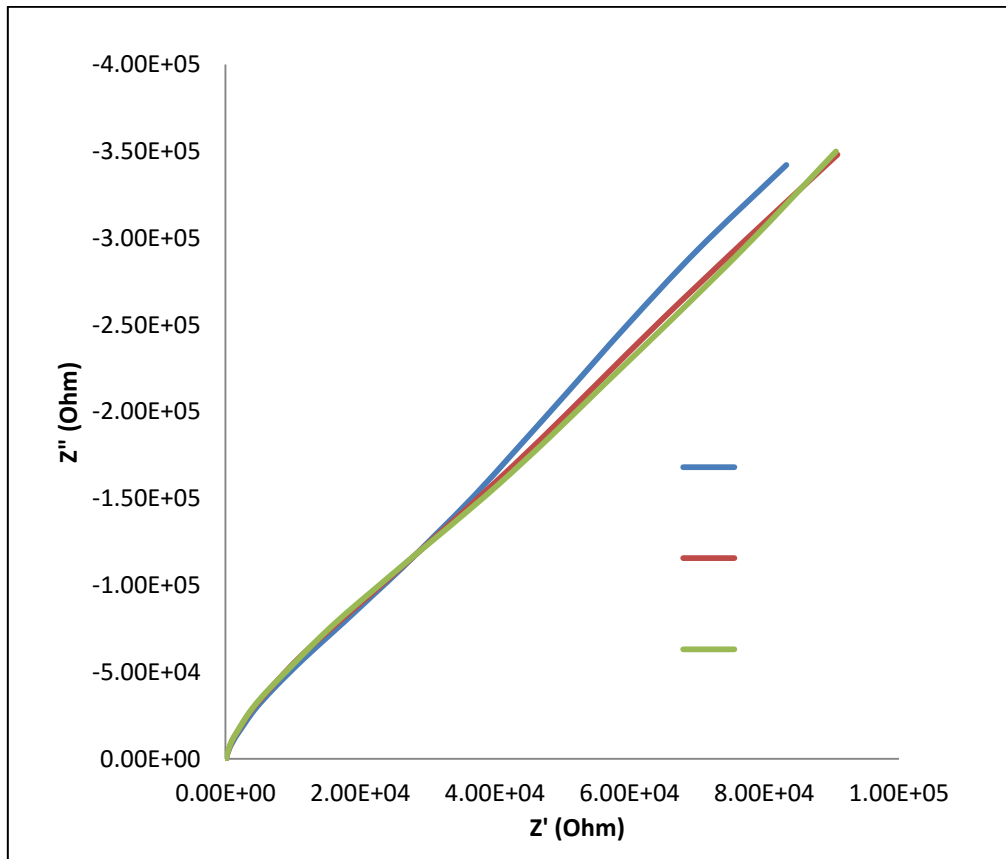


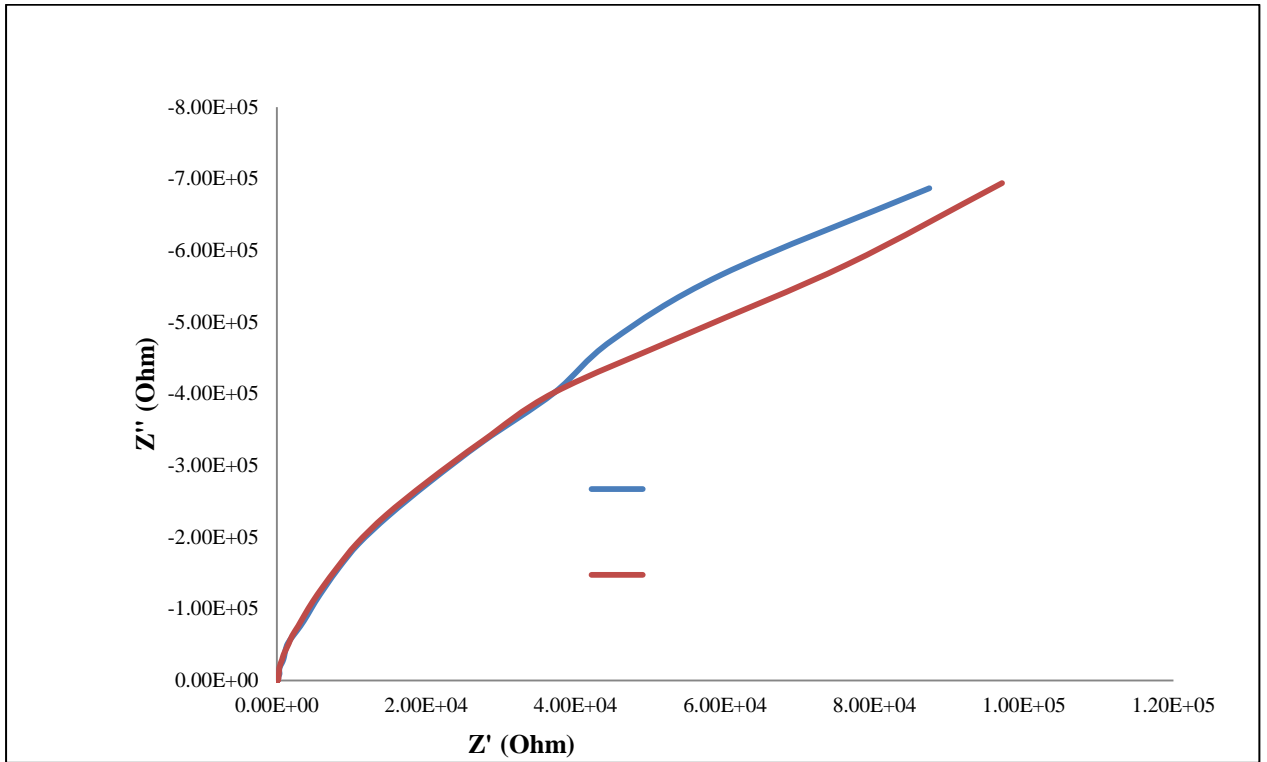












4.6 References

- Becucci, L. Vizza, F., Duarte, Y. and Guidelli, R. 2014. The GM1 Ganglioside Forms GM1-Rich Gel Phase Microdomains within Lipid Rafts. *Coatings*, 4, pp. 450-464.
- Chuang, C.H. 2014. Immunosensor with well-separated polyaniline nanowires for determination of isoelectric point based on electrochemical impedance spectroscopy. *Nano/Micro Engineered and Molecular Systems (NEMS)*, pp. 604-608.
- Fajka-Boja, R., Blaskó, A., Kovács-Sólyom, F., Szebeni, G.J., Tóth, G.K. and Monostori, E. 2008. Co-localization of Galectin-1 with GM1 ganglioside in the course of its clathrin- and raft-dependent endocytosis. *Cellular and Molecular Life Sciences*, 65, pp. 2586-2593.
- Fortuna-Costa, A., Gomes, A.M., Kozłowski, E.O., Stelling, M.P. and Pavão, M.S.G. 2014. Extracellular Galectin-3 in Tumour Progression and Metastasis. *Frontiers in Oncology*, 4(138), pp. 1-9.
- Fu-Tong, L. and Rabinovich, G. 2010. Galectins: Regulators of acute and chronic inflammation. *Annals of the New York Academy of Sciences*, 1183(1), pp.158-182.
- Gao, P., Simpson, J.L., Zhang, J. and Gibson, P.G. 2013. Galectin-3 its role in asthma and potential as an anti-inflammatory target. *Respiratory Research*, 14(1), pp.136.
- Gupta, R.K., Pande, A.H., Gulla, K.C., Gabius, H.J. and Hajela, K. 2006. Carbohydrate-induced modulation of cell membrane. VIII. Agglutination with mammalian lectin galectin-1 increases osmofragility and membrane fluidity of trypsinized erythrocytes. *FEBS Letters*, 580(6), pp. 1691-1695.
- Hirabayashi, J. 1997. *Galectin: Definition and history* [Online]. Available from: <http://www.glycoforum.gr.jp/science/word/lectin/LEA01E.html> [Accessed August 19 2015].
- Johannes, L., Parton, R.G., Bassereau, P. and Mayor, S. 2015. Building endocytic pits without clathrin. *Nature Reviews Molecular Cell Biology*, 16, pp. 311 - 321.
- Jose, B., Mallon, C., Forster, R.J. and Keyes, T.E. 2011. Lipid bilayer assembly at a gold nanocavity array, *Chemical Communications*, 47, pp. 12530-12532

Kopitz, J., Vértesy, S., Sabine, A., Fiedler, S., Schnolzer, M. and Gabius, H. 2014. Human chimera-type Galectin-3: Defining the critical tail length for high-affinity glycoprotein/cell surface binding and functional competition with Galectin-1 in neuroblastoma cell growth regulation. *Biochimie*, 104, pp.90-99.

Lajoie, P., Partridge, E.A., Guay, G., Goetz, J.G., Pawling, J., Lagana, A., Joshi, B., Dennis, J.W. and Nabi, I.R. 2007. Plasma membrane domain organization regulates EGFR signaling in tumor cells. *The Journal of Cell Biology*, 179(2), pp.341-356.

Ledeen, R.W., Wu, G., Bleich, D., Lu, Z.H. and Gabius, H.J. 2012. Galectin-1 Cross-Linking of GM1 Ganglioside in Autoimmune Suppression IN: *Galectins and Disease Implications for Targeted Therapeutics*. American Chemical Society, pp. 107 - 121.

Lingwood, C.A. 2011. Glycosphingolipid functions. *Cold Spring Harb Perspect Biol*, 3

Lopez, P.H. and Schnaar, R.L. 2009. Gangliosides in cell recognition and membrane protein regulation. *Current Opinion in Structural Biology*, 19(5), pp.549-557.

Mader, S.S. 2001. *Biology*. 7th ed. New York: McGraw-Hill.

Novák, J., Kriston-Pá, É., Czibula, A., Deák, M., Kovács, L., Monostori, E. and Fajka-Boja, R. 2014. GM1 controlled lateral segregation of tyrosine kinase Lck predispose T-cells to cell-derived Galectin-1-induced apoptosis. *Molecular Immunology*, 57(2), pp. 302-309.

Radosavljevic, G., Volarevic, V., Jovanovic, I., Milovabovic, M., Pejnovic, N., Arsenijevic, N., Hsu, D.K. and Lukic, M.L. 2012. The roles of Galectin-3 in autoimmunity and tumor progression. *Immunologic Research*, 52pp.100-110.

Rapoport, E.M., Andre, S., Kurmyshkina, O.V., Pochechueva, T.V., Severov, V.V., Pazynina, G.V., Gabius, H.J. and Bovin, N.V. 2008. Galectin-loaded cells as a platform for the profiling of lectin specificity by fluorescent neoglycoconjugates: A case study on Galectins-1 and -3 and the impact of assay setting. *Glycobiology*, 18(4), pp.315-324.

Roisen, F.J., Bartfeld, H., Nagele, R. and Yorke, G. 1981. Ganglioside stimulation of axonal sprouting in vitro. *Science (New York, N.Y.)*, 214(4520), pp.577-578.

Rondelli, V., Fragneto, G., Motta, S., Del Favero, E., Brocca, P., Sonnino, S. and Cantù, L. 2012. Ganglioside GM1 forces the redistribution of cholesterol in a biomimetic membrane. *Biochimica Et Biophysica Acta*, 1818(11), pp.2860-2867.

Ryan, M. and Washburn, L. 2014. *Quorum sensing in vibrio cholerae: Pathogenicity of cholera* [Online]. Available from: <http://sites.tufts.edu/quorumsensing/qs-in-vibrio-cholerae/pathogenicity-of-cholera/> [Accessed August 19 2015].

Schnaar, R.L., Suzuki, A. and Stanley, P. 2009. Chapter 10 Glycosphingolipids *IN: Varki, A., Cummings, R.D., Esko, J. and et al. (eds.) Essentials of Glycobiology. 2nd edition.*

Schnaar, R.L. 2004. Glycolipid-mediated cell–cell recognition in inflammation and nerve regeneration. *Archives of Biochemistry and Biophysics*, 426(2), pp.163-172.

Szklarczyk, O.M., González-Segredo, N., Kukura, P., Oppenheim, A., Choquet, D., Sandoghdar, V., Helenius, A., Sbalzarini, I.F. and Ewers, H. 2013. Receptor concentration and diffusivity control multivalent binding of Sv40 to membrane bilayers. *PLOS Computational Biology*, e1003310

Varki, A. 2007. Glycan-based interactions involving vertebrate sialic-acid-recognizing proteins. *Nature*, 446pp.1023-1029.

Varki, A., Cummings, R.D. and Esko, J.D. 2009. *Essentials of Glycobiology*. 2nd ed. New York: Cold Spring Harbour.

Varki, A. and Lowe, J.B. 2009. Chapter 6 Biological Roles of Glycans *IN: Anonymous Essentials of Glycobiology*. 2nd Ed ed. Cold Spring Harbor Laboratory Press,

Varki, A., Cummings, R., Esko, J., Freeze, H., Hart, G. and Marth, J. 1999. *Essentials of Glycobiology*. 1st ed. New York: Cold Spring Harbor Laboratory Press.

Vasta, G.R. 2012. Galectins as pattern recognition receptors: Structure, function and evolution. *Advances in Experimental Biology and Medicine*, 946pp.21-36.

Vasta, G.R. 2009. Roles of Galectin in infection. *Nature Review Microbiology*, 7pp.424-438.

Wang, J., Lu, Z., Gabius, H., Rohowsky-Kochan, C., Ledeen, R.W. and Wu, G. 2009. Cross-linking of GM1 ganglioside by Galectin-1 mediates regulatory T cell activity involving TRPC5 channel activation: Possible role in suppressing experimental autoimmune encephalomyelitis. *Journal of Immunology*, 182pp.4036-4045.

Chapter 5: Conclusions and Future Work

5.0 Conclusions and Future Work

This thesis focussed on the development of a suitable model of the cell membrane to provide a realistic representation of an organism's bilayer. This model was used to investigate the effects of ibuprofen and diclofenac on the lipid bilayer and also to assess GM1-galectin interaction when GM1 was incorporated into the membrane itself. Chapter 2 detailed the fabrication of the DOPC lipid bilayer suspended across a gold microcavity array. Lipid bilayers have been fabricated previously but this is the first model which supports a bilayer between two aqueous environments and has a stability surpassing that of the BLM. The gold substrate enables EIS analysis which was used in Chapters 3 and 4.

Chapter 3 demonstrated the application of the model in assessing drug plasma membrane interactions, specifically focusing on ibuprofen and diclofenac. This work showed that diclofenac interacted more strongly with the bilayer and induced nanoscale defects in the layer, mainly in the lipid tails. Alternatively, ibuprofen increased the resistance of the bilayer indicating that it was adding to the films thickness. This is in keeping with previous research which shows this drug as primarily interacting with the polar headgroups and having little effect on the hydrocarbon chains.

Chapter 4 uses the biomimetic microcavity supported lipid bilayer to study the interaction between the ganglioside, GM1 and various galectins by fabricating GM1 containing cell membranes to investigate GM1-galectin binding and network formation; the influence of lipid/sterol integration on GM1-galectin recognition, aggregation and crosslinking across disease relevant members of the galectin family: galectin-1 and galectin-3, followed by galectin-3t.

The MSLBs are a significant and necessary advance on current lipid membrane models as they permit accurate representations of cell membrane in elements of composition, fluidity, asymmetry and microenvironment. To conclude, MSLBs pose a unique, electrochemical alternative to investigate the affect that various drugs have when they permeate through the membrane and also how various proteins affect the bilayer, particularly when they bind with external compounds. This is a much needed technique in

current membrane research as MSLBs are a unique and robust approach to investigate numerous membrane properties with bounds of potential in variation and optimisation. They offer a very significant improvement on the state of the art including liposomes and conventional and tethered supported lipid bilayers in terms of versatility, reproducibility, biomimicry and, in particular, amenability to analytical interrogation. In particular the deep fluid well below as well as above the bilayer and ability to address both sides of the layer is novel and desirable.

There is still work to be done to improve and optimise the performance of the array - reproducibility and stability of response is very good in single substrates but the substrate to substrate variation has to be addressed by a method which will make pore deposition and substrate size as uniform as possible. Additionally, various surface modifications to the substrate and for Chapter 3, a broader range of drugs needs to be assessed to further validate model. This work should include an assessment of the cell membrane following permeation to ensure serious damage is not being done to the cell or alternatively, some drugs may function in destroying this barrier and so this method is needed. MSLBs surpass their industrial counterparts additionally as various cell membrane compositions can be constructed and improvements and alternations to the surface modification compounds can be utilised to increase sensitivity. Finally, the incorporation of proteins into the MSLBs, as demonstrated in Chapter 4, is catered for as the cavity arrays provide an environment where proteins can position themselves through the membrane and extrude in the intracellular and extracellular environments without being restricted or impeded by support materials. Regarding the experiments using galactose to inhibit the galectin-GM1 interaction, this is not the ideal sugar and future work would include a lactose investigation. Additionally increased variations in concentration of the GM1 and the galectin should be further assessed to understand the variation in response. Cholesterol incorporation was assessed minimally; lipid composition and its influence is a growing area of study and these platforms provide the ideal substrate for analysis.

Appendix 1: FLCS Results

Table A1: FLCS data analysis of ibuprofen for 2 probes

1. Atto655-DOPE

Conc. (μM)	Mol. Brightness (X 1000)	Fluor. lifetime (ns)	Anomalous exponent α	N	D ($\mu\text{m}^2/\text{s}$)
0	6.3 ± 0.9	3.3 ± 0.03	1.00 ± 0.03	3.0 ± 1	11.7 ± 0.8
1	6.7 ± 1.0	3.3 ± 0.01	0.98 ± 0.03	3.0 ± 1	10.7 ± 1.0
4	6.35 ± 1.2	3.34 ± 0.01	1.0 ± 0.02	2.0 ± 1	10.64 ± 0.6
20	6.1 ± 0.8	3.32 ± 0.01	0.98 ± 0.02	3.0 ± 0.5	10.66 ± 0.8
40	6.4 ± 0.65	3.30 ± 0.01	1.0 ± 0.03	3.0 ± 0.5	12.0 ± 1.1
100	5.9 ± 0.74	3.29 ± 0.01	0.98 ± 0.02	2.0 ± 0.5	11.6 ± 0.75
400	6.56 ± 0.5	3.28 ± 0.05	1.00 ± 0.02	3.0 ± 1.0	10.7 ± 1.0
800	6.95 ± 0.5	3.3 ± 0.01	0.99 ± 0.04	2.0 ± 1.0	11.6 ± 1.1
1000	6.12 ± 1.1	3.3 ± 0.02	0.97 ± 0.04	1.5 ± 0.5	11.27 ± 1.2
After wash		3.29 ± 0.01	0.99 ± 0.04	2.5 ± 0.5	11.5 ± 1.2

2. β -BODIPY-C5-HPC

Conc. (μM)	Mol. Brightness (X 1000)	Fluor. lifetime (ns)	Anomalous exponent α	N	D ($\mu\text{m}^2/\text{s}$)
0	12.7 ± 2.0	5.94 ± 0.14	0.98 ± 0.03	2.0 ± 0.5	14.35 ± 1.52
1	13.0 ± 1.2	5.97 ± 0.05	0.97 ± 0.03	2.0 ± 0.5	13.73 ± 1.70
4	12.2 ± 1.5	5.89 ± 0.10	0.96 ± 0.02	2.0 ± 1.0	12.38 ± 1.50
20	11.8 ± 1.5	5.92 ± 0.04	0.95 ± 0.04	3.0 ± 0.5	11.30 ± 1.10
40	11.74 ± 1.7	5.87 ± 0.05	0.97 ± 0.02	2.0 ± 0.5	12.10 ± 1.10
100	11.82 ± 1.1	5.83 ± 0.08	0.98 ± 0.03	2.0 ± 0.5	12.63 ± 1.20
400	11.57 ± 0.90	5.82 ± 0.07	0.96 ± 0.03	2.0 ± 0.5	11.22 ± 1.2
800	11.30 ± 1.2	5.83 ± 0.09	0.97 ± 0.03	2.0 ± 0.5	13.20 ± 1.0
1000	12.48 ± 1.5	5.82 ± 0.10	0.97 ± 0.02	2.0 ± 0.5	11.00 ± 1.15
After wash	11.74 ± 1.3	5.84 ± 0.10	0.96 ± 0.03	2.5 ± 0.5	11.90 ± 1.0

Table A2: FLCS data analysis of diclofenac for 2 probes

1. Atto655-DOPE

Conc. (μM)	Mol. Brightness (X 1000)	Fluor. lifetime (ns)	Anomalous exponent α	N	D ($\mu\text{m}^2/\text{s}$)
0	6.3 ± 0.9	3.3 ± 0.03	0.98 ± 0.03	3.0 ± 1	11.7 ± 0.8
1	6.2 ± 0.9	3.3 ± 0.01	0.99 ± 0.02	3.0 ± 1	12.0 ± 0.5
4	6.1 ± 0.8	3.3 ± 0.02	1.0 ± 0.03	3.0 ± 1	11.9 ± 1.3
20	6.2 ± 0.7	3.24 ± 0.01	1.15 ± 0.04	2.0 ± 0.5	16.6 ± 1.4
40	5.0 ± 0.65	3.16 ± 0.02	1.08 ± 0.06	1.5 ± 0.5	18.0 ± 2.1
100	3.9 ± 0.8	3.04 ± 0.02	1.19 ± 0.07	1.0 ± 0.2	24.0 ± 4.3
400	1.6 ± 0.35	2.78 ± 0.08	1.21 ± 0.11	1.0 ± 0.4	34.3 ± 5.2
800	1.1 ± 0.2	2.5 ± 0.13	1.16 ± 0.10	1.0 ± 0.5	43.5 ± 8.0
1000	1.0 ± 0.16	2.44 ± 0.12	1.21 ± 0.15	1.5 ± 0.5	41.5 ± 8.0
After wash		3.15 ± 0.03	1.14 ± 0.04	1.0 ± 0.5	22.0 ± 3.5

2. β -BODIPY-C5-HPC

Conc. (μM)	Mol. Brightness (X 1000)	Fluor. lifetime (ns)	Anomalous exponent α	N	D ($\mu\text{m}^2/\text{s}$)
0	12.7 ± 2.0	5.94 ± 0.14	0.98 ± 0.03	2.0 ± 0.5	14.35 ± 1.52
1	12.0 ± 1.0	5.90 ± 0.10	0.97 ± 0.04	2.0 ± 0.5	12.22 ± 2.0
4	13.2 ± 2.0	5.97 ± 0.10	0.97 ± 0.02	2.5 ± 0.5	12.27 ± 1.30
20	10.8 ± 1.1	5.70 ± 0.10	0.97 ± 0.03	2.5 ± 0.5	11.40 ± 1.10
40	11.2 ± 1.3	5.63 ± 0.12	0.96 ± 0.05	2.5 ± 0.5	11.50 ± 1.40
100	7.0 ± 1.5	5.10 ± 0.07	0.97 ± 0.02	2.5 ± 0.5	10.60 ± 1.60
400	6.45 ± 1.0	4.72 ± 0.07	0.97 ± 0.03	2.0 ± 0.5	10.95 ± 1.0
800	4.42 ± 0.9	4.24 ± 0.09	0.96 ± 0.03	2.5 ± 0.5	10.20 ± 1.0
1000	3.4 ± 0.7	4.12 ± 0.06	0.95 ± 0.05	3.0 ± 0.5	10.00 ± 0.9
After wash		5.62 ± 0.17	0.96 ± 0.03	2.5 ± 0.5	12.00 ± 1.5